

Porosity in wire-arc directed energy deposition of aluminum alloys: Formation mechanisms, influencing factors and inhibition strategies

Hao Yi^{a,b,*}, Liu Yang^{a,b}, Le Jia^{a,b}, Yuze Huang^c, Huajun Cao^{a,b,**}

^aState Key Laboratory of Mechanical Transmission, Chongqing University, Chongqing 400044, China

^bCollege of Mechanical and Vehicle Engineering, Chongqing University, Chongqing 400044, China

^cSchool of Engineering, Lancaster University, Lancaster, LA1 4YW, UK

*Corresponding author. Email: haoyi@cqu.edu.cn (H. Yi)

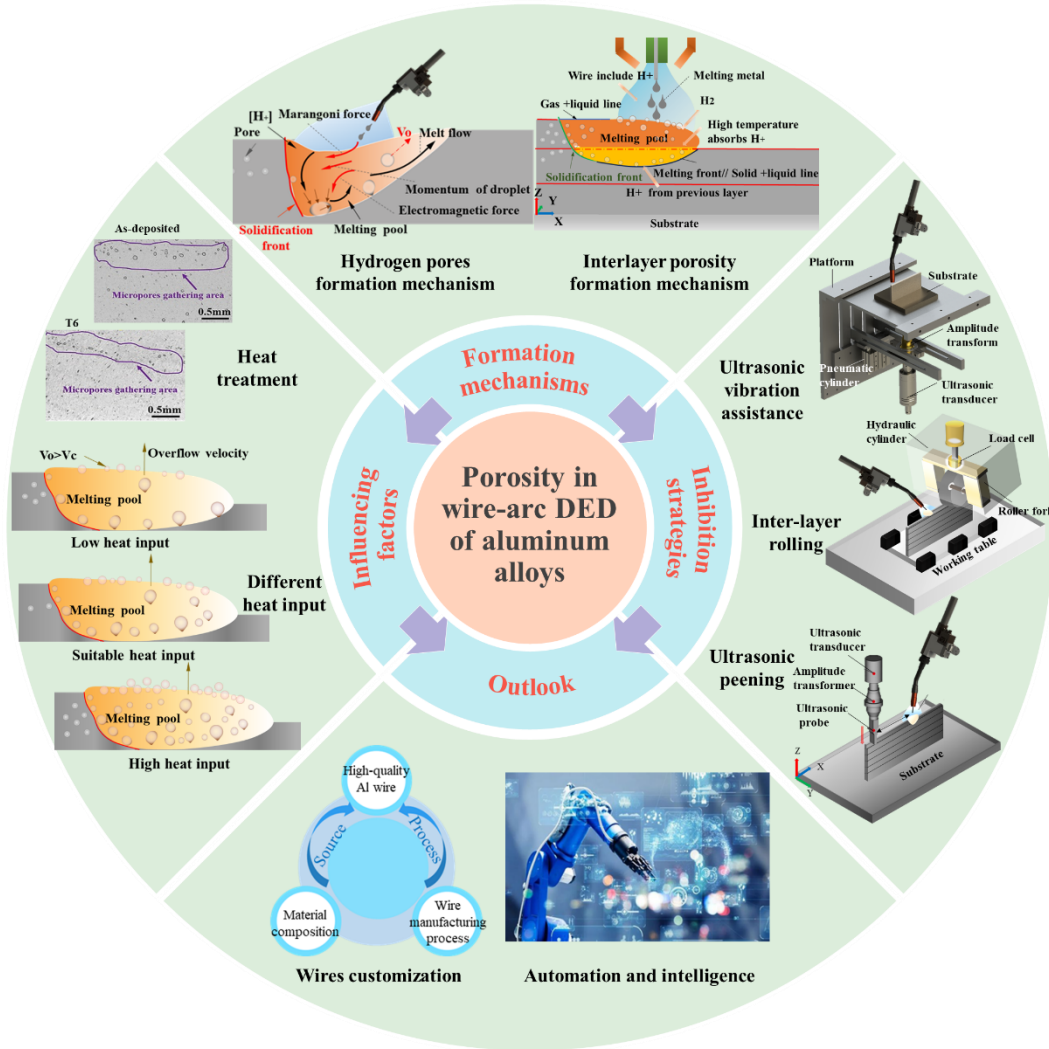
**Corresponding author. Email: hjcao@cqu.edu.cn (H. Cao)

Abstract

Wire-arc directed energy deposition (DED) offers advantages such as high forming efficiency and the ability to create parts without potential constraints on size. It possesses unique advantages in the high-efficiency production of large or ultra-large alloy metal components, for example aluminum. However, the issue of porosity in wire-arc DED aluminum alloys has been a subject of widespread discussion. Porosity defects can induce stress concentration and site for crack formation and propagation. This deterioration results in diminished tensile strength and fatigue resistance, limiting the potential applications of wire-arc DED in aluminum alloy builds. To this end, for the first time, this review offers a thorough examination of prevalent porosity imperfections in wire-arc DED aluminum alloys, including gas pores, shrinkage cavities and porosity arising from the volatilization of elements. Particular emphasis is placed on elucidating the formation mechanisms and spatial distribution of hydrogen pores, which constitute the primary pore defects in wire-arc DED aluminum alloys. Moreover, the research scrutinizes the influence of various wire-arc DED techniques, arc modes, process parameters, and shielding gas environments on porosity formation. The inhibition strategies of porosity defects in wire-arc DED aluminum alloys, including laser-arc hybrid additive manufacturing, ultrasonic vibration assistance, external magnetic field, inter-layer rolling, inter-layer friction stir processing, ultrasonic peening treatment, laser shock peening, and hot isostatic pressing, are further summarized. Ultimately, this work anticipates the future trajectory of wire-arc DED aluminum alloys, offering valuable guidance for the fabrication of high-quality

wire-arc DED aluminum alloy intricate components.

Keywords: Wire-arc directed energy deposition; Aluminum alloys; Porosity; Formation mechanisms; Influencing factors; Inhibition strategies.



Graphical Abstract

Table of Contents

1. Introduction	5
2. Wire-arc directed energy deposition	8
3. Porosity formation mechanism	9
3.1. Hydrogen pores.....	10
3.2. Shielding gas pores	20
3.3. Shrinkage cavity.....	20
3.4. Element volatilization porosity	21
4. Porosity influencing factors	22
4.1. Heat input.....	23
4.1.1 Current and travel speed	23
4.1.2 Wire feed speed.....	25
4.1.3 Wire-arc DED methods.....	26
4.1.4 Arc mode.....	26
4.2. Shielding gas environment.....	33
4.3. Heat treatment.....	36
4.4. Other influencing factors	40
5. Porosity inhibiting strategies	42
5.1. Multi-energy sources.....	43
5.1.1. Laser-arc hybrid additive manufacturing	43
5.1.2. Ultrasonic vibration assistance.....	47
5.1.3. External magnetic field	50
5.2. Post-processing	53
5.2.1. Inter-layer rolling	53

5.2.2. Inter-layer friction stir processing.....	58
5.2.3. Ultrasonic peening treatment	61
5.2.4. Laser shock peening.....	64
5.2.5. Hot isostatic pressing	67
6. Conclusions and outlook.....	69
6.1. Conclusions.....	69
6.2. Outlook	70
Acknowledgements	73
References.....	73

1. Introduction

Aluminum alloys are extensively utilized in diverse industries, including aerospace, automotive, and shipbuilding, owing to their remarkable blend of high specific strength, exceptional corrosion and heat resistance, excellent electrical conductivity, and lightweight properties [1, 2]. In recent years, the manufacturing of structural components made from aluminum alloys has witnessed progressive advancements in terms of intricacy, precision, and scale. Additive manufacturing (AM) has demonstrated as a pivotal technology in enhancing the production efficacy of high-quality aluminum alloys [3, 4]. Its intrinsic capacity to surmount erstwhile perceived limitations in mass production has rendered it particularly advantageous. Noteworthy advantages include the fabrication of intricate geometries, facile customization of structures, and substantial weight reduction while simultaneously preserving strength and structural integrity. The past decade has witnessed a discernible surge in the attention devoted to additive manufacturing of aluminum alloys. Wire-arc directed energy deposition (wire-arc DED) stands out as a noteworthy subset within the realm of AM, offering an array of advantages. These advantages encompass cost-effective equipment, high production rates, the versatility to work with a variety of materials, and the capacity to fabricate large-sized components without encountering dimensional constraints [5-7].

However, the substantial size of melt pool in wire-arc DED, coupled with the specific material properties (e.g., hydrogen solubility) of aluminum alloys, boosting the formation of porosity defects in wire-arc DED fabricated aluminum alloy components [6, 8]. Consequently, the application of this technology is severely constrained. When fabricating aluminum alloy, porosity defects are more prone to occur due to contamination of the wire surface in compared to that of other metallic materials, such as titanium and stainless steel [9, 10]. During the cooling and solidification process, the hydrogen solubility in aluminum alloys experiences a drastic reduction, approximately by a factor of 20, resulting in the formation of numerous hydrogen pores [9, 11]. Moreover, the higher thermal conductivity of aluminum alloys in comparison to that of other metallic materials, such as steel and titanium alloys, results in reduced opportunities for bubbles to escape, thereby facilitating the formation of pores [6]. Research has demonstrated that the existence of porosity has a substantial negative impact on the fatigue life of a material [12]. Furthermore, fatigue properties are primarily affected by the surface or sub-surface porosity, especially large-size porosity [13, 14]. When

subjected to internal and external stresses, pores may propagate and expand, initiating cracks, which, in turn, lead to a significant reduction in fatigue strength under dynamic loading conditions [15]. Additionally, a high number of microporous defects in the matrix can cause a decrease in the microhardness of the alloy [16]. Xie et al. [17] have identified that the occurrence of cracks in the material can be attributed to defects, including pores and lack of fusion. Pores serve as preferred points for crack initiation and can significantly diminish the mechanical properties of the specimen [18]. This effect is particularly pronounced when the diameter of the pore exceeds 50 μm [19, 20]. The presence of a porous zone within the material restricts the effective bearing area of the built part and induces stress concentration. This heightened stress concentration can trigger the formation of microcracks inside the material, potentially leading to fracture [21]. According to Zhang et al. [22], the presence of pores in wire-arc DED components can lead to an uneven distribution of microhardness within each layer, potentially causing abrupt variations in hardness at specific locations. Fang et al. [23] identified that pores also represent the primary factor contributing to differences in mechanical properties between specimens oriented in parallel and perpendicular directions. As depicted in Fig. 1, porosity serves as a pivotal process parameter for evaluating the performance of wire-arc DED aluminum alloy components, garnering extensive attention in the manufacturing of components [8, 9, 24].

Currently, porosity can be effectively controlled in wire-arc DED aluminum alloys by adjusting heat input [25-27], shielding gas environment [28-30], and the implementation of composite fabrication processes such as laser-arc hybrid additive manufacturing [31-33], ultrasonic vibration assistance [34-36], external magnetic field [37, 38], inter-layer rolling [16, 17, 39], inter-layer friction stir processing [18, 40, 41], ultrasonic peening treatment [42, 43], laser shock peening [44, 45], and hot isostatic pressing [46, 47]. For instance, Williams et al. [48] achieved reduced porosity in 2319Al alloy specimens by adjusting travel speed and wire feed rates. Sun et al. [49] explored the impact of air and argon environments on porosity while maintaining appropriately controlled heat input conditions, and found that argon environments significantly diminished internal porosity defects. Ding et al. [48] significantly decrease porosity in 2319Al alloy through the use of the cold metal transfer-incorporated pulse and polarity (CMT-PADV) process. Cong et al. [50] employed ultrasonic frequency pulsed variable polarity TIG to successfully mitigate porosity in wire-arc DED of 2024 Al alloy. This approach not only reduced porosity but also improved microhardness and

homogeneity. Zhang et al. [51] utilized laser-assisted MIG to fabricate 5356 Al alloy. Their findings revealed that the addition of the laser resulted in a reduction in the number of hydrogen porosities and led to a finer and more homogeneous microstructure, thereby enhancing tensile strength. Through the application of workpiece vibration, Gao et al. [52] achieved a 22.5% reduction in the average grain size compared to that of non-vibrated samples. Additionally, the tensile fracture porosity decreased from 6.66% to 1.52% due to the vigorous swirling of the melt pool caused by the workpiece vibration. Gu et al. [53] employed inter-layer rolling to reduce micropores in the deposition process of 2319 and 5087 alloys. He et al. [18] demonstrated that the introduction of interlayer friction stir processing (FSP) effectively eliminated pores. This treatment significantly damaged both α -Al dendritic and Si-rich eutectic networks, resulting in improved plasticity and fatigue properties when compared to the conventional wire-arc DED process for Al-Si alloys.

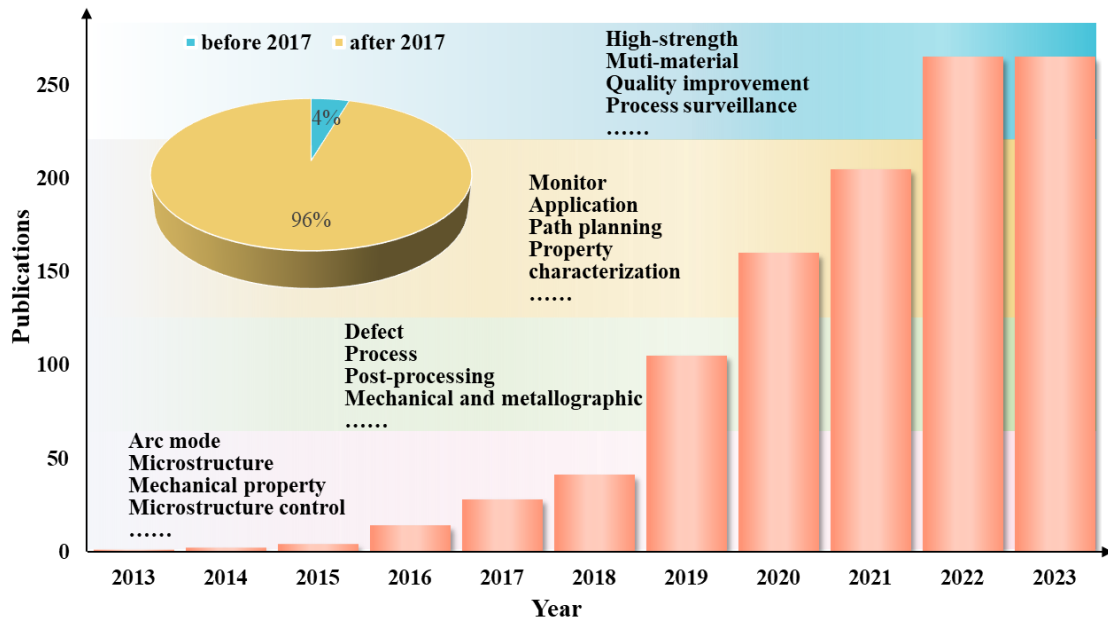


Fig. 1. Findings from the Science Citation Index on wire-arc DED aluminum alloy.

Nonetheless, a noticeable gap exists in the systematic review of porosity defects within wire-arc DED aluminum alloy. The existing literature lacks a comprehensive synthesis of the formation mechanisms, influencing factors, and strategies for mitigating porosity. This paper aims to bridge this gap by offering an in-depth examination of common porosity defects encountered in wire-arc DED aluminum alloy. It places particular emphasis on elucidating the formation mechanism and distribution patterns of hydrogen pores. Furthermore, it conducts a comprehensive review of the impacts of different wire-arc DED methods, arc modes, process parameters, and shielding gas environments on the occurrence of porosity. Moreover, this paper provides a concise summary of

strategies to suppress porosity defects in wire-arc DED aluminum alloy. Finally, it outlines potential future development trends for wire-arc DED aluminum alloy, offering valuable insights for the preparation of high-quality complex components from wire-arc DED aluminum alloy.

2. Wire-arc directed energy deposition

Wire-arc DED utilizes an electric arc as a heat source to melt metal wire, with the welding torch or substrate following a predetermined path. Upon completing the deposition of one layer, the process continues in the next weld path, repeating until the entire three-dimensional structure of the specimen is formed [1, 4, 54]. The wire-arc DED technology offers a host of benefits, including high productivity, cost-effectiveness in equipment, a more open production environment, and the absence of size limitations for structural parts. Furthermore, wire-arc DED can accommodate a wide range of materials, is unaffected by material reflectivity, and exhibits notably higher energy and stacking efficiency under certain conditions compared to high-energy beam processes. These characteristics render it exceptionally suitable to produce large-scale integrated structural components [4, 6, 8]. Wire-arc DED technology is typically categorized into three main variants: gas tungsten arc welding (GTAW), plasma arc welding (PAW), and gas metal arc welding (GMAW) [8]. To address the potential for surface defects resulting from the high heat input of the GMAW technology, the cold metal transfer (CMT) process was developed as an extension of this technology. CMT technology offers the advantages of low heat input, a stable welding process, minimal spatter, and high-quality weld seams [10]. Fig. 2 depicts their technical schematics.

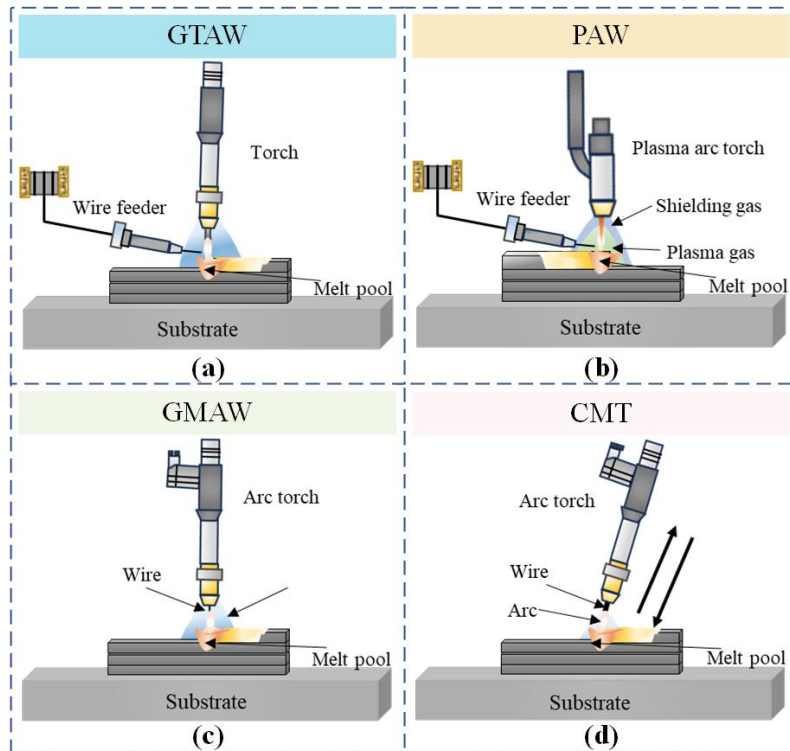


Fig. 2. Schematic illustration of various wire-arc DED technologies: (a) GTAW. (b) PAW. (c) GMAW. (d) CMT.

3. Porosity formation mechanism

Porosity is a common defect in wire-arc DED aluminum alloy [1, 4, 48]. Fig. 3 illustrates the classification of porosity based on its formation, which includes hydrogen pores, shielding gas pores, shrinkage cavities and porosity resulting from the volatilization of elements [9]. Shielding gas pores stems from the mixing of shielding gases into the melt pool, such as argon and nitrogen. The first two types of pores typically exhibit a more regular shape with sphericity close to one. In contrast, shrinkage cavities tend to display irregular and twisted shapes with sharp curvatures and crack-like features, potentially leading to higher stress concentrations [6, 9, 10]. When compared to pores, shrinkage cavities are potentially more detrimental due to their irregular morphology, often resulting from improper process parameters, suboptimal path planning, as well as unstable deposition process [17].

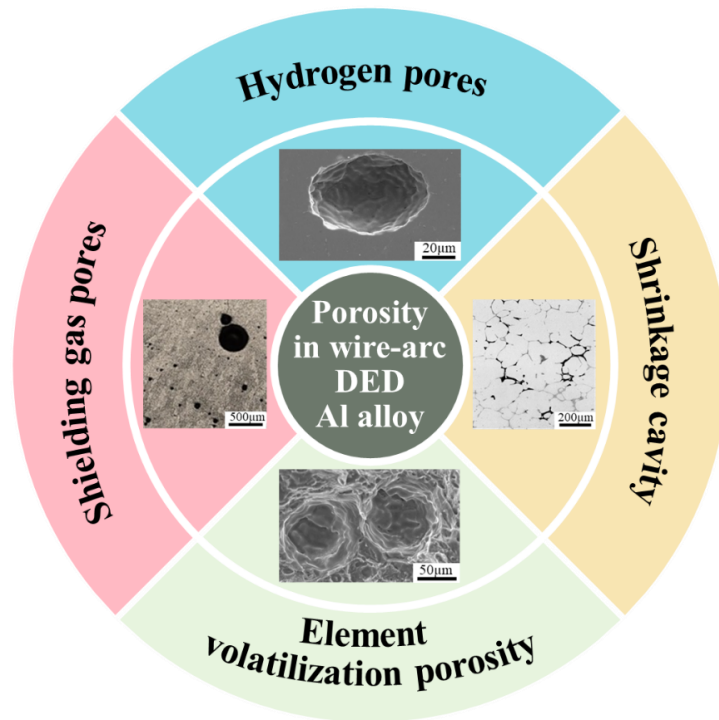


Fig. 3. Porosity in wire-arc DED aluminum alloys [55-57].

3.1. Hydrogen pores

Hydrogen pore formation is the primary driver of porosity defects in wire-arc DED aluminum alloy [27, 48]. This section delves into the mechanism of hydrogen pore formation during wire-arc DED aluminum alloy processes. The presence of hydrogen is a fundamental prerequisite for the creation of hydrogen porosity [2, 5, 6]. Hydrogen in wire-arc DED Aluminum alloys primarily originates from three sources, including the metal wires, substrates, and water vapor in the ambient air [6, 8]. The internal hydrogen content is generated during the primary metal casting process [4]. The main contributors to increased hydrogen content are abrasive materials, grease, or other hydrocarbons present on the surface of the formed wires [4, 58]. As depicted in Fig. 4(a)-4(b), variations in the surface roughness of the wire material influence the hydrogen content in the melt pool and the shape of the arc. Wires with inferior surface quality tend to trap grit and moisture more readily [59]. When the wires are melted by the arc, they release free hydrogen, leading to an increased porosity rate in the wire-arc DED aluminum alloy builds [60].

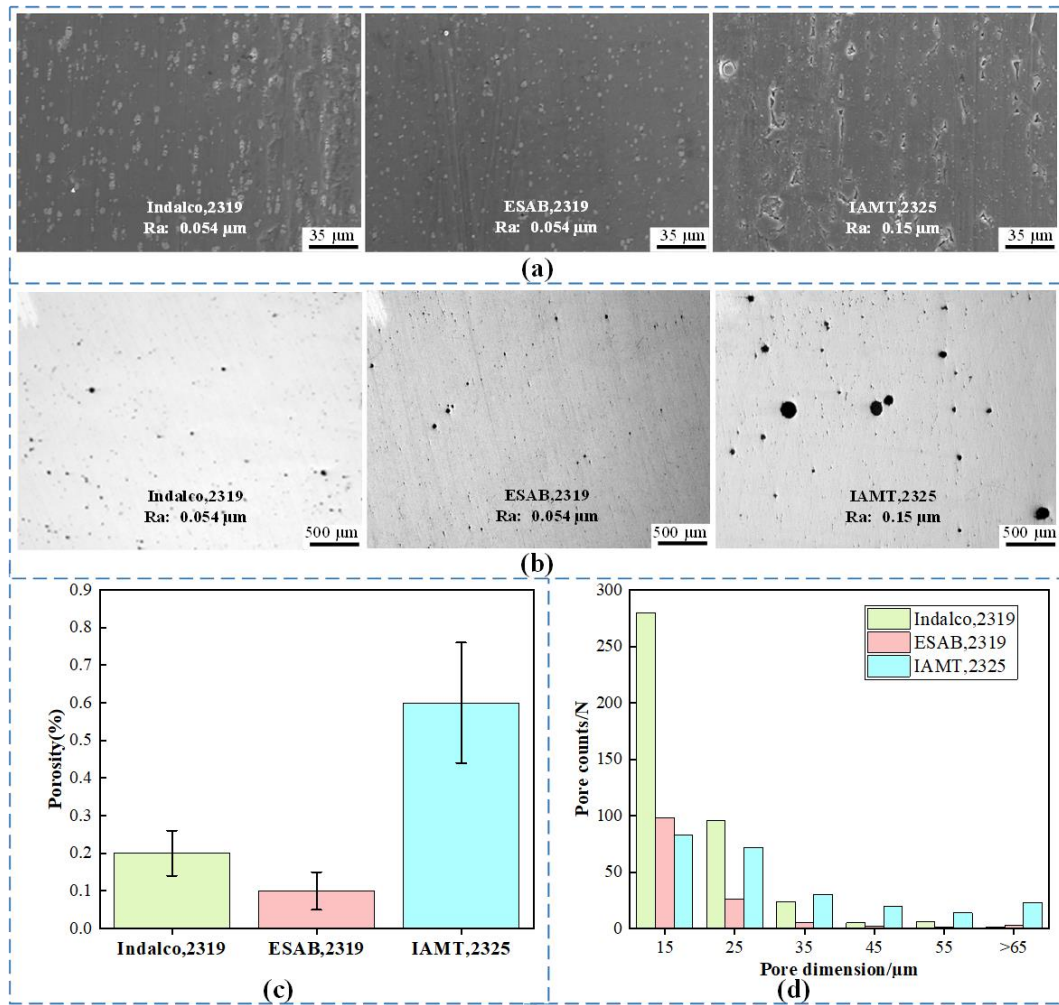
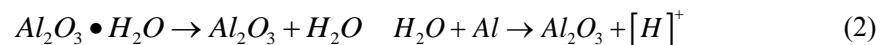
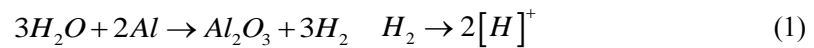


Fig. 4. Findings from the literature of the effect of wire surface roughness over hydrogen gas pores. (a) SEM image of wire surface. (b) Metallography of wire-arc DED samples. (c) Porosity of the wire-arc DED samples. (d) Statistic results of pore dimension and counts of wire-arc DED samples [59].

Aluminum wire has a tendency to adsorb moisture on its surface during storage [58]. Additionally, aluminum readily reacts with oxygen and ambient humidity, even at room temperature. When aluminum comes into contact with oxygen, it forms a thin layer of aluminum oxide (Al_2O_3). This oxide layer further undergoes hydration when exposed to atmospheric humidity, resulting in the formation of amorphous aluminum oxide hydroxide ($Al_2O_3 \cdot 3H_2O$) [48, 61]. Although the alumina film on pure aluminum is typically dense and does not readily absorb water in dry environments, the mechanical properties of pure aluminum are often insufficient for industrial applications. Instead, aluminum alloys are extensively used in various industry sectors. Among the most common are Al-Mg alloys, in which magnesium (Mg) has a strong affinity for oxygen,

resulting in the formation of an oxide film that is a mixture of Al_2O_3 and MgO . This oxide film is loose, porous, and easily absorbs water [4, 8]. While the source of hydrogen from the aqueous oxide layer can be eliminated through processes like heat treatment [4], the presence of other alloying elements can indeed influence the solubility of hydrogen in the aluminum solution [25]. For instance, magnesium and its associated phases exhibit a strong capacity for hydrogen absorption, with hydrogen solubility in molten magnesium reaching as high as 60 ml/100 g at approximately 630°C. This solubility is 92.5 times greater than the solubility of hydrogen in aluminum [9, 61]. Furthermore, while the arc deposition process establishes a shielding gas environment, it is not entirely pure. The high-temperature process tends to absorb moisture simultaneously, which also contributes to the increased hydrogen content during the wire-arc DED process [48].

Fig. 5 illustrates that the formation of hydrogen bubbles during the process involves four additional stages: nucleation, growth, detachment from the melt pool wall, upwelling and overflow [62]. These stages collectively determine the residual pore content in the sample and consequently impact the properties of the specimen. In the wire-arc DED aluminum alloy, hydrogen-containing substances will decompose under high-temperature conditions to produce atomic hydrogen [48, 55, 60], as described in Equations (1) and (2). When the local hydrogen content exceeds the maximum solubility in the aluminum liquid, the liquid metal becomes supersaturated with gases, leading to the nucleation and growth of hydrogen pores [63]. It should be noted the solubility of hydrogen in the liquid and solid phases of Al alloys differs significantly, with a factor of nearly 20 (0.69 ml/100 g in the liquid phase and 0.036 ml/100 g in the solid phase) [57, 64, 65]. This means that if the hydrogen content in the melt exceeds the solubility of hydrogen in the solid phase, hydrogen becomes concentrated at the solidification front.



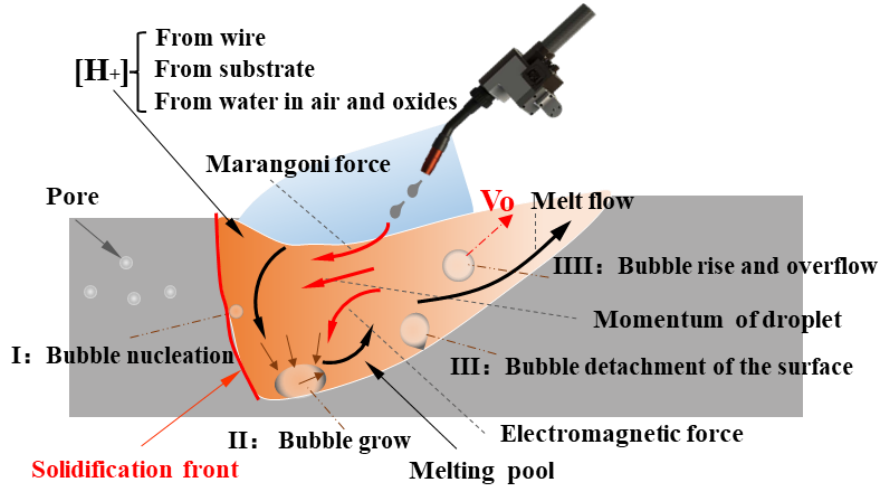


Fig. 5. Four stages of forming hydrogen pores.

Bubbles tend to grow after nucleation that adhere Equation (3) [62], where bubble growth occurs when the pressure inside the bubble surpasses the sum of the additional pressure components: atmospheric pressure and surface tension. In Equation (3), P_h represents the internal pressure of the pore, $\delta_{2,g}$ denotes the surface tension between the pore and the liquid metal, and r signifies the radius of curvature of the pore.

$$P_h > 1 + \frac{2\delta_{2,g}}{r} \quad (3)$$

During the wire-arc DED process, the alteration in surface tension between the gas and the liquid is considered insignificant [63]. By modifying the process parameters and implementing other measures to enhance the arc pressure, the melt pressure increases uniformly to maintain force equilibrium. Consequently, the bubble is extruded and distorted by the liquid pressure, resulting in an ellipsoidal shape with an increase in radius of curvature and a corresponding reduction in additional pressure. Another approach is to elevate the gas pressure within the bubble, a condition that is known to increase with temperature [66]. This facilitates the necessary circumstances for pore growth.

The ability of the bubble to detach from the wall of the melt pool is governed by the surface tension between the liquid metal, the gas phase, and the wall of the melt pool. This process is characterized by the wetting angle (θ), which is a critical parameter shown in Equation (4). When the wetting angle is relatively large (typically $>90^\circ$), bubbles tend to remain attached to the wall even after detaching. Due to the short heating and cooling times involved in the wire-arc DED process, it is less likely for the residual bubbles to escape once attached. Conversely, when the

wetting angle is small (typically $<90^\circ$), the bubble detaches from the wall, and no residual bubbles remain. In such cases, the susceptibility of the deposited parts to pore formation is significantly reduced [62].

$$\cos \theta = \frac{\delta_{1,g} - \delta_{1,2}}{\delta_{2,g}} \quad (4)$$

In the provided context, $\delta_{2,g}$ represents the surface tension between the pore and the liquid metal, $\delta_{1,g}$ denotes the surface tension between the solid and the gas, and $\delta_{1,2}$ denotes the surface tension between the liquid and the solid. It is known that surface tension is inversely related to temperature [66]. To influence these surface tensions, process parameters and other measures that affected the process temperature can be adjusted to decrease $\delta_{2,g}$ and $\delta_{1,2}$. Reducing these values results in a larger radius of curvature, which increases the contact area between the pore and the detached surface. This larger contact area leads to an increase in $\delta_{1,g}$.

The ability of bubbles to escape from the molten metal is determined by the difference between the cooling rate of the melt pool (V_c) and the bubble spillage rate (V_o) [27]. If $V_c > V_o$, there may not be sufficient time for the bubbles to overflow and form a pore. Conversely, if $V_o > V_c$, a single-pass multilayer member without pore may be obtained [63]. The cooling rate of the melt pool V_c in aluminum processing, which is also known as the crystallization rate of the aluminum alloy, can be controlled by adjusting the process parameters [9, 60]. The bubble spillage rate (V_o) is primarily influenced by factors such as the radius of curvature of the bubble (r), the liquid density (ρ_1), the density of the bubble (ρ_2), and the viscosity of the liquid (η), as outlined in Equation (5) [67].

$$V_o = \frac{2(\rho_1 - \rho_2)gr^2}{9\eta} \quad (5)$$

The viscosity of a liquid is primarily influenced by its temperature, with higher temperatures resulting in lower viscosity [9]. At elevated temperatures, the cooling rate of the melt pool (V_c) decreases, the viscosity of the metallic liquid decreases, and the radius of curvature of the bubbles increases. Consequently, there is a faster rate of bubble overflow and a reduced propensity for pore formation in the process. It is important to mention that while an increase in temperature facilitates

a higher rate of bubble overflow, simply elevating the melt pool temperature to reduce porosity is not a desirable approach [49, 61]. This aspect will be explored in more detail in Section 4.1.

Porosity in wire-arc DED aluminum alloys is distributed throughout the deposited specimen, but is usually most prominent in its interlayer region, as depicted in Fig. 6(b) [65, 68]. In the interlayer region, the number of hydrogen pores is greater, and their dimensions are larger. As seen in Fig. 6(a), hydrogen pores tend to distribute at the interlayers. In each X_{i+1} layer deposition, the top surface of X_i is the preferred location for pore formation due to reduced energy requirements for bubble nucleation [63]. Consequently, pores are most likely to be generated at the semi-molten interface between adjacent layers. One significant factor is that the pores generated in the interlayer are less likely to escape [67]. This is because of the "solid-liquid" phase transition between X_{i+1} and X_i layers, which results in a faster cooling rate in this region compared to other parts of the melt pool. As a result, the hydrogen bubbles generated here have difficulty escaping in a timely manner, leading to pore defects in this area. Meanwhile, the surface of each layer is susceptible to accumulating more hydrogen pores [27, 69]. For instance, in the case of X_{i+1} layer deposited, the surface of X_{i+1} belongs to the "gas-liquid" junction, where the cooling rate of the melt pool is higher. Many bubbles generated between the X_{i+1} layer and the X_i layer cannot overflow in time due to limited upward mobility. Consequently, they persist on the surface of X_{i+1} and evolve into pore defects [65]. Simultaneously, the rapid solidification of the X_{i+1} layer surface makes it prone to reacting with oxygen in the air, forming a dense oxide film. This oxide film further hinders the escape of hydrogen bubbles [2, 10]. Furthermore, during X_{i+2} layer deposition, the porosity trapped on the surface of the X_{i+1} layer can act as a non-uniform phase nucleation site. Simultaneously, the oxides present on the surface of the X_{i+1} layer, when they enter the melt pool, contribute to the formation of new pores in the region between the X_{i+2} layer and the X_{i+1} layer. Additionally, there are two distinct mechanisms that charging for the growth of micropores, one is Ostwald maturation and the other is migration and aggregation [70]. Remelting of the X_i layer occurs during X_{i+1} layer deposited. The X_i layer surface retains numerous tiny hydrogen pores that do not have sufficient time to overflow. Some of these pores may be in close proximity to each other and, due to their higher density, they can recolonize and grow to form larger bubbles that continue to rise [70]. Nevertheless, due to the limited heat input and the capacity for bubble rising, some of the larger bubbles fails to escape and become trapped on the surface of the X_{i+1} layer, leading to the

formation of larger pores [9, 48]. When depositing the X_{i+2} layer, the same process repeats, and the X_{i+1} layer is equivalent to the X_i layer in this regard. This repetition of processes leads to the characteristic distribution of hydrogen pores in the interlayer. Additionally, more pores are formed between the first wire and the substrate [39]. This is attributed to the fact that the substrate contains a higher concentration of elemental hydrogen. When the first layer is formed, the melt pool becomes richer in elemental hydrogen, resulting in the nucleation of more hydrogen bubbles.

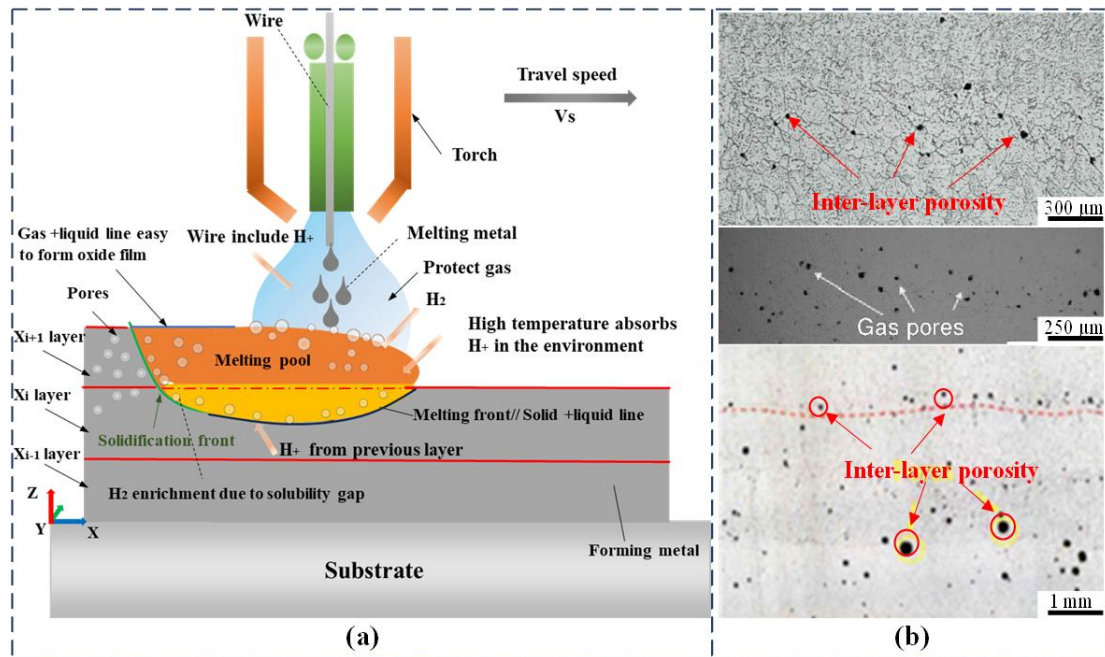


Fig. 6. (a) Schematic diagram of interlayer porosity formation. The interlayer region corresponds to the junction of layer X_i and layer X_{i-1} , as well as layer X_i and layer X_{i+1} . (b) Inter-layer porosity of as-deposited wire-arc DED aluminum alloy [61].

The characteristics of the interlayer distribution of hydrogen pores are the primary reason for differences in the mechanical properties of specimens in the vertical and horizontal directions [23, 67, 71, 72]. Table 1 provides an overview of the literature that discussing the differences in mechanical properties caused by porosity. Table 1 also demonstrates that the mechanical properties in the horizontal direction are generally higher than those in the vertical direction. The impact of porosity on tensile properties is attributed to the reduction of the loaded area [17, 18, 69]. As depicted in Fig. 7, pores in the horizontal direction exhibit minimal deformation during stretching and maintain a round shape. However, the specimens tend to crack, and the fracture crack typically extends through the pore. The necking of the pore near the fracture crack further triggers crack initiation. Conversely, pores in the vertical direction undergo significant deformation during tensile

stress, exhibiting an irregular shape. The propagation of cracks along the deformed pores is exacerbated compared to the horizontal direction, owing to the deformation pores. The primary fracture modes consist of through-crystal cracking and along-crystal cracking [73]. This discrepancy is due to the alignment of the tensile direction in horizontal specimens with the direction of porosity distribution. In this case, the reduction in the loaded area is insignificant, and tearing phenomena do not occur. In vertical specimens, the stretching direction and the direction of porosity distribution are perpendicular, leading to a significant reduction in the loaded area. Consequently, cracks propagate along the surface of porosity distribution, resulting in diminished mechanical properties [69].

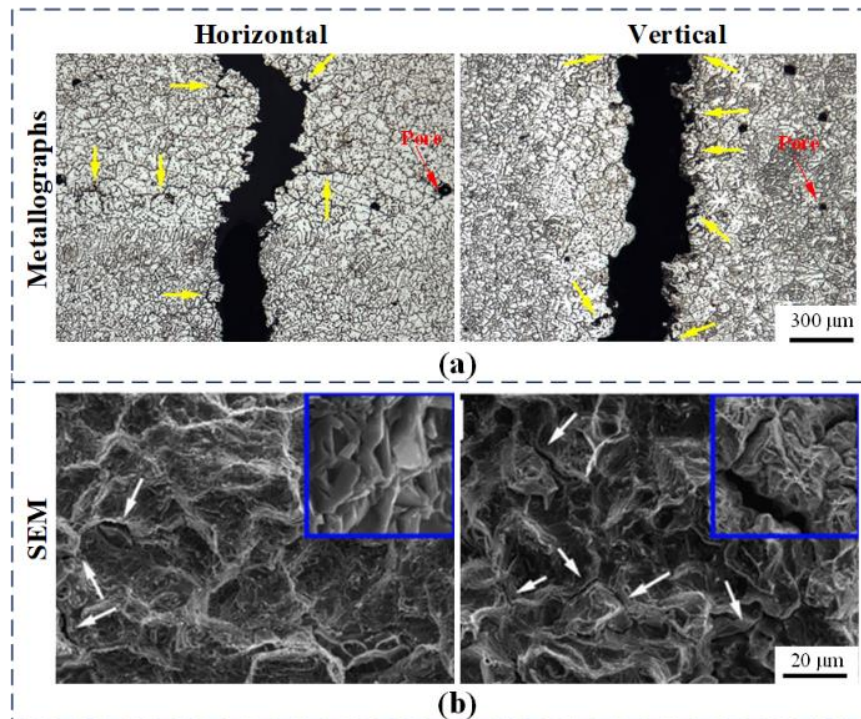


Fig. 7. (a) Metallographs of the fractured position of wire-arc DED alloys [74]. (b) SEM fractographic morphology for tensile samples of wire-arc DED alloys [74].

Table. 1. Differences in mechanical properties of specimens in vertical and horizontal reverse directions due to porosity

Al alloy	Process	Ultimate tensile strength (Mpa)	Yield strength (Mpa)	Elongation (%)	Ref.
2319 Al-6.3Cu	CMT (As deposited) (V)	258.4	106	13.3	[55]
	(H)	262.6	113	14.7	
	MIG-P (V)	277	175	5.6	
2024 Al-4.4Cu-1.5Mg	(H)	284	177	6.0	[50]
	+H-T (V)	375	294	4.3	
	(H)	458	310	12.7	
	MIG-UP (V)	290	186	6.0	
	(H)	299	189	6.6	
	+H-T (V)	437	281	10.4	
	(H)	471	302	14.0	
	CMT-P As deposited (V)	186	163	1.4	
	(H)	204	178	2.9	
	+rolled (V)	313	210	6.2	
2024	(H)	328	221	12.4	[75]
	rolled & HT (V)	444	290	9.8	
	(H)	468	301	20.6	
	CMT-PA (As deposited) (V)	267	186	2.4	
	(H)	324	204	7.7	
	+rolled (V)	280	273	0.5	
	(H)	394	308	7.3	
	+rolled & HT (V)	411	284	6.0	
	(H)	467	283	22.6	
	5356-O (As cast) (V)	130	285	/	
5356 Al-5Mg	(H)	83	172	/	[67]
	MIG (As deposited) (V)	257.5	/	/	
4043	(H)	262	/	/	[76]
	4043-O (As cast)	125	60	5.0	

Al-5Si	CMT (As deposited) (V)	177	/	20	
	(H)	164	/	17	
Al-7Si	CMT+T6 (V)	347	298	4.5	[77]
	(H)	332	293	4.4	
4047	CMT (As deposited) (V)	267.6	114.9	28.3	
Al-12Si	(H)	254.0	114.8	17.1	[78]
7075	CMT (As deposited) (V)	204	348	18.8	
Al-Zn-Cu	(H)	265.5	401.75	17.53	[79]

3.2. Shielding gas pores

Insufficient flow rate and inadequate purity of shielding gas can easily cause the surface fluctuation of the melt pool, leading to the formation of shielding gas pores. High arc temperatures can cause nitrogen (N_2) in the shielding gas environment to melt into the molten metal. As the melt pool undergoes solidification and the temperature decreases, the solubility of N_2 in the liquid metal diminishes, with a notable drop in solubility occurring during the crystallization process. If the N_2 is unable to escape in a timely manner, it often manifests as honeycomb-like pores on the surface of the deposited layer or in the form of diffuse micropores distributed within the deposited metal [35, 80]. It is important to note that pores formation due to shielding gas (argon, nitrogen) mixing into the melt pool is generally more pronounced and often found in the specimens with lower heat input, as depicted in Fig. 8.

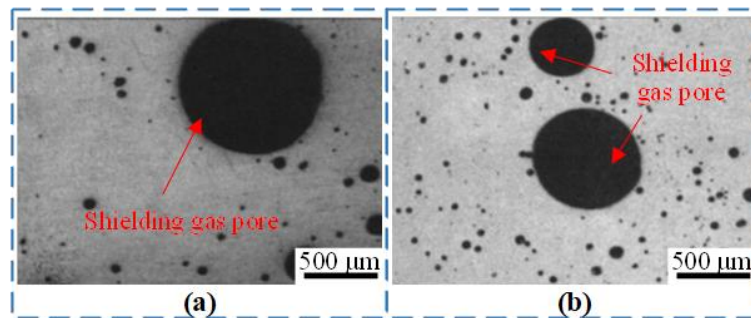


Fig. 8. Shielding gas pores [81]: (a) 100% Ar; (b) 50%Ar+50%He.

3.3. Shrinkage cavity

Solidification shrinkage cavities predominantly arise due to the volume differential between the solid and liquid phases of aluminum alloys during the solidification process [17]. As the melt pool undergoes the cooling process, the solid phase contracts at a higher rate than that of the liquid phase, owing to their different thermal contraction coefficients. When the liquid phase tends to solidify at the same rate as the solid phase, tensile stresses surpass the surface tension at the liquid-solid interface, resulting in the formation of cavities between the liquid and solid phases [82]. As depicted in Fig. 9, these cavities are typically situated in the vicinity of incipient phases, particularly α -Al dendrites [6]. As the number of dendrites increases and local solidification commences, the flow resistance of the liquid phase intensifies, which also leads to the formation of shrinkage pores [57]. Furthermore, the occurrence of shrinkage pores is also contingent upon factors such as backfilling and the temperature range during solidification of the aluminum alloy. Xie et al. [17]

observed in single-pass experiments that improper selection of process parameters may prevent the Al alloy from reaching its metallurgical bonding temperature during deposition. This can result in insufficient heat input during deposition, leading to fusion defects. Meanwhile, if the temperature of the melting pool is too low, the liquid metal cools rapidly, solidifies before it can completely fill the cavities, thereby generating solidification shrinkage cavities. In multi-channel experiments, continuous remelting and a low cooling rate can also contribute to the formation of inter-dendritic shrinkage cavities [39].

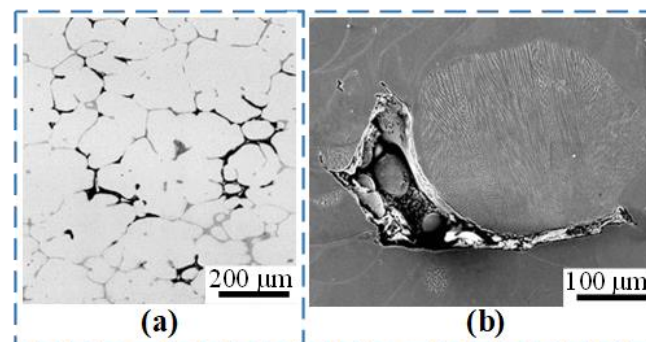


Fig. 9. (a) Shrinkage cavity. (b) Lack of fusion [56, 82].

3.4. Element volatilization porosity

The formation of pores due to the volatilization of alloying elements, such as Mg, Zn, and Li, represents another significant factor contributing to porosity in wire-arc DED Aluminum alloys [2, 8]. As depicted in Fig. 10, Li et al. [57] identified two distinct forms of porosity in the deposited material of Al-Zn-Mg alloys: porosity stemming from the presence of hydrogen and porosity resulting from the loss of Zn due to combustion. The loss of Zn content can reach as high as 44.7% with increasing heat input. Dong et al. [83] conducted a comparative analysis of the chemical composition of 7055 Al alloy and found an 11.8% loss in Zn content. This loss is attributed to the low boiling point of Zn, which results in its combustion during the wire-arc DED process. The vapors generated from these combustion losses do not entirely escape the melt pool, subsequently forming pores upon solidification [84]. In the case of Al alloy 5000, wire-arc DED can lead to Mg losses of up to 20%, with volatilization primarily dependent on heat input [4, 6, 27]. It is worth noting that the impact of elemental losses on mechanical properties has received more attention than the porosity formation associated with these losses [6].

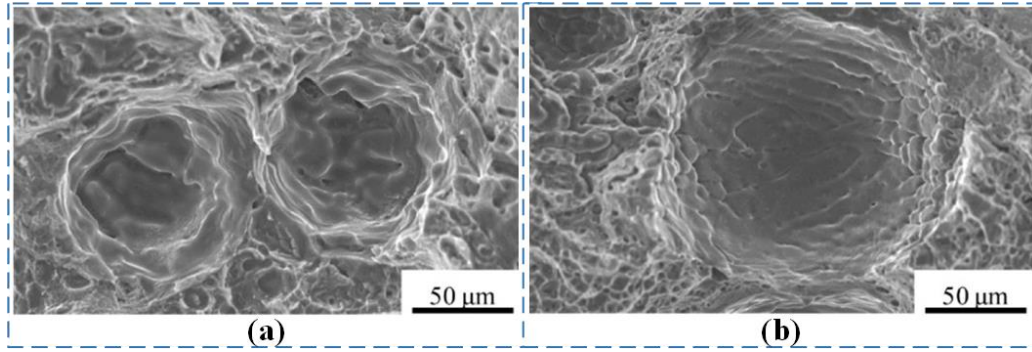


Fig. 10. Two distinct forms of porosity in Al-Zn-Mg alloys sample: (a) Zn volatilization porosity; (b) hydrogen pore [57].

4. Porosity influencing factors

The presence of porosity severely limits the application of wire-arc DED Aluminum alloys. As shown in Fig. 11, different wire-arc DED methods (GMAW, GTAW and PAW), arc modes (CMT, cold metal transfer–incorporated pulse (CMT-P), cold metal transfer–incorporated polarity (CMT-ADV), cold metal transfer-incorporated pulse and polarity (CMT-PADV), etc.), process parameters (welding current/voltage, wire feed speed and travel speed, etc.), and shielding gas environment all have an effect on the porosity of wire-arc DED Aluminum alloys. This section reviews the factors affecting porosity of wire-arc DED Aluminum alloy.

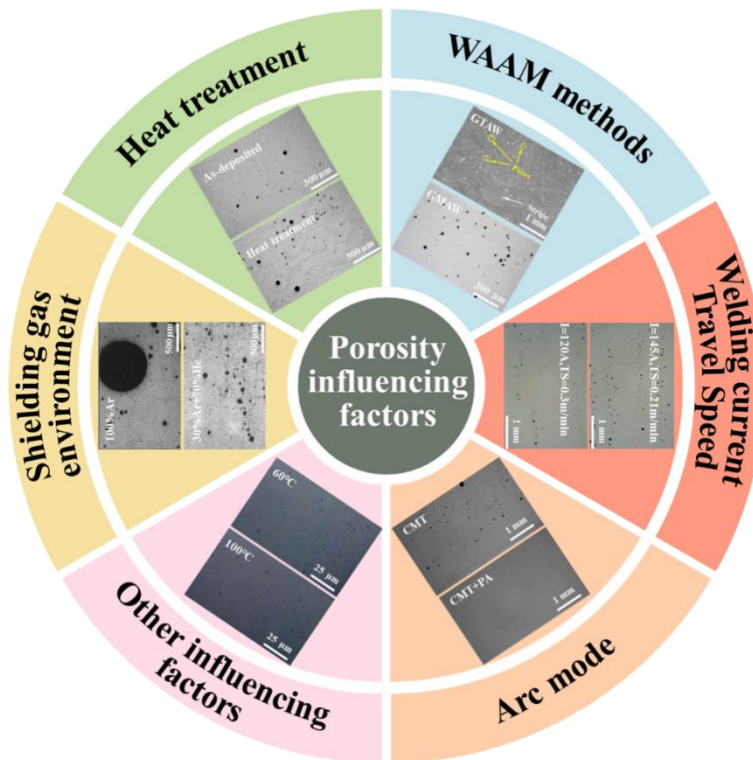


Fig. 11. Porosity influencing factors in wire-arc DED Aluminum alloys.

4.1. Heat input

The heat input in wire-arc DED aluminum alloys plays a pivotal role in determining the quality of the formed components and their resulting microstructure. Effective control over the number and size of pores within the specimens can be achieved by precisely managing the heat input [48]. Several researchers have substantiated that the porosity rate in the deposited components can be significantly influenced by manipulating the process parameters to alter the heat input. Equation (6) presents the formula for calculating the heat input in wire-arc DED [9, 55]:

$$HI = \eta \times \frac{UI}{TS} \quad (6)$$

Equation I - instantaneous current (A); U -instantaneous voltage (V); TS -travel speed (mm/s). η -thermal input efficiency coefficient, which is process-dependent. The η value is 0.9 for the CMT process and 0.8 for the GMAW process.

Based on the Equation (6), the heat input is directly correlated with the current, voltage, and travel speed. Fig. 12(d) demonstrates a distinct positive correlation between the pore volume fraction and the welding current [25, 27]. Additionally, as the travel speed escalates, there is a discernible decline in both the quantity and percentage of pores, as illustrated in Fig. 12(e) [27]. In the realm of wire-arc DED, it is worth noting that adjustments in wire feed speed (WFS) also have a direct impact on the heat input [48, 61, 85]. Consequently, these changes in heat input subsequently influence the level of porosity within the fabricated components [49].

4.1.1 Current and travel speed

In Fig. 12(a), Cong et al. [48] examined the porosity in 2319 aluminum alloy specimens at different travel speeds. **Their investigation revealed that excessive heat input results in a substantial rise of porosity flaws within the specimen.** Fig. 12(b) and (c) clearly demonstrate that excessive heat input results in a significant presence of pore defects in the interlayer region, accompanied by larger pore size and coarse grain size. Conversely, when the heat input is lower, both the quantity and size of pore defects decreased, and the grain structure exhibited refinement [86]. This phenomenon can be attributed to the competitive growth relationship between pores and grains [81, 87]. Hydrogen pores primarily undergo growth via processes involving heterogeneous nucleation, autonomous diffusion, or merging. The solidification interface of **cellular** or dendritic crystals, as well as certain inclusions, serve as heterogeneous nucleation sites for these pores. In the presence of equiaxial

dendrites within the material structure, they act to segregate and bifurcate pores, leading to a reduction in pore size [9]. A lower heat input is instrumental in grain refinement [49, 80] which, in turn, effectively hinders the diffusion of hydrogen within the liquid metal. This limitation on hydrogen diffusion curtails the nucleation and the growth of hydrogen pores [49]. Conversely, under conditions of high heat input, hydrogen atoms struggle to escape effectively from the melt pool, particularly within a coarsely columnar grain structure [14]. This phenomenon aligns well with the research conducted by Zhu [27] and Liu [25] on wire-arc DED Al-Mg alloys. Furthermore, Li et al. [57] have also reported similar observations for that of Al-Zn-Mg alloys.

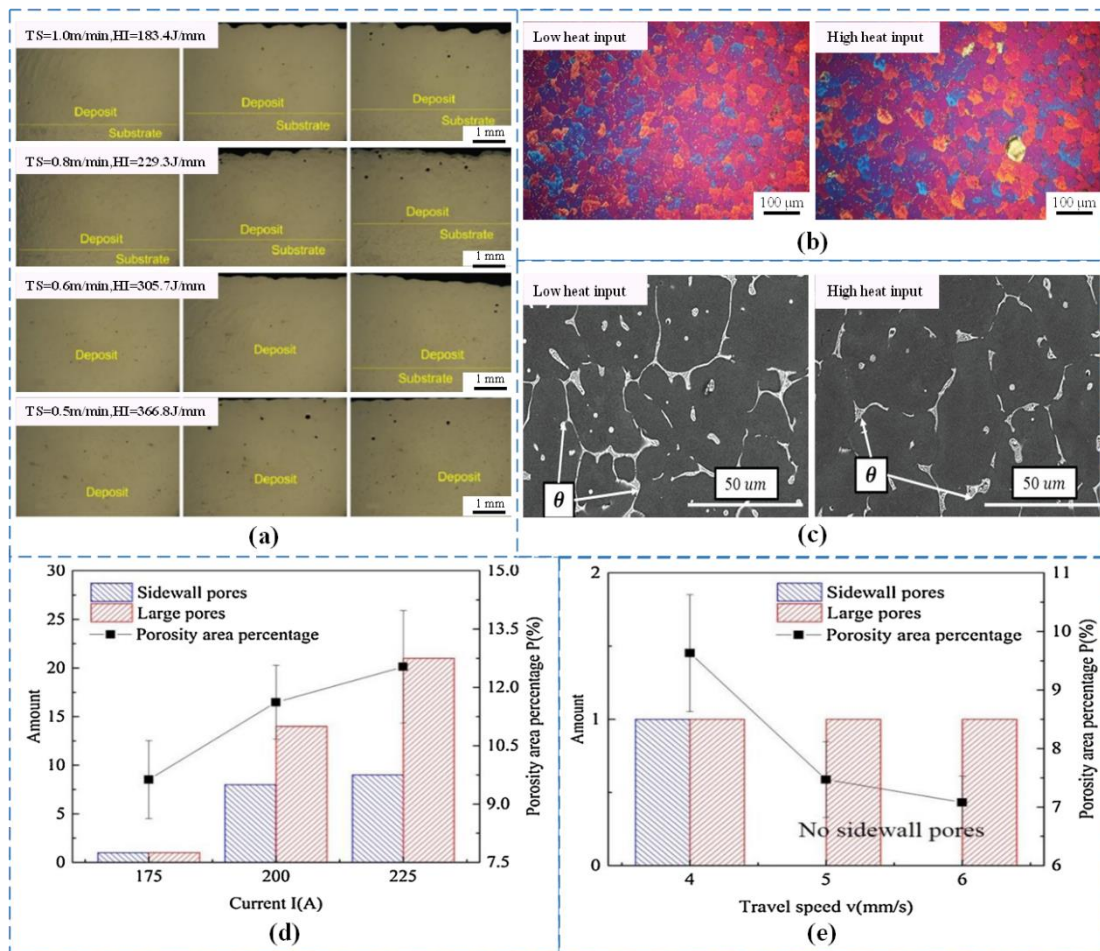


Fig. 12. (a) Al-Cu alloy porosity with CMT-P process over the left, middle, and right of the deposited samples [48]. (b) Samples with different heat input under polarized light optical microscope [86]. (c) 2319 aluminum alloy with different heat input [86]. Influence of parameters on 5083 pore amounts and porosity area percentage: (d) Influence of welding current; (e) Influence of travel speed [27].

An excessive or insufficient travel speed often leads to the formation of hydrogen pores in the deposited components [22]. When the travel speed is high, it leads to a low heat input and an

accelerated cooling rate of the melt pool. This accelerated cooling rate impedes the timely escape of gas bubbles within the melt pool, ultimately leading to the formation of internal pores upon solidification. Conversely, a low travel speed prolongs the arc's residence time in the high-temperature zone. This extended exposure to high temperatures has a dual effect: firstly, it elevates the melt pool temperature, reducing its surface tension, causing it to spread to the side, and potentially resulting in overflow after solidification. Secondly, the elevated melt pool temperature can lead to the volatilization of certain low-boiling-point metal elements within the melt pool, consequently increasing the porosity rate [83]. **Moreover, compared with the normal residence time, the prolonged residence time of the melt pool in the high-temperature region will aggravate the oxidation of aluminum alloy [83].**

As depicted in Fig. 13(a) and (b), the influence of heat input on porosity exhibits similar characteristics in both air and argon environments [49]. By adjusting welding current, travel speed, and wire feed speed to gradually reduce heat input, a discernible trend emerges: a decrease in both the number and diameter of pores within the specimens. However, further reduction in heat input results in a counterintuitive effect: the number of pores increases, while a smaller number of larger-sized pores appear. One issue is that the arc current is insufficient, leading to a deterioration in the cleaning effect of the oxide film on the surface of the aluminum alloy wire by AC arc. Additionally, the oxide film is not being cleaned and can act as a highly efficient nucleation plasma point, promoting the formation of pores [80, 81]. Secondly, a reduction in the current amplitude diminishes the stirring effect of the arc on the melt pool, which is not conducive to facilitating the escape of pores. With a significant reduction in heat input, the residence time of the liquid metal within the melt pool in the high-temperature region becomes too brief, resulting in a delay in both pore growth and escape after nucleation has occurred [80, 87].

4.1.2 Wire feed speed

As illustrated in Fig. 13(b) for wire-arc DED under an argon environment, it is evident that decreasing the wire feed speed can effectively diminish the occurrence of internal pore defects while keeping the heat input constant [49]. This phenomenon could be attributed to the thermal action and unavoidable arc disturbance during wire deposition [74]. Due to constraints associated with the smelting and preparation procedures of aluminum alloy wires, the wire surface often exhibits certain pits that are prone to impurity and moisture adsorption. Moreover, the wire material can contain a

substantial number of internal porosities. As the wire feed speed increases, the quantity of wire material being melted likewise escalates. If the arc cleaning effect on the wire surface is suboptimal, it can lead to a heightened presence of impurities, hydrogen, and oxides within the melt pool. Consequently, this results in a significant increase in the nucleation rate of hydrogen pores as well as an enlargement of pore size [61].

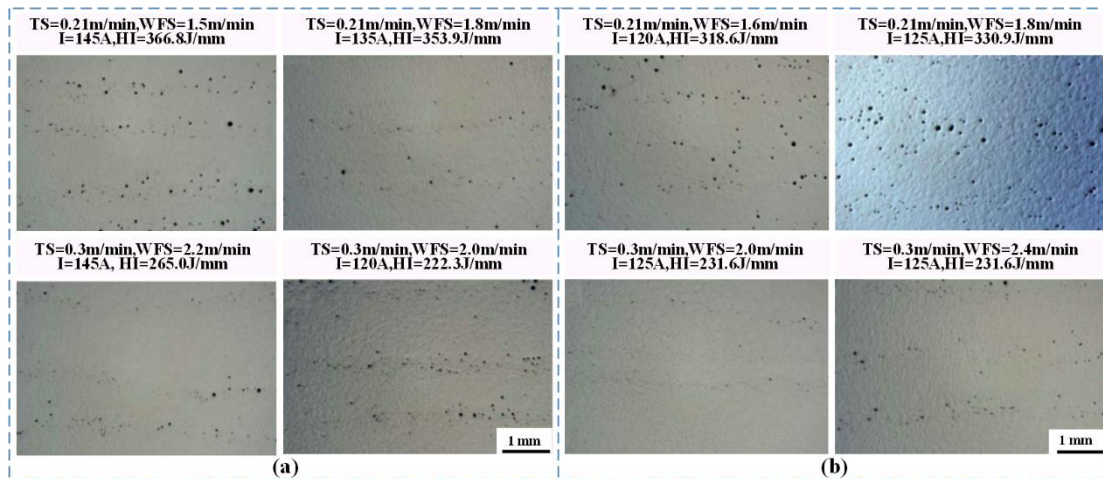


Fig. 13. Wire-arc DED of aluminum alloy under different shielding gases (a) Common air environment [49]. (b) Argon environment [49].

4.1.3 Wire-arc DED methods

Meanwhile, different process selections and arc modes also affect the porosity in specimen [48, 50]. In the contemporary landscape for wire-arc DED aluminum alloy fabrication, GTAW, GMAW and CMT represent the dominant processes. CMT technology has garnered significant attention in academia due to its inherent merits, characterized by low heat input, a stable welding process, negligible spatter and diminished porosity [9, 50]. Notably, the GTAW process excels in achieving a more stringent control over material and heat input when juxtaposed with the GMAW process, thereby yielding fewer pores in the deposited specimens [21, 33, 88].

4.1.4 Arc mode

In the context of 5356 aluminum alloy, Jiang [89] and Feng [67] conducted a comparative study between the GMAW and GMAW-Pulse (GMAW-P) processes. Through the modulation of additional pulses, the GMAW-P process can effectively mitigated porosity. As depicted in Fig. 14(a), when the additional pulse frequency was set at 0 Hz in the GMAW process, porosity levels reached their maximum values. This finding is attributed to the unique nature of the GMAW-P process, where in double pulses are employed. The strong pulse component facilitates the melting of

transition melt droplets from the wire material, while the low-frequency pulse contributes to the agitation of the melt pool. This dual effect not only accelerates the upward movement of hydrogen pores but also induces oscillations in the melt pool. Under identical operating conditions, the rate of metal crystallization can be somewhat diminished, hence decreasing the porosity of the specimen. Aldalur et al. [90] conducted an extensive study on the 5356 aluminum alloy employing three distinct modes: pulsed-GMAW, CMT, and pulsed-Alternating Current (pulsed-AC) mode. Their investigation revealed that the pulsed-AC mode proved exceptionally effective in porosity reduction. As depicted in Fig. 14(b) and (c), the porosity reduction achieved with the pulsed-AC mode exceeded that of the pulsed-GMAW mode by over sixfold and surpassed the pulsed-AC mode by a staggering tenfold. This remarkable performance can be attributed to the AC pulse mode's unique feature of alternating current signals with both positive and negative polarities. When the current signal is positive, the wire is heated in the direction of electron motion and subsequently fuses with the deposited material in the substrate, akin to other operational modes. However, when the current signal is negative, the polarity undergoes a reversal, causing the current to heat the previously welded beads. This process effectively removes the surface oxide film on the Al alloy's surface, where the removal allows the material to expel hydrogen that was previously trapped within the molten material, thus leading to a substantial reduction in porosity.

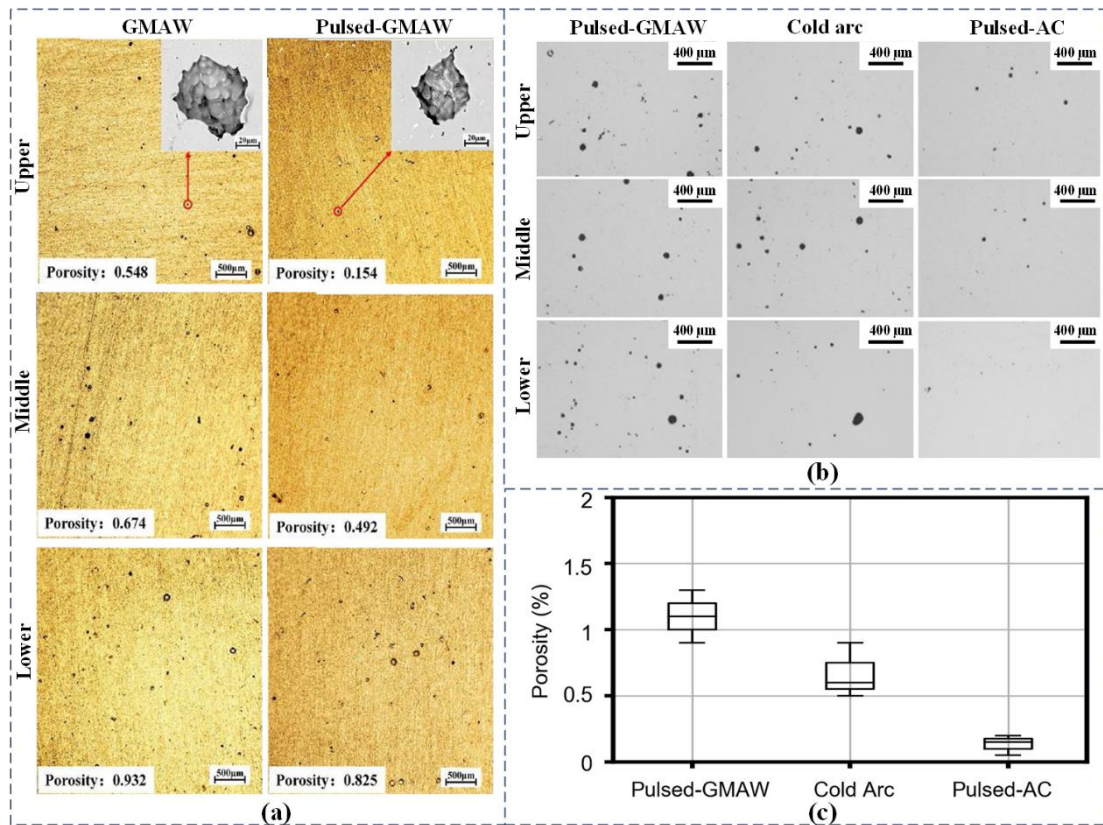


Fig. 14. (a) Distribution of pores of the two arc modes [89]. (b) Non-etching micrographs for porosity analysis [90]. (c) Average porosity values obtained with different working modes [90].

In the case of alloy 2024, utilizing the AC-GTAW technique, Yu et al. [91] observed that the sample densities exhibited a pattern of initially growing and then dropping as the pulse frequency increased, as illustrated in Fig. 15(c). Small pore is predominant in the low pulse frequency samples, while large pore is more frequent in the high pulse frequency samples, as in Fig. 15(a). A discernible correlation between pore size and pulse frequency is also observed. Fig. 15(b) reveals that within the samples processed with lower pulse frequencies, the proportion of small area pores is relatively higher, whereas in samples subjected to higher pulse frequencies, the number of large area pores is comparatively elevated. Cong et al [50]. introduced ultrasonic frequency pulses into conventional variable polarity TIG, leading to grain refinement, substantial reduction in porosity, and enhancement in microhardness and homogeneity of the treated specimens. This effect is highlighted in Fig. 16(a) and (d), which demonstrates that the **ultrasonic frequency pulsed variable polarity (UFPVP) arc mode**, when compared to the **conventional variable polarity (VP) arc mode**, can effectively reduce the occurrence of porosities in wire-arc DED components. **Since hydrogen exhibits lower solubility in solid aluminum alloys compared to liquid aluminum alloys,**

oversaturated hydrogen tends to form gas pores within the structure. Moreover, in contrast to conventional VP arc processes, the utilization of UFPVP arc deposition leads to an increase in liquid pressure within the melt pool. Consequently, the growth of gas pores is more pronounced, resulting in an increase in the radius of curvature. Furthermore, through the analysis of penetration angle and surface tension, it has been observed that gas bubbles are more readily detached during this process. The combination of a larger radius of curvature and low viscosity contributes to an enhanced bubble spillage rate, thereby reducing specimen porosity.

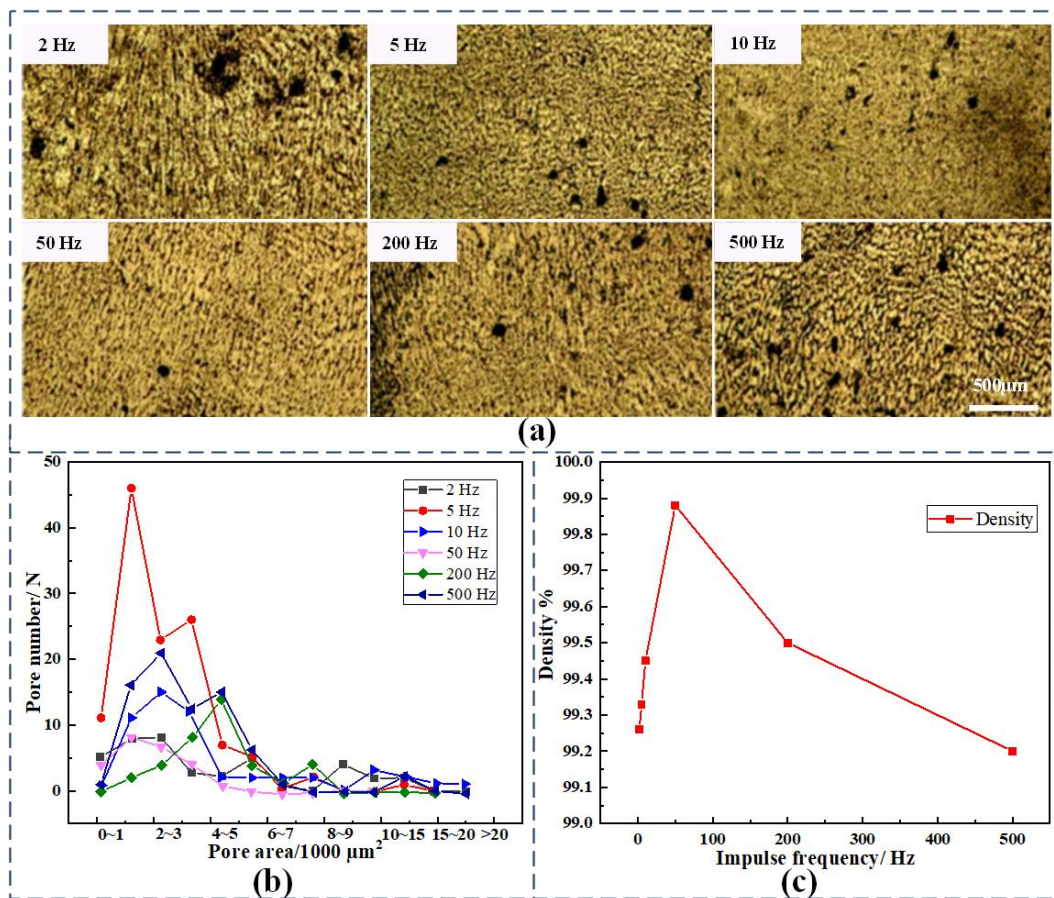


Fig. 15. (a) Porosity of 2024 aluminum alloy under different pulse frequencies [91]. Stomatal statistics, pore number (b) and density (c), of samples with different frequencies [91].

In the context of alloy 2319, Cong et al. [61] conducted a comprehensive investigation into the impact of four distinct CMT process methods, namely CMT, CMT-P, CMT-ADV, and CMT-PADV, on the porosity formation of Al-Cu alloy. As depicted in Fig. 16(b), the current waveforms associated with these processes exhibit variations. Their findings, illustrated in Fig. 16(c), revealed that the CMT and CMT-P processes resulted in a higher accumulation of pores in the 2319 alloy, while the employment of CMT-ADV and CMT-PADV processes yielded a notably lower number of

pores. The CMT-PADV process proved particularly advantageous in reducing or even eliminating pores due to its lower heat input and the enhanced efficiency of the arc in removing the oxide film from the end of the Al-Cu alloy wire. The results agree with the research that was conducted by Gu [9] and Fang [92], as illustrated in Fig. 16(e) and Fig. 17(a) and (b). Notably, this conclusion also holds true for the 7075 aluminum alloy, as demonstrated in Fig. 17(c) and (d) [23]. Nevertheless, the volatilization of low-melting-point alloying elements induced by large heat input emerged as a significant factor on the variations of specimen porosity [83], as discussed in Section 3.2.

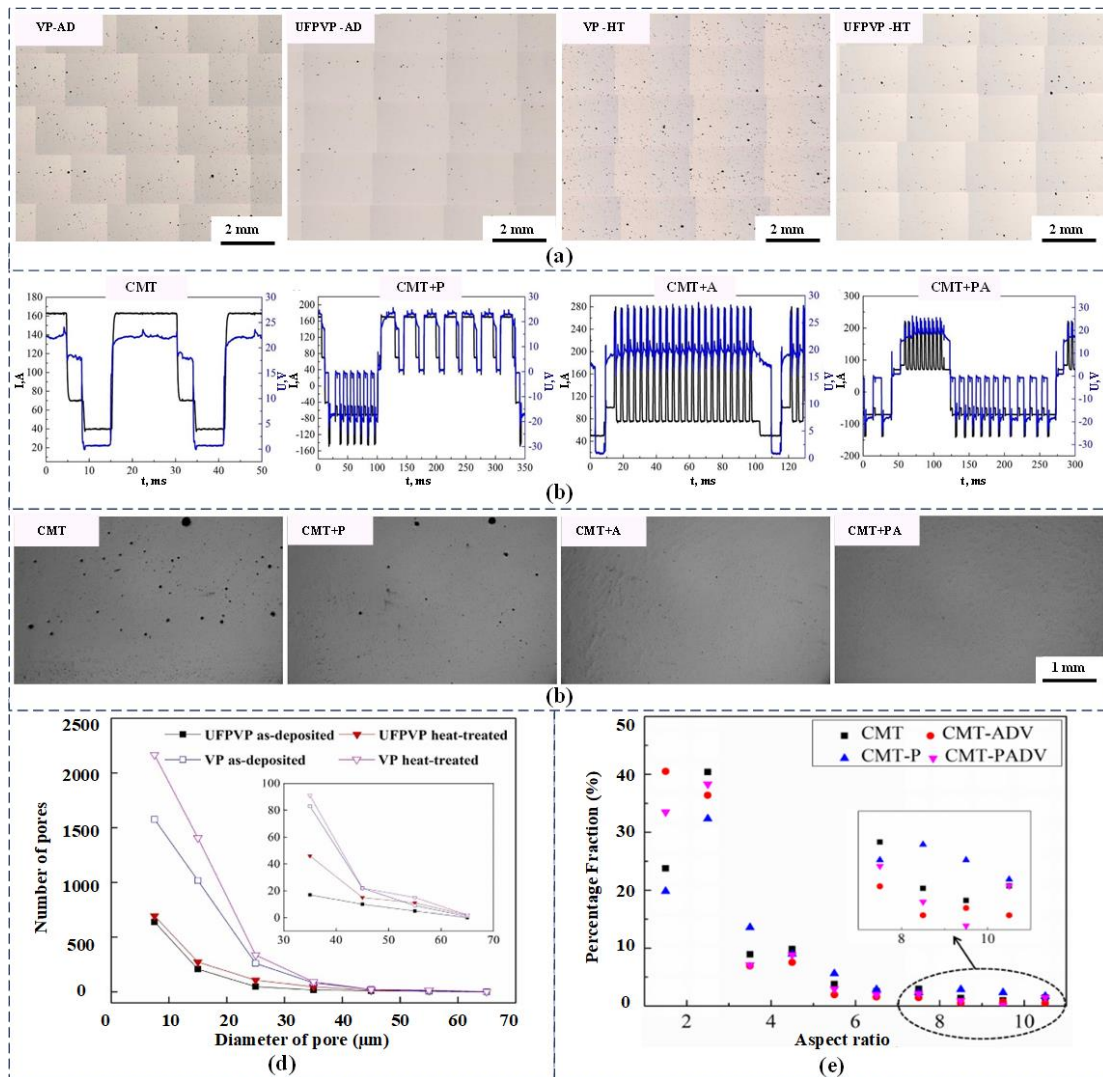


Fig. 16. (a) Porosity results of wire-arc DED 2024 aluminum alloys [50]. (b) Measurements of arc current and voltage waveforms [92]. (c) Single layer deposition porosity of wire-arc DED 2319 alloy [61]. (d) Porosity statistical results of wire-arc DED 2024 aluminum alloys [50]. (e) Pore aspect ratio distribution in percentage fraction for the 2219Al alloys [92].

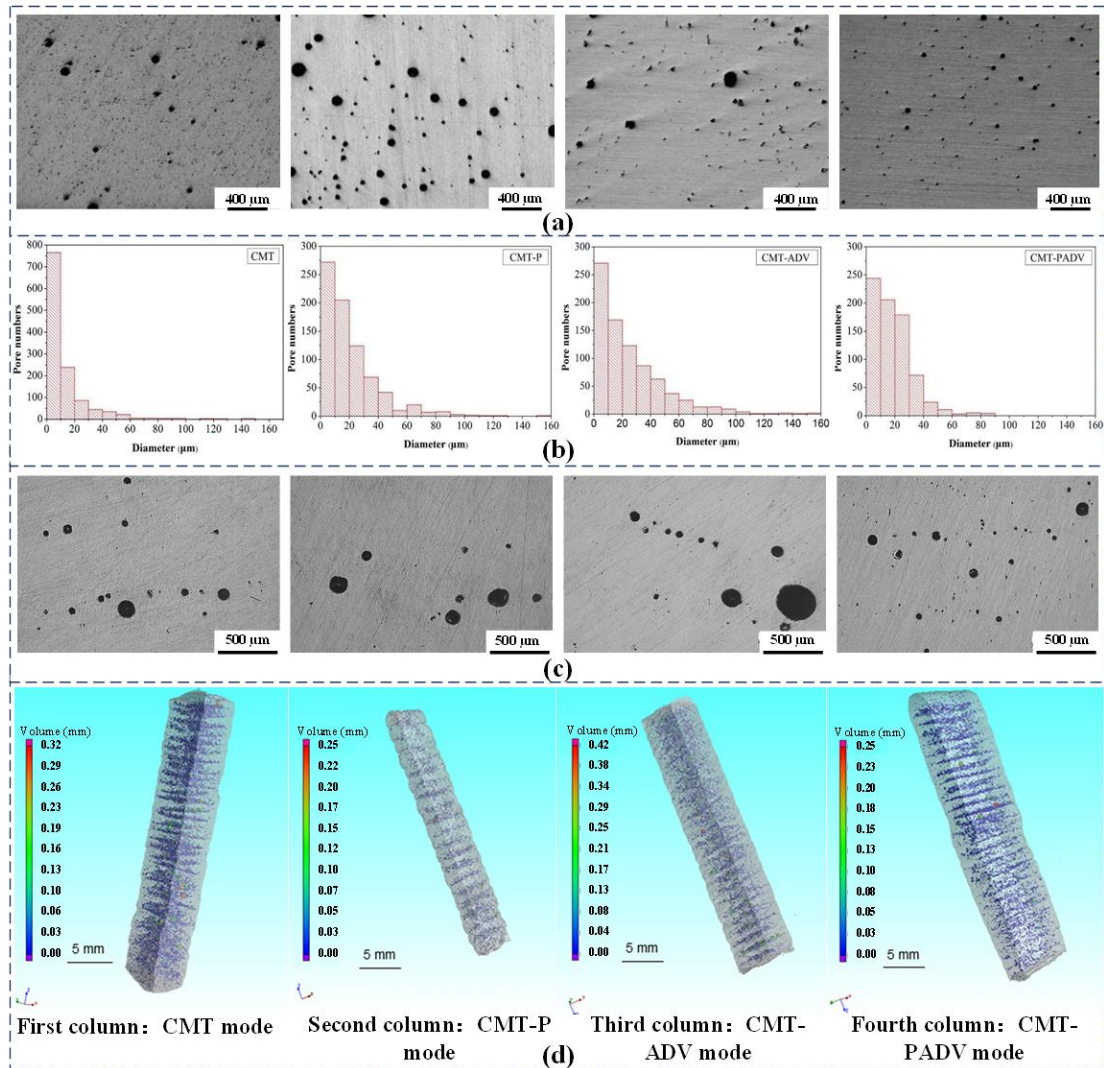


Fig. 17. (a) Optically observed porosity for the wire-arc DED 2219 Al alloys [92]. (b) Pore size distribution in numbers for the 2219 Al alloys [92]. (c) Porosity morphology in samples [23]. (d) Porosity distribution, 3D-morphology, and location inside the samples [23].

The observations presented above highlight that reducing the power supply current and wire feed speed while increasing the travel speed can effectively lower the heat input and consequently diminish the porosity of the specimen. Section 3.4 reveals that there are four stages involved in the production of hydrogen pores. It is evident that the temperature of the melt pool increases when there is a greater amount of heat input. During the nucleation stage, the hydrogen absorption capacity is enhanced at elevated temperatures, resulting in a greater production of hydrogen bubbles. Subsequently, in the growth stage, the larger heat input amplifies the arc pressure, thereby increasing the liquid pressure within the melt pool. As a consequence, hydrogen bubbles develop a larger radius of curvature and grow in size. Moving forward to the detachment and overflow stages, the elevated

temperature of the melt pool leads to a decrease in the wetting angle (θ) and the cooling rate of the melt pool (V_c), while increasing the rate of overflow (V_o). Those combined factors result in fewer hydrogen bubbles being trapped within the melt pool. Additionally, it's worth noting that at higher heat input, the deposition layer thickness reduces, and the distance from the bottom of melt pool to its top becomes shorter, facilitating the escape of bubbles. Fig. 18(a) demonstrates that at low heat input, the melt pool's temperature is relatively low. Consequently, there is a minimal change in the number of grain boundaries needed for H^+ elemental and porosity formation. As a result, the number of pores formed in the specimen is also reduced. An appropriate increase in heat input eases the detachment and spilling of pores. Therefore, when the heat input is appropriately increased within a lower overall heat input range, the pores are more likely to overflow with fewer numbers and smaller size, as illustrated in Fig. 18(b). When the heat input is excessively high, the more sensitive elevation in temperature leads to a significant increase in H^+ elemental uptake. Although pore detachment and spilling are more readily achieved under these conditions, the number of generated bubbles surpasses the number of spilled bubbles, resulting in an increased quantity of hydrogen pores being trapped within the melt pool. Simultaneously, the size of the generated pores becomes substantial due to the excessive radius of curvature of the bubbles, as exemplified in Fig. 18(c).

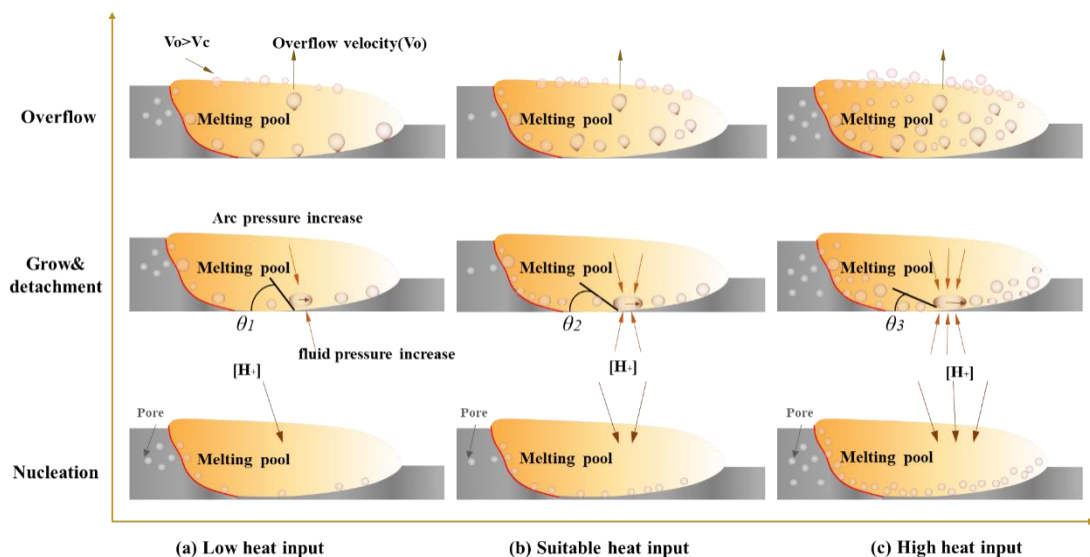


Fig. 18. Effect of different heat input on porosity formation and detachment. (a) low heat input. (b) suitable heat input. (c) high heat input.

Overall, it becomes evident that an appropriate increase in heat input augments the

nucleation rate and thus results in a higher number of bubbles. Concurrently, the overflow rate is heightened, leading to increased hydrogen bubble overflow. However, when the heat input is excessively low, the solidification rate of the melt pool becomes too fast. This, in turn, leads to a greater deposition layer height, a larger escaping distance from the bottom of the melt pool to the top. Additionally, the formation of a small number of bubbles becomes more difficult to escape from the melt pool [48, 61]. Consequently, both excessively high and excessively low heat inputs are unfavorable for controlling specimen porosity. It is imperative to employ an appropriate heat input to regulate the rate of bubble generation and spillage to attain components with low porosity or even the elimination of porosity, as supported by previous research [49, 61]. Furthermore, it is worth noting that the effect of heat input on porosity generation in the above wire-arc DED aluminum alloy reports, has primarily been explored in the context of single-wire deposition. There are also relevant studies investigating the effect of heat input on porosity in dual-wire [65, 93, 94] and multi-wire [95] arc additive manufacturing methods. These studies provide valuable insights into how heat input influences porosity, contributing to a more comprehensive understanding of this critical parameter.

4.2. Shielding gas environment

To solve the hydrogen pore, Kang et al. [96] conducted experiments on wire-arc DED aluminum alloys using the GMAW process. They compared the effects of three different shielding gas supplies: conventional argon (Ar), a mixture of Ar + 67% helium (He) supplied conventionally, and an alternating supply of pure Ar and He. Their focus was on evaluating the pore rate and shape of the deposited aluminum alloy specimens. As illustrated in Fig. 19(a) and (b), the results show that welding with alternating pure Ar and He yielded lower weld porosity as well as deeper and wider weld profiles compared to that of welding with pure Ar and Ar + 67% He supplied by conventional methods. Under appropriately controlled heat input conditions, Cong et al. [49] investigated the effect of different environments, including air and argon, on porosity. Their findings indicated that using argon environments leads to a significant reduction in internal porosity defects, as depicted in Fig. 19(d) and (e).

As illustrated in Fig. 19(f), the size and number of pores in wire-arc DED aluminum alloys are influenced by the composition of the shielding gas environment [81]. NUÑEZ et al. [97] observed that the pore rate in wire-arc DED aluminum alloys was lower when the shielding gas comprised

Ar-He-O₂ compared to when it was composed of Ar-He alone. Moreover, with an increase in He content, the fluidity of the melt pool improved, creating favorable conditions for the escape of hydrogen and further reducing the pore generation rate. JURIC et al. [29] utilized a shielding gas environment consisting of 97.5% He + 2.5% CO₂ by volume fraction, resulting in wire-arc DED aluminum alloy specimens with uniform organization and negligible pore defects. LI et al. [30] found that aluminum alloys protected by nitrogen (N₂) exhibited the presence of numerous flake nitrides, which acted as nucleation points for pores. This presence of nitrides diminished the plasticity and tensile strength of the components. These findings highlight the critical role of shielding gas composition in determining the porosity and mechanical properties of wire-arc DED aluminum alloy parts.

The flow rate of the shielding gas is also a significant factor in determining the likelihood of pore formation, as it has an impact on the melt droplet transfer process and the shape of the melt pool [28]. Cong et al. [98] conducted an analysis of how the shielding gas flow rate influences pore formation in wire-arc DED aluminum-Cu alloy. As shown in Fig. 19(c), it is evident that increasing the flow rate of pure Ar shielding gas assists in reducing pore formation when other factors such as *WFS* and *TS* are held constant. This reduction occurs because an elevated shielding gas flow rate can limit the entry of external gases into the melt pool, consequently reducing porosity [98]. At lower shielding gas flow rates, the protective atmosphere of the wire-arc DED process weakens. Any disturbances in the shielding gas environment are more likely to result in oxidation and the formation of pores during the deposition process of aluminum alloys, even with low heat input [28]. Additionally, micro-pores can serve as new nucleation sites for pores, promoting pore growth. Simultaneously, the shielding gas flow rate should also not be too high, which can lead to both the wastage of shielding gas and undesirable interference with the welding arc [49, 61]. Therefore, regulating the appropriate shielding gas flow rate is beneficial to reduce the formation of porosity.

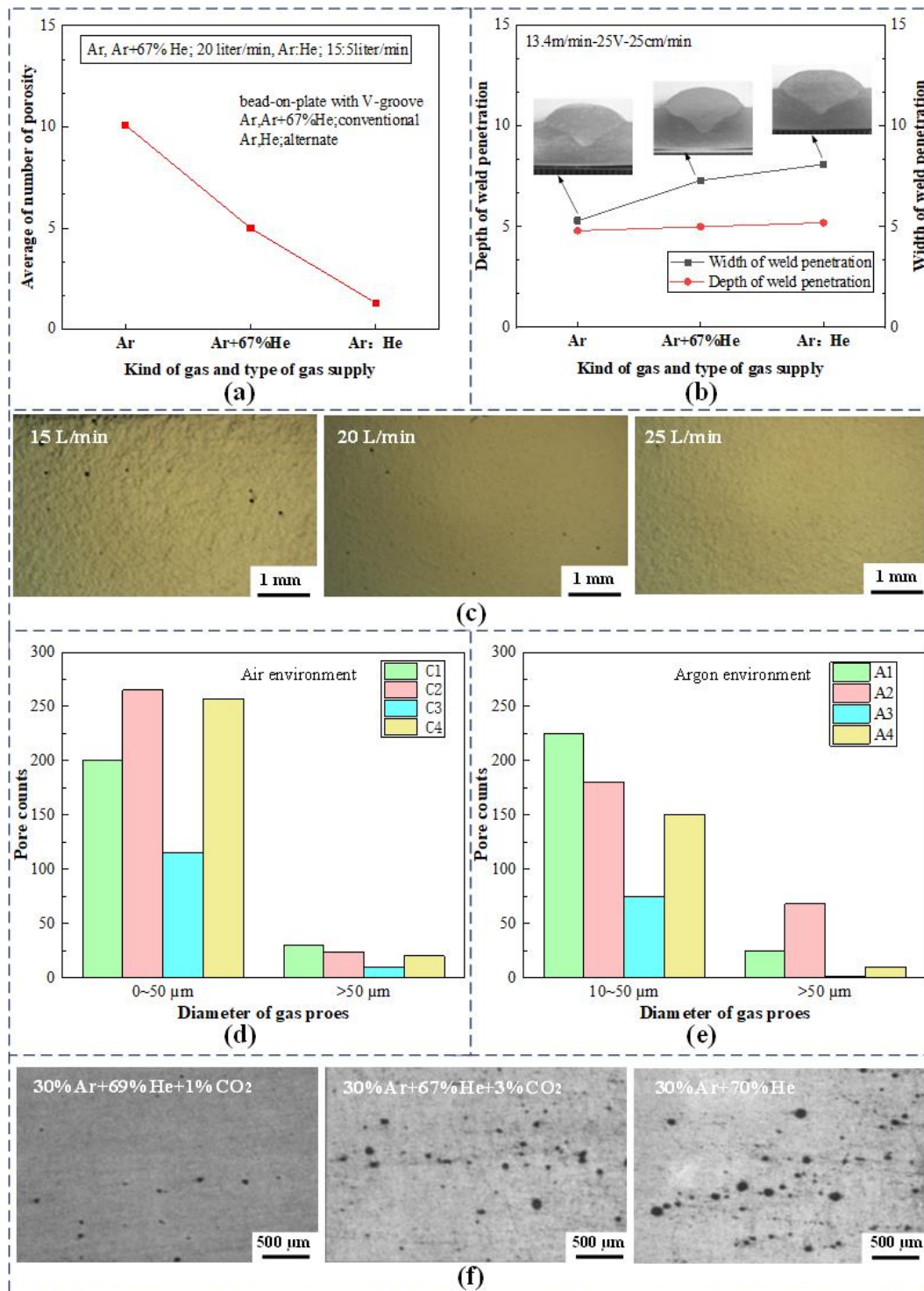


Fig. 19. (a) Porosity under different shielding gases [96]. (b) Weld shape under different shielding gases [96].

(c) Effect of shielding gas flow rate on porosity [98]. (d) (e) Pore counts for as-deposited samples [49]. (f)

Blowholes appearance in joints welded by different shielding gases [81].

The purity of the shielding gas is indeed a critical factor in preventing porosity, with gases like Ar and He being among the most commonly used for this purpose [98]. High purity levels are required for optimal performance. For Ar, a purity of 99.99% is the standard requirement, and when

producing precision components, even higher purity of 99.999% is necessary. The presence of impurities such as O₂, H₂, N₂, and H₂O in the shielding gas should be minimized, with content requirements of less than 0.005% for O₂, less than 0.005% for H₂, less than 0.015% for N₂, and less than 0.02mg/L for H₂O. When the O₂ content exceeds or equals 0.1%, the component's surface may appear dark grey, and in severe cases, it may become contaminated with a black slag-like material that hinders further deposition and complicates cleanup. Furthermore, during the wire-arc DED aluminum alloy process, certain shielding gases have the potential to react with the raw material, leading to the formation of impurities that can contribute to porosity in the fabricated parts. Therefore, maintaining high gas purity is paramount to achieving porosity-free, high-quality components in wire-arc DED processes [28].

In summary, it is evident that the composition, flow rate, and purity of shielding gas significantly affect the porosity in wire-arc DED aluminum alloys. These parameters play a crucial role in achieving low-porosity, high-quality components in wire-arc DED processes.

4.3. Heat treatment

To achieve high strength in wire-arc DED built aluminum alloy components, heat treatment is commonly employed to improve the microstructure [99]. For instance, applying T6 treatment to the specimen mitigates stress and structural defects within the metal, leading to a homogeneous and refined microstructure. Consequently, this enhancement bolsters the strength and toughness of the metal specimen. One of the heat treatment processes used for aluminum alloys is solution treatment. This process involves heating an aluminum alloy to a specific temperature and holding it there, followed by a rapid cooling. During the solution treatment of an aluminum alloy, solute atoms are dissolved in the matrix, and after cooling, a supersaturated solid solution is formed in the alloy's matrix. The supersaturated solid solution formed in the matrix of the aluminum alloy following the solution treatment is highly unstable. Subsequent aging treatment allows for the precipitation of hard, small-sized reinforcing phases, which leads to an increase in the alloy's strength. The degree of solute atom saturation plays a crucial role in this process. A higher degree of saturation results in a greater driving force for recrystallization, making it easier to form high-density precipitated phases during aging [100]. Several studies have demonstrated that thermal stresses generated at high temperatures during heat treatment can promote the aggregation of pores, leading to an increase in the total volume and size of the pores [9, 50, 70].

As demonstrated in Fig. 20, Gu et al. [9, 53, 55] observed significant changes in the microstructure of both wire-arc DED 2319 Al and 5087 Al alloys after heat treatment. Following the heat treatment of the 2319 Al alloy, the average diameter and sphericity of the pores did not undergo significant alterations, but there was a notable increase in both the total number and area ratio of the pores. This phenomenon can be attributed to the presence of a large number of dendrites, grain boundaries, or fine uniformly distributed second-phase particles that serve as non-homogeneous nucleation points during heat treatment. As a result, a substantial quantity of fine secondary pores forms in the top and bottom regions. As shown in Fig. 22(b), most of the micropores in the heat-treated 2319 Al alloy specimens are around 5 μm , providing evidence of that the secondary pores generation is caused by heat treatment. The diameters of the pores in the upper and lower regions of the specimen shift to the left of the diagram (Fig. 22(b)) after heat treatment, indicating that the primary factor influencing pore evolution in these areas is the formation of secondary pores. Meanwhile, the diameter of the pores in the central region moves to the right and becomes concentrated around 10 μm , suggesting that pore evolution in the central region is primarily driven by the coarsening of pores.

Following the heat treatment of 5087 Al alloy, several notable changes were observed: the average size and sphericity of the pores increased, the number of pores decreased, and the area covered by porosity expanded. Those phenomena are resulting from the collective impact of numerous tiny pore clusters (known as Ostwald maturation) and subsequent hydrogen diffusion. Additionally, in the 5087 Al alloy deposited specimens, many small pores with a diameter of approximately 2 μm were distributed. This distribution could be attributed to the volatilization of Mg or the influence of alloying elements on metal solidification and pore formation. Subsequently, these small pores gradually grew during heat treatment to form larger pores. This observation aligns with the findings reported by Liu et al. [101], as illustrated in Fig. 21(a).

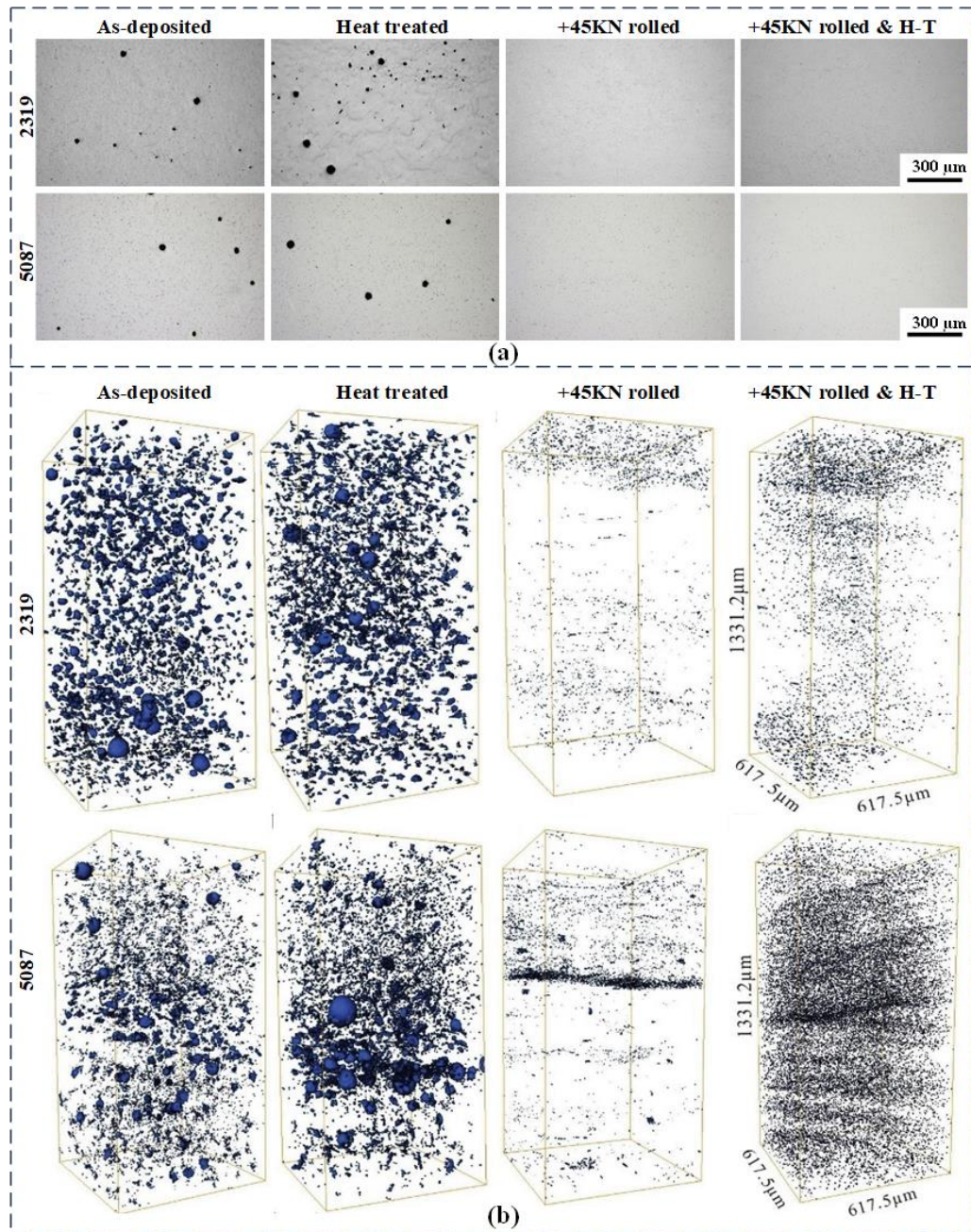


Fig. 20. (a) Optically observed porosity and 3D view of micropores for the wire-arc DED 2319 and 5087 aluminum alloy with different state [53, 55].

Fig. 20 demonstrates that heat treatment resulted in an increased pore area in the deposited specimens of both alloys. Nevertheless, when the specimens were subjected to rolling at 45 KN before heat treatment, the diameter of the pores in both alloys remained below 5 μm. In the case of the Al-Cu-Mg alloy, it was observed that after heat treatment, the density of pores in the specimens decreased, while the equivalent diameter (d), sphericity (S_p), and porosity area (V) of the pores increased [74], as depicted in Fig. 21(c) and (d).

During the wire-arc DED process of the 2196 Al-Li alloy, Xue et al. [68] noticed a significant presence of pores in the directly deposited parts, with sizes primarily clustered in the range of 10-30 μm . As shown in Fig. 21(e) and (f), T6 heat treatment exacerbated this situation, leading to a higher proportion of microporosities larger than 50 μm and an increase in the maximum pore size to 107 μm . Fig. 22(a) displays the three-dimensional (3D) and two-dimensional (2D) representations of porosity in the samples before and after heat treatment, characterized by X-ray Computed Tomography (XCT). These observations are consistent with the findings following the heat treatment of wire-arc DED 2024 and 7055 aluminum alloys [84, 94].

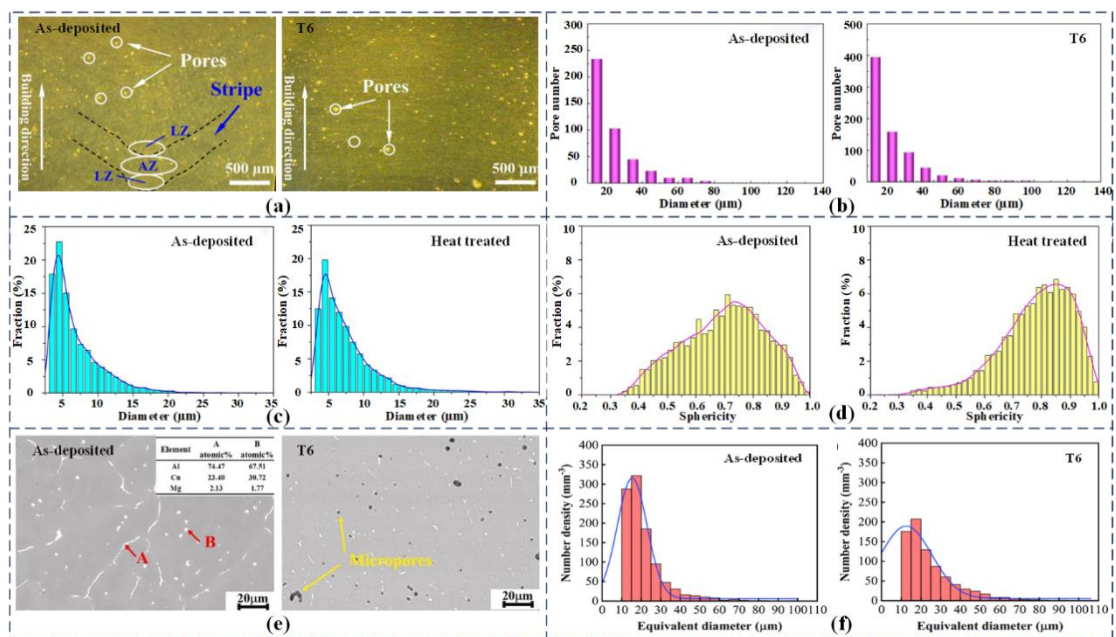


Fig. 21. (a) Macro characteristics in the cross section. (b) Pore size distribution in numbers [101]. (c) (d) Micro-pore number fraction in wire-arc DED aluminum alloys as a function of equivalent diameter and sphericity [74]. (e) (f) SEM images and equivalent diameter distribution frequency of the AA2196 Al-Li alloy [68].

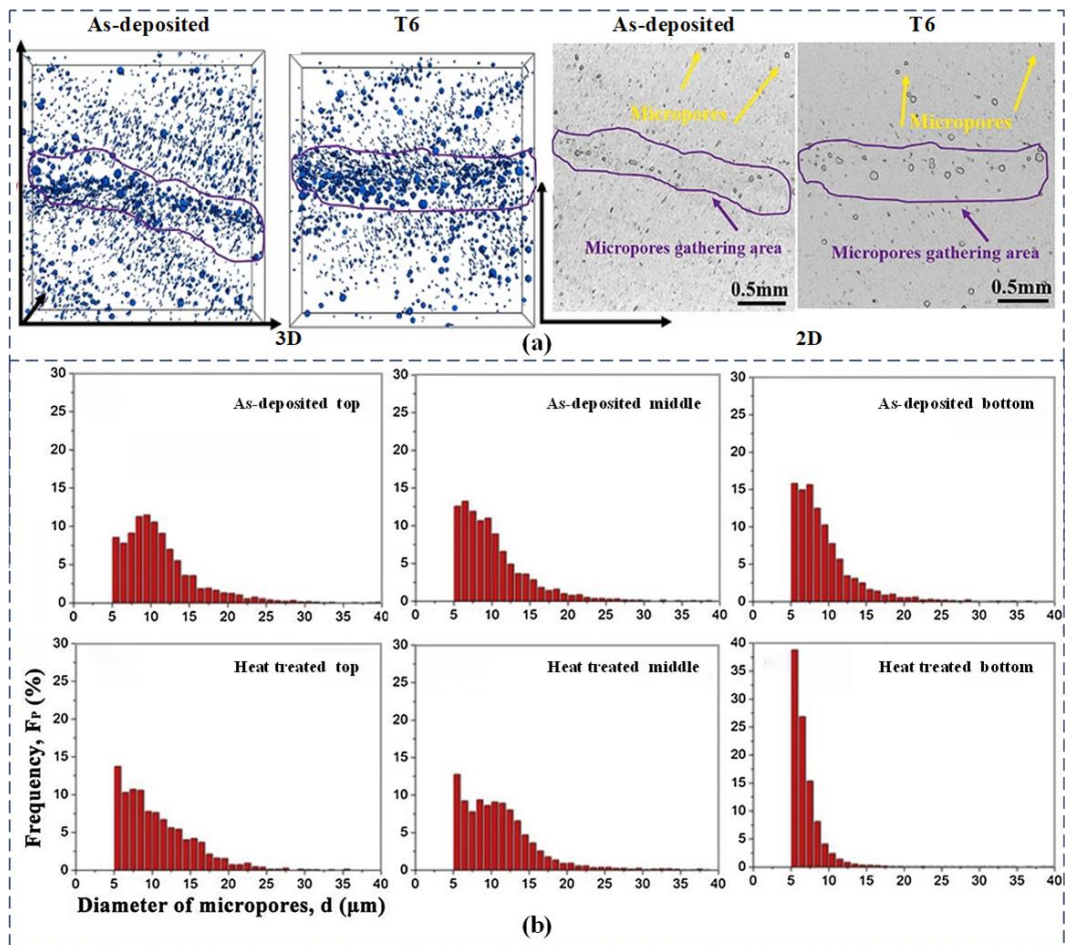


Fig. 22. (a) XCT characterized micropores in 3D and 2D in AA2196 Al-Li alloy at different conditions [68]. (b)

Diameter distribution of micropores in wire-arc DED 2319 alloy [9].

In summary, heat treatment leads to an increase in the pore volume rate of wire-arc DED aluminum alloys. This increase is primarily attributed to three evolutionary mechanisms: the precipitation of hydrogen micropores, the dissolution of phase particles, and the growth of micropores [9].

4.4. Other influencing factors

Interlayer cooling time and interlayer temperature also affect wire-arc DED aluminum alloy porosity. According to the findings of Gao et al. [102], the pore content decreases and then increases with increasing interlaminar cooling time, while maintaining the same travel speed and wire feed speed. When the interlayer specimens were either short or long, a significant quantity of pores were generated. When the interlayer cooling time is too short, it results in excessive heat accumulation, slower solidification, prolonged exposure of the liquid metal, and coarser grain formation. The surface of the deposition layer experiences excessive heating and is susceptible to the formation of

an oxide film. This wire has a higher tendency to absorb moisture from the surrounding air, resulting in the generation of more hydrogen pore [103]. On the contrary, when the cooling time between layers is prolonged, it can result in increased shrinkage cavity formation due to inadequate fusion, ultimately leading to the emergence of larger pores. This occurs because the process gas is introduced into the melt pool, coupled with its rapid cooling rate as well as the minimal heat accumulation, prevents the gas bubbles from escaping before they are caught by the solidification front. As a result, these trapped gas bubbles produce enormous pores [103].

The interlayer temperature and cooling time exhibit an inverse relationship, which has implications for controlling pore formation in aluminum alloy specimens. When the interlayer temperature is excessively high, the heat dissipation conditions of the produced sections deteriorates, even when all other process variables are constant. The excess heat in the melt pool cannot dissipate efficiently, leading to an overheated melt pool with an extended residence time and increased fluidity. After solidification, this overheating may result in the occurrence of "flow" phenomena, as well as porosity, liquified phase, and even thermal cracking defects in the deposited parts [25]. **Additionally, when the lifting height of the welding torch is fixed, it will cause the excessive dry elongation of the wire, which will also cause an increase in specimen porosity.** The phenomenon occurs because as the deposition height increases, the accumulation of heat elevates the melt pool temperature, enhancing its fluidity. This, in turn, causes an increase in the width of the monolayer and a decrease in height. **When the risen height of welding torch is fixed of each layer, if the height of the deposited layer is less than the lifting height of the torch, the length of the protruding wire will progressively rise with each additional layer. Conversely, it will progressively decrease in length. When the wire extends excessively, the shielding effect of the protective gas on the surrounding air weakens significantly. This allows the surrounding air to enter the melt pool, leading to the formation of large-sized process pores in the specimen. Excessive travel speed may also weaken the shielding gas, resulting in a higher incidence of large process pore sizes in the specimen.**

The aforementioned elements that influence porosity pertain to items deposited in wire-arc DED single-pass monolayer or single-pass multilayer experiments. Zhang et al. [22] discovered that the porosity in the multi-pass multilayer experiment, laser-MIG arc hybrid additive manufacturing process is also influenced by the lap rate. When the lap rate is excessively high, the surface height of the specimen exhibits a progressive increase in the direction of the lap, accompanied by

significant heat accumulation and excessive remelting of the metal. On one side, the remelted portion of the metal experiences grain growth during the second melting. On the other hand, the remelted surface of the Al alloy accumulates more oxides, which increases the likelihood of pore formation and other defects, ultimately reducing the performance of the specimen. Furthermore, the preparatory steps before the wire-arc DED process is initiated, such as the meticulous removal of oxide films, oils, and other surface impurities from both the wire and base material also constitute a crucial factor, impacting the quality of the final specimen [27, 67].

5. Porosity inhibiting strategies

Researchers have also implemented various strategies to minimize or eliminate the porosity formation. This section explores the role of laser-arc hybrid additive manufacturing, ultrasonic vibration assistance, inter-layer rolling, inter-layer friction stir processing, ultrasonic peening treatment, and other composite manufacturing processes in reducing the porosity of wire-arc DED aluminum alloys, as illustrated in Fig. 23. These approaches aim to improve the overall quality and performance of wire-arc DED aluminum alloys. Furthermore, meticulous pre-process surface preparation involving the thorough removal of oxide films, oil, and moisture from both the filament and base material surfaces prior to wire-arc DED has been demonstrated to be an effective approach in addressing the hydrogen source issue. This comprehensive surface cleaning procedure helps control hydrogen generation at its origin, thereby reducing the nucleation rate of pore formation [27, 67]. Additionally, the preliminary pre-heating of wires prior to their utilization plays a pivotal role in diminishing the heat input during the process, leading to a notable reduction in pore formation within wire-arc DED aluminum alloys [84].

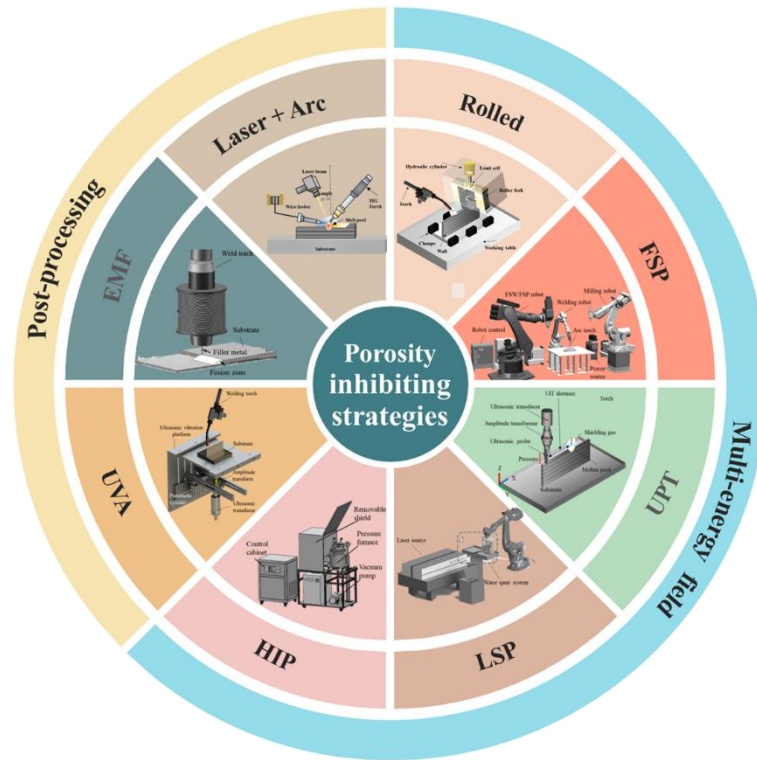


Fig. 23. An overview of porosity inhibiting strategies.

5.1. Multi-energy sources and external fields

5.1.1. Laser-arc hybrid additive manufacturing

The concept of the laser-arc hybrid process was initially introduced by Steen [104]. This process combines two distinct heat sources, namely laser and arc, which possess contrasting energy transmission methods and physical features. Laser-arc hybrid additive manufacturing is an innovative technique that merges the advantages of these two heat sources [105]. The two are coupled by adding a low-power laser to induce the arc. The laser creates a keyhole in the melt pool, which has an anodic spot effect. This effect attracts the arc towards the anodic spot, resulting in improved arc precision and stability [51].

Laser-arc hybrid additive manufacturing process is further categorized into paraxial and coaxial composite, as depicted in Fig. 24(a) [104]. Laser-arc paraxial hybrid additive manufacturing refers to a process where the laser and the arc are not aligned along the same axis at a specific angle. This technique is characterized by its simple device structure and limited flexibility [104]. Laser-arc coaxial hybrid additive manufacturing refers to a process where a laser and an arc are aligned closely in the same axis. This technique involves a more intricate internal structure and requires higher device specifications, resulting in improved flexibility. Laser-arc hybrid additive

manufacturing encompasses three techniques: laser-MIG arc hybrid additive manufacturing (Laser+ MIG) [88], laser-TIG arc hybrid additive manufacturing (Laser + TIG) [21, 105], and laser-PTA arc hybrid additive manufacturing (Laser + PTA) [31]. The principles of these techniques are illustrated in Fig. 24(b).

Laser+ MIG is a process where a low-power laser is combined with the MIG arc to generate an electric arc. This approach delivers a high arc heat input and excellent fabrication efficiency, with an aluminum alloy deposition efficiency of up to 2.0 m³/h. However, the process may suffer from poor stability and excessive spatter [51]. Laser + TIG integrates a low-power laser into the TIG arc, where a tungsten electrode is used to melt the wire. This process offers greater stability and reduced spatter compared to Laser + MIG, but it comes at the cost of lower welding efficiency [51, 88]. Laser + PAW integrates a low-power laser into the PAW arc, which also utilizes a non-consumable tungsten electrode. Compared with conventional TIG arc, the PAW arc offers higher energy density, improved control over heat input, enhanced resistance to external interference, and easier management of the shaping process. However, it is worth noting that this method demands higher equipment standards [31, 106]. It is important to note that when the laser power exceeds 300 W and the energy density surpasses 106 W/cm², keyholes can form in the specimen [31]. Therefore, it is advisable to avoid excessively high laser power.

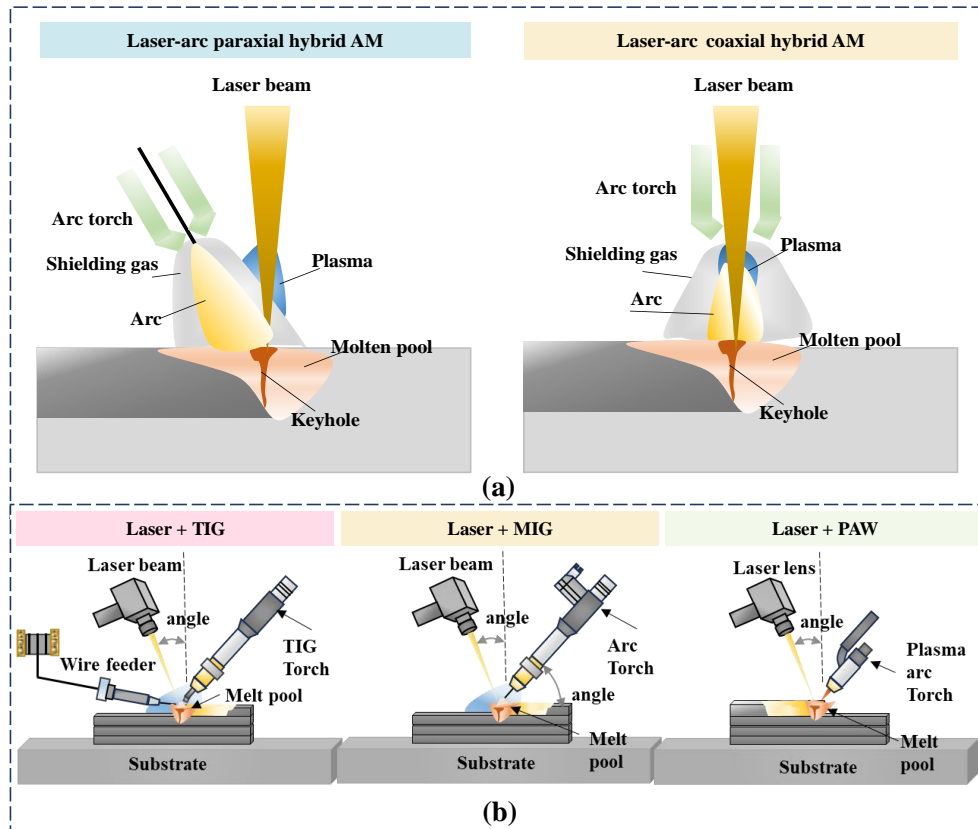


Fig. 24. (a) Laser-arc hybrid additive manufacturing classification. (b) Schematic diagram of laser-arc hybrid additive manufacturing.

As depicted in Fig. 25(a), Zhang et al. [88] conducted a study by incorporating a low-power laser to induce the MIG arc and investigating the impact of welding parameters on the porosity of 6082 aluminum alloy joints. They discovered that the characteristics of the melt pool shape were closely linked to the weld porosity. To predict the porosity of hybrid welds, they introduced a volumetric characteristic coefficient, denoted as Φ . As demonstrated in Fig. 25(c), their findings indicated that as Φ increased, it became easier for bubbles to escape from the melt pool, leading to lower weld porosity. When $\Phi > 0.52$, the weld porosity was reduced to less than 0.5%. In the case of 2319 aluminum alloy, Zhang et al. [22] observed that the introduction of the laser led to a decrease in both the diameter of the pores and the number of pores per unit area in the deposited aluminum alloy specimens, as shown in Fig. 25(b). This reduction in porosity can be attributed to the stirring effect of the laser, which enhanced the mobility of the melt pool, making it more conducive for the hydrogen gas pore to escape from the melt pool. **When the laser is applied to the melt pool, the melt flow initiates at the rear surface of the keyhole, then flows downward to the rear of the keyhole and rises along the contour of the melt pool [107]. This leads to a rapid melt flow towards to the rear of**

molten pool, rapidly expanding the length of the molten pool. Consequently, the introduced laser enhances the stirring of the melt pool flow, causing the generated bubbles to overflow in the major molten pool flow direction, shown in Fig. 25(c).

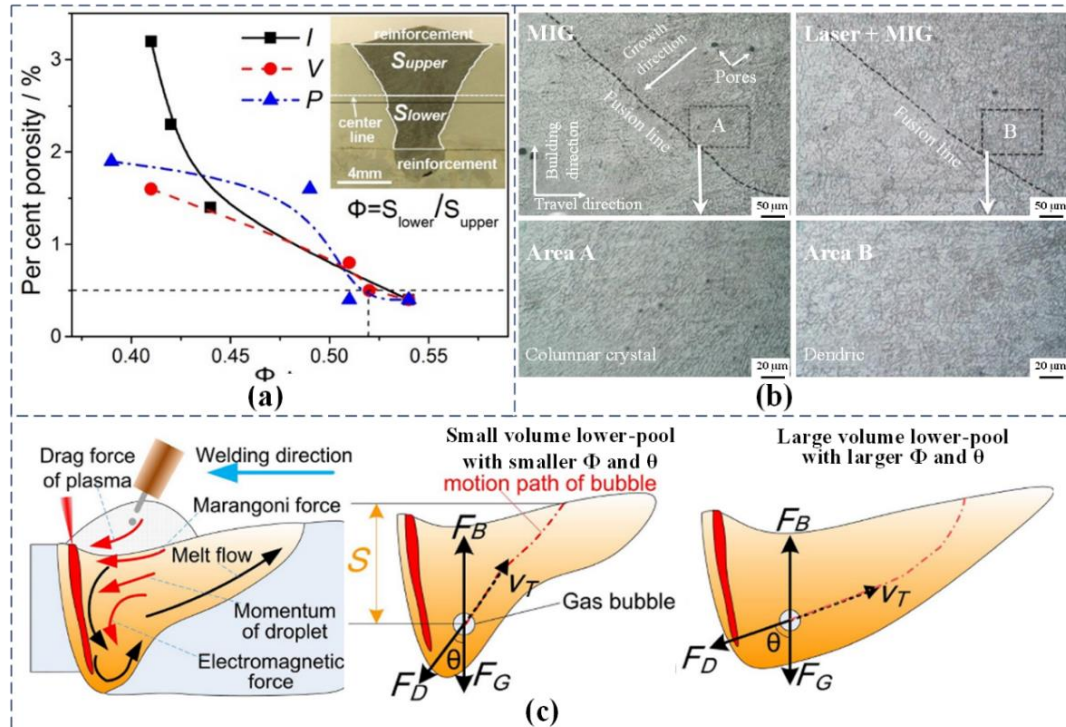


Fig. 25. (a) Weld percent porosity as a function of the Φ [88]. (b) Microstructure of 2319 Al perpendicular to the scanning direction [22]. (c) Movement and force condition of gas bubbles within LAHW melt pool [88].

In Fig. 26(a), Liu et al. [21] employed pulsed laser-TIG arc hybrid additive manufacturing (LAHAM) to investigate the Al-Zn-Mg-Cu (7075) alloy. They observed that there were no crack defects and only a few pores in the y-z plane of the specimens produced using both the conventional wire-arc DED and the LAHAM process. The porosity of the deposited specimens was determined using Archimedes' method, and they found that the porosity of wire-arc DED and LAHAM specimens was 99.87% and 99.68%, respectively. Similarly, Wu et al. [33] conducted a study on 2319 aluminum alloy and observed the presence of micropores in the cross-section of the deposited specimens. However, the size of these pores was generally less than 200 μm , and the percentage of the pore area was only 0.82% (counting only pores with a diameter of more than 5 μm), as shown in Fig. 26(b). Examination of the fracture surface with a scanning electron microscope revealed the presence of uniform spherical micropores, as shown in Fig 26(c). The fracture mechanism seen is microporosity through fracture, which is a typical ductile fracture. To analyze the effect of pulsed laser on the microstructure, Chen et al. [31] compared laser-PTA samples with

PTA samples. They found that without the application of the laser, there were more porosity defects distributed around the grain boundaries. In contrast, the laser-PTA process resulted in no obvious porosity defects inside the deposited layer. This was attributed to the pulsed laser that promotes the motion of melt pool flow and thus boosts the escaping of gas pore, increasing the density of the solidified metal.

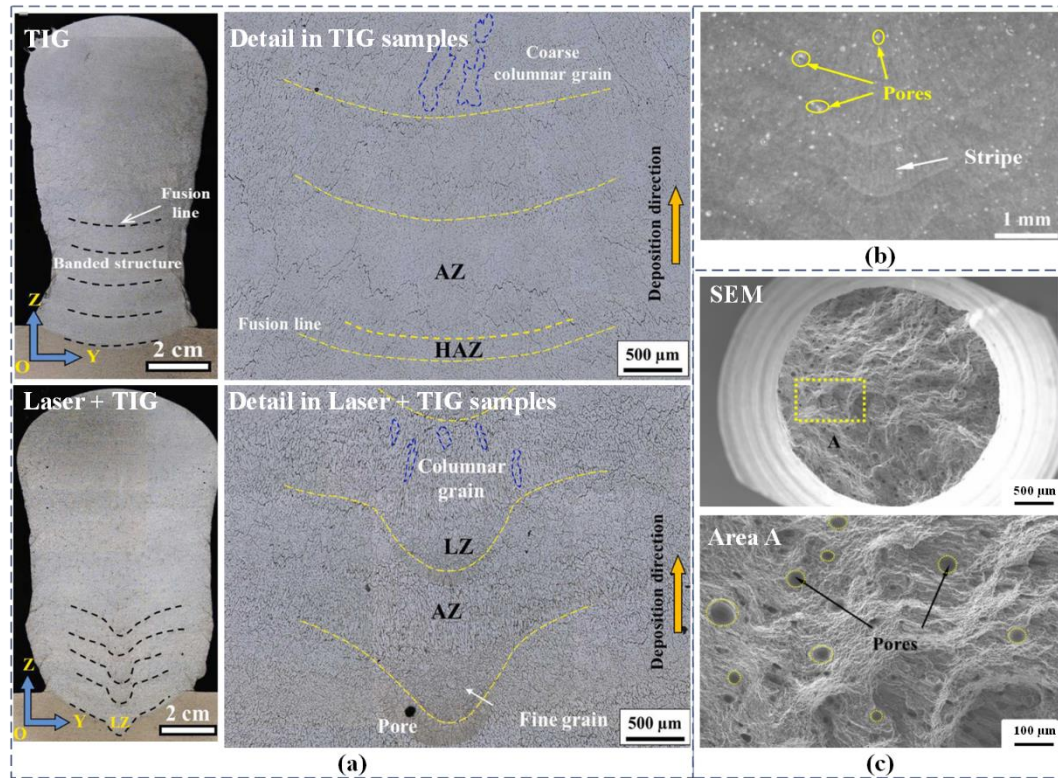


Fig. 26. (a) Macrostructure morphologies of YOZ plane for Al-Zn-Mg-Cu alloy specimen [21].

(b) Macro morphology of a deposited specimen in cross section [33]. (c) The surface of tensile fracture [33].

In summary, laser-arc hybrid additive manufacturing processes effectively reduce the porosity of aluminum alloy specimens. This reduction in porosity can be attributed to several factors. First, the introduction of a laser enhances the flow of liquid metal in the melt pool, improving the escape rate of pores. Second, the anode spotting effect of the laser stabilizes the arc, reducing the likelihood of hydrogen absorption during the welding process in wire-arc DED. These combined effects result in lower porosity levels in the final aluminum alloy components.

5.1.2. Ultrasonic vibration assistance

Ultrasonic vibration assistance (UVA) is a mechanical vibration-based method used in wire-arc DED for improving material properties. The basic principle involves converting standard 220V, 50Hz alternating current into ultrasonic frequency alternating current of 20kHz and above. This

ultrasonic frequency alternating current is then transformed into mechanical vibrations with the same frequency by a transducer. These mechanical vibrations are transmitted to the tool head via an amplifier rod, and the tool head applies the high-frequency vibrations to the working part, such as the substrate or workpiece, to enhance material properties [35, 108]. The experimental schematic for UVA is shown in Fig. 27(a).

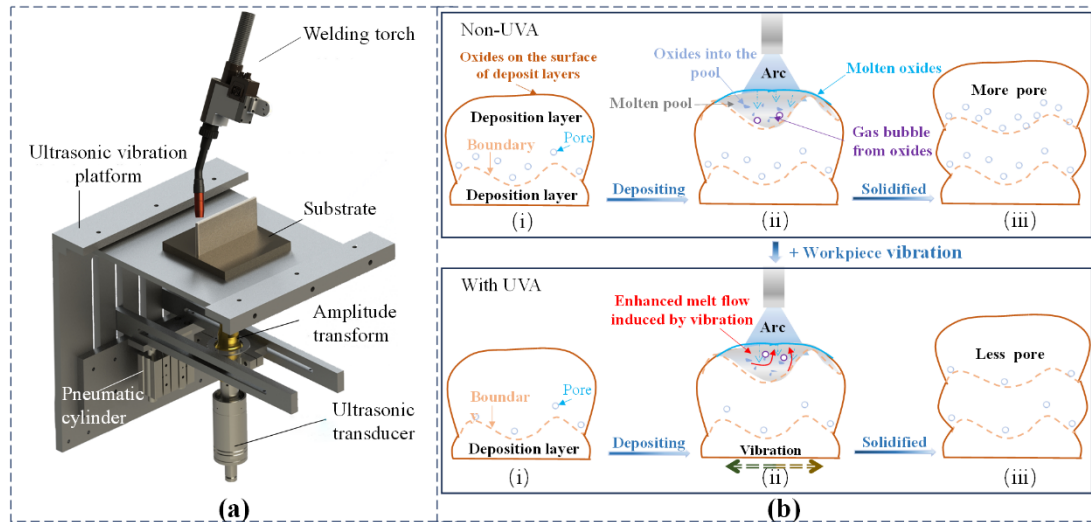


Fig. 27. (a) Schematic diagram of ultrasonic vibration of substrate [36]. (b) Schematic diagram of ultrasonic vibration reducing porosity.

The use of workpiece vibration to study Al-Mg alloys by Zhang et al. [52] showed that it promoted grain refinement and reduced porosity. When vibration was introduced to the substrate, Gao et al. [52] observed a significant reduction in both the number and size of pores within the aluminum alloy specimens, as shown in Fig. 28(a). This aligns with the findings of Zhang et al. [109]. As shown in Fig. 27(b), wire-arc DED is a multilayer deposition process, and completely removing the oxides on the surface of the deposited layers can be challenging. During the remelting process, these oxides can enter the melt pool. Therefore, the main method to suppress porosity is to encourage bubbles in the melt pool to overflow [52]. Ultrasonic waves, as a form of high-frequency sound waves, produce various nonlinear effects, including cavitation, acoustic flow, mechanical impact, and radiation pressure, during melt propagation [52]. When the impact needle periodically strikes the surface of the substrate or workpiece, the saturated hydrogen in the liquid aluminum alloy precipitates due to the ultrasonic vibration, leading to the formation of numerous small "cavitation bubbles" in the liquid metal. The sound pressure amplitude inside these cavitation bubbles reaches a critical value and causes them to rupture. This rupture generates a strong shock wave that promotes

the flow of molten metal and accelerates the escape of gas bubbles [34]. Meanwhile, the rupture also increases the localized melt pool temperature, which extends the solidification time of the pool, providing more time for the escape of gas bubbles, resulting in reduced porosity [110].

Fig. 28(c) and (e) show that when the ultrasonic vibration power is too high, it leads to an increase in porosity [111]. This happens because the acoustic pressure inside the melt pool gradually increases with the rising amplitude. When the acoustic pressure reaches a certain threshold, the distance between molecules exceeds a limiting value, and the structural integrity of the liquid metal medium is compromised, resulting in the formation of pores. Simultaneously, the amplification of the acoustic pressure results in the augmentation of the acoustic flow, so intensifying the fluidity of the melt pool. The vortex effect within the melt pool fluid causes bubbles that rise to the surface to be swept back into the interior of the melt pool, ultimately increasing the porosity of the aluminum alloy [112].

The use of UVA also affects the location of pores, as shown in Fig. 28(b). The specimens without UVA had fewer pores on the surface, most of which were located below the weld seam. In contrast, specimens with UVA had more pores concentrated at the centerline of the weld seam. This difference is attributed to the ultrasonic vibrations promoting the upward escape of tiny bubbles. However, due to the rapid cooling of the melt pool, these bubbles are unable to escape completely and remain trapped at the shallow surface of the deposited parts [109]. It's worth noting that torch or wire vibration can also accelerate the flow of the melt pool and reduce heat input, as mentioned in the references [35, 113, 114].

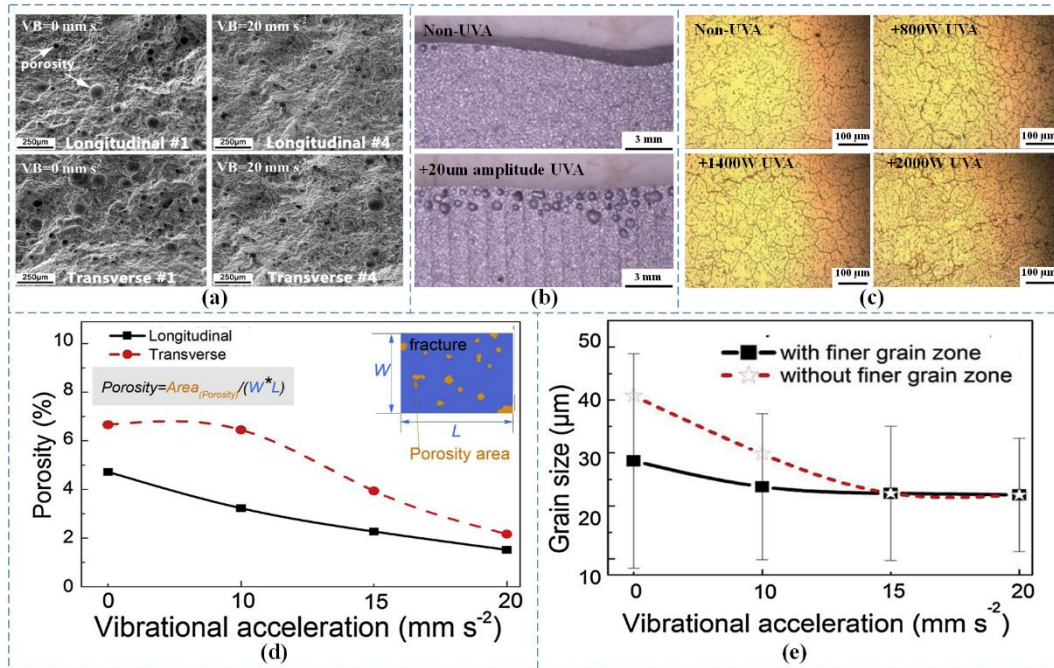


Fig. 28. (a) Fracture surface morphology with different vibration acceleration [52]. (b) Pores on the weld surface of specimens [109]. (c) Microstructure of the additive sample under different ultrasonic vibration power [111]. (d) Porosity percentages of fracture surfaces [52]. (e) Average grain size of the additive manufactured specimens [52].

In summary, the application of ultrasonic vibration assistance (UVA) strengthens the flow of the melt pool, promoting the effective overflow of internal bubbles and leading to improved microstructure morphology and mechanical properties of wire-arc DED aluminum alloys [52].

5.1.3. External magnetic field

In recent years, external magnetic fields (EMF) have been employed as a facilitative measure to enhance the forming process [37, 115]. Various types of magnetic fields, including transverse magnetic fields [116], longitudinal magnetic fields [117-119], and alternating magnetic fields [120, 121], have been investigated. The underlying principle involves the interaction between the magnetic field and charged particles within the welding arc, resulting in the generation of Lorentz force. This force induces periodic rotational motion in the charged particles, thereby prompting the rotation of the welding arc. Consequently, the flow direction of molten metal in the melt pool undergoes alteration, influencing the crystallization process of the metal within the melt pool. Hence, the external magnetic field serves to effectively regulate the transition of melt droplets and the flow dynamics of the melt pool [122, 123]. In comparison with alternative auxiliary methods, EMF exhibits the advantages of cost-effectiveness, high flexibility, and ease of implementation, rendering

it highly promising for application in wire-arc DED. Fig. 29 displays the experimental apparatus.

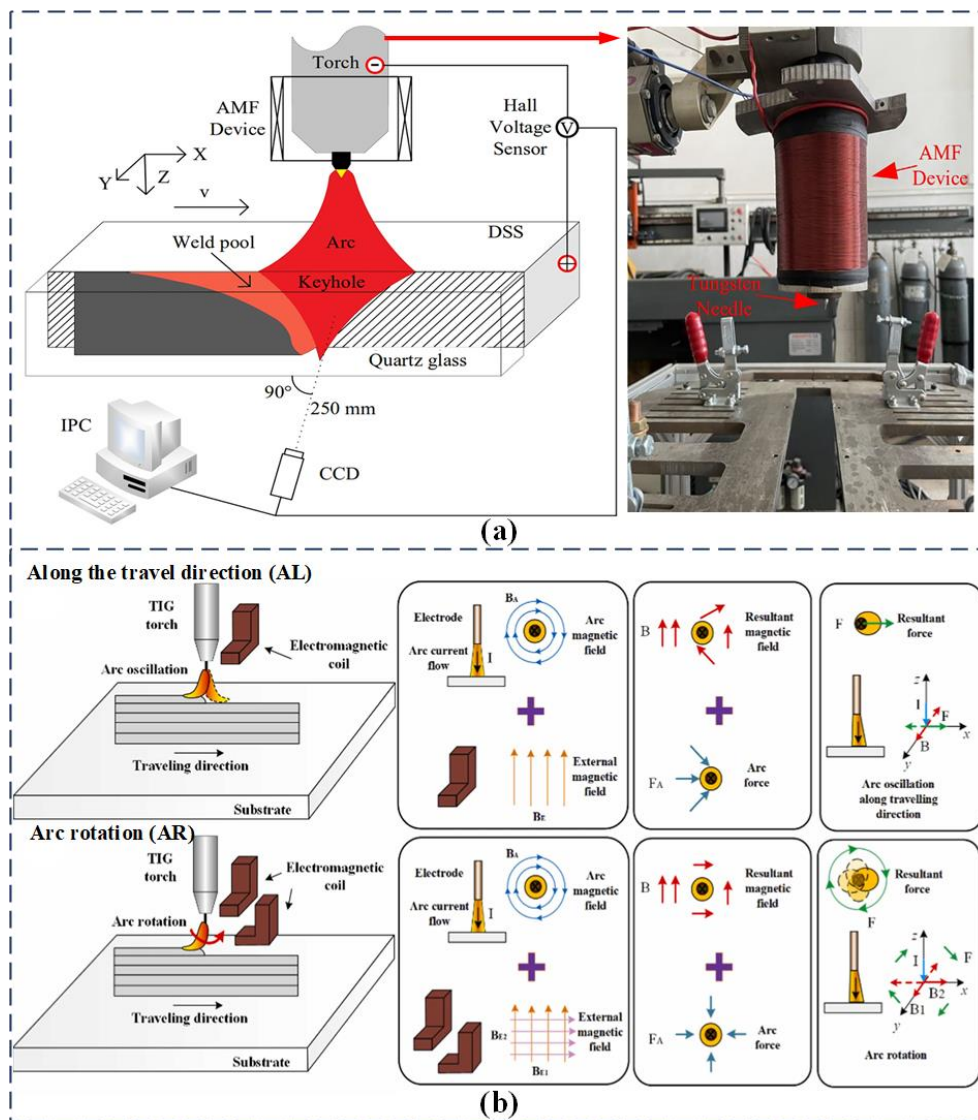


Fig. 29. (a) Schematic of the experimental system of magnetic field-assisted wire-arc direct energy deposition [119]. (b) Schematic illustration of the magnetic oscillation mechanism and resultant force on the arc for AL and AR [123].

By using an **alternating** magnetic field assisted wire-arc DED, Bai et al. [73] successfully produced a thin-walled steel component. The application of the **alternating** magnetic field was observed to impede the melting or collapse of liquid metal at the boundary. Wang et al. [117] utilized a longitudinal static magnetic field to refine dendritic crystals, diminished the segregation of reinforcing elements, and enhanced the mechanical properties of the fabricated specimen. In a study by Corrad et al. [120], it was discovered that magnetic arc oscillations could effectively inhibit melt pool overcurrent, leading to an increased deposition uniformity and a reduced heat flow density of the plasma arc. This, in turn, minimized heat accumulation. Furthermore, Zhao et al. [38]

implemented a longitudinal alternating magnetic field to facilitate electromagnetic stirring in the wire-arc DED process for Al-Mg alloy. This innovative application induced significant alterations in the melt pool's shape and solidification behavior, leading to a notable reduction in droplet splashing, refinement of grain size, and a substantial decrease in the maximum pore size, as depicted in Fig. 30(a). Wang et al. [37] employed a self-designed external composite magnetic field (ECMF) to concurrently enhance the efficiency and forming accuracy of the wire-arc DED process for aluminum alloy. The utilization of the EMF proved instrumental in effectively reducing porosities in the single-layer specimen, as illustrated in Fig. 30(b). Two primary factors contribute to this observed phenomenon. Firstly, when subjected to the alternating electromagnetic force, the arc and the melt droplets exhibit periodic oscillations in the forward and leftward directions. This phenomenon enhances the stirring effect on the melt pool and contributes additional energy to facilitate the overflow of bubbles. Secondly, the spread ability of molten metal is significantly augmented with the assistance of EMF, resulting in an increased melt pool width and a reduction in both reinforcing and melt pool penetration depth. The diminished reinforcement and penetration serve to shorten the escape distance of bubbles, thereby increasing the likelihood of their expulsion from the melt pool.

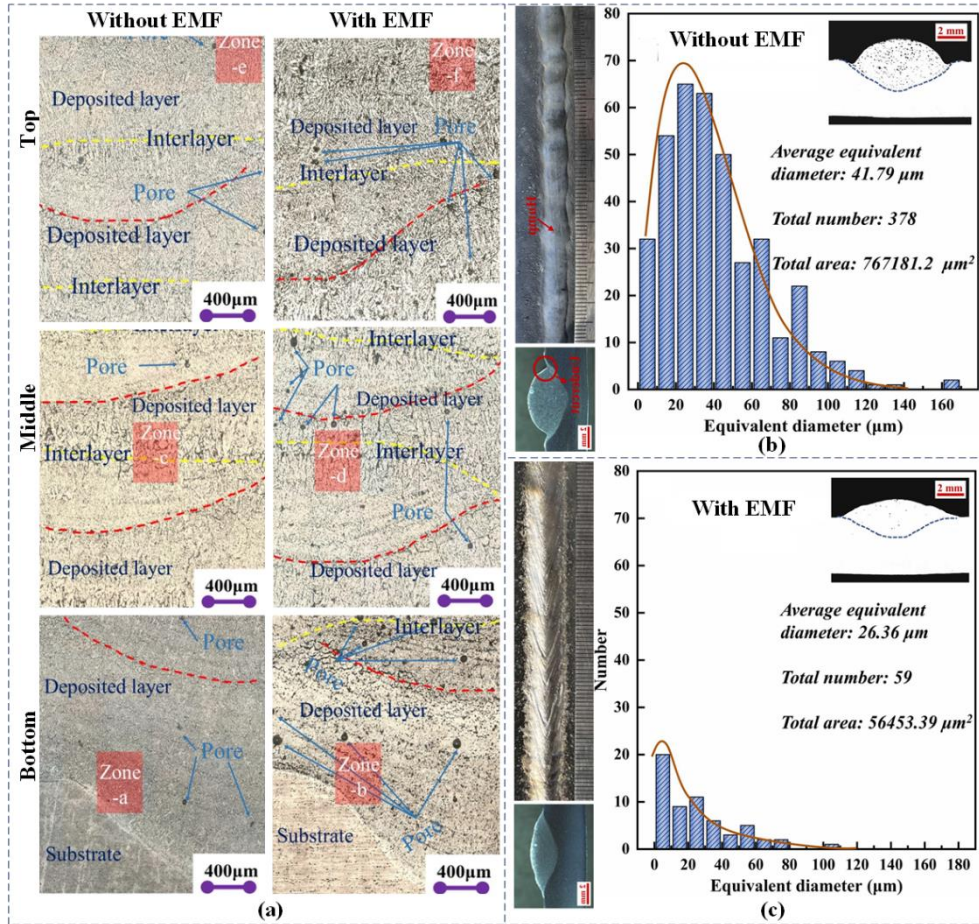


Fig. 30. (a) Microstructure of sample deposited with and without EMF [38]. (b) Deposition morphologies and the statistical results of porosity without EMF [37]. (c) Without EMF [37].

In conclusion, electromagnetic stirring emerges as the principal factor influencing both the configuration of the melt pool and the alteration of solidification behavior in the wire-arc DED process. The application of an external magnetic field plays a multifaceted role, mitigating heat accumulation through arc modification, diminishing melt pool overflow, amplifying the stirring effect on the melt pool, and supplying additional energy for bubble overflow. Simultaneously, the substantial enhancement in the spread ability of molten metal contributes to a reduction in the escape distance of gas bubbles, thereby elevating the likelihood of successful gas bubble expulsion from the melt pool.

5.2. Post-processing

5.2.1. Inter-layer rolling

The principle of inter-layer rolling in the wire-arc DED process involves applying constant pressure to the upper surface of the deposited metal by a roller during the interlayer dwell time [55].

Several investigations have demonstrated that the inter-layer rolling procedure is highly effective in enhancing residual stress and improving the microstructure in wire-arc DED aluminum alloy [124, 125]. Fig. 31(a)-31(c) depicts the experimental setup. As reported, the effectiveness of inter-layer rolling is influenced by various factors, including the roller's shape, rolling pressure, and the number of rolls applied [124, 126]. Additionally, the rolling parameters may need to be adjusted based on the layer's distance from the substrate [75]. Fig. 31(d) illustrates two different types of rollers used for specimens. The first type, "shaped" rollers, feature a grooved profile that engages with the convex top of the weld head. The second type, "slotted" rollers, incorporate a 10 mm deep slot to restrict lateral deformation of the deposited material. Slotted rollers require lubrication before rolling, and the lubricant is removed before the next layer is deposited. It's worth noting that slotted rollers might not be used to roll the first several layers because the depth of the grooves may exceed the deposited height [126].

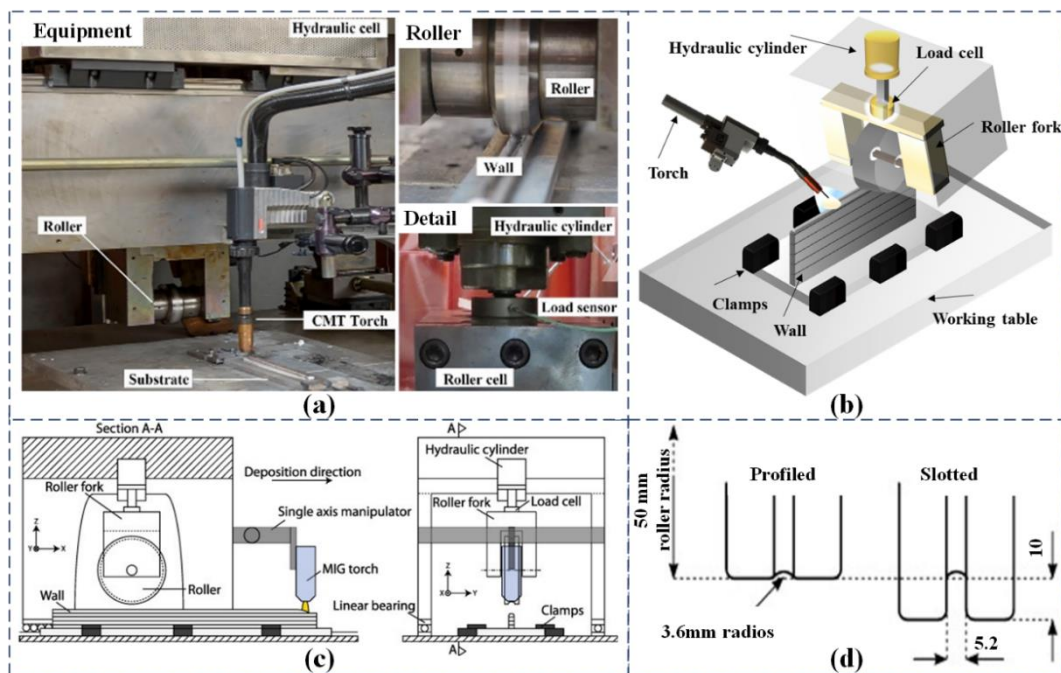


Fig. 31. (a) Experimental schematic diagram of interlayer rolling [55]. (b) Schematic diagram. (c) Planar schematic diagram [126]. (d) Roller designs applied to the wire-arc DED deposits [126].

Using 2319 and 5087 aluminum alloy wires, Gu et al. [55] fabricated straight-walled specimens with inter-layer rolling process during wire-arc DED. The impact of inter-layer rolling on the porosity of these straight-walled specimens was investigated. As seen from Fig. 32(a) and (c), rolling loads of 15 kN, 30 kN, and 45 kN were applied, resulting in varying degrees of reduction in the

number of pores in both 2319 and 5087 aluminum alloys. The x-ray diffraction tomography shown in Fig. 34(a) illustrates the distribution characteristics and individual morphology of the micropores. The results indicated that the number, volume, size, and sphericity of the micropores in the rolled alloy decreased with increasing load, ultimately achieving a final density of more than 99.9%, as depicted in Fig. 32(b).

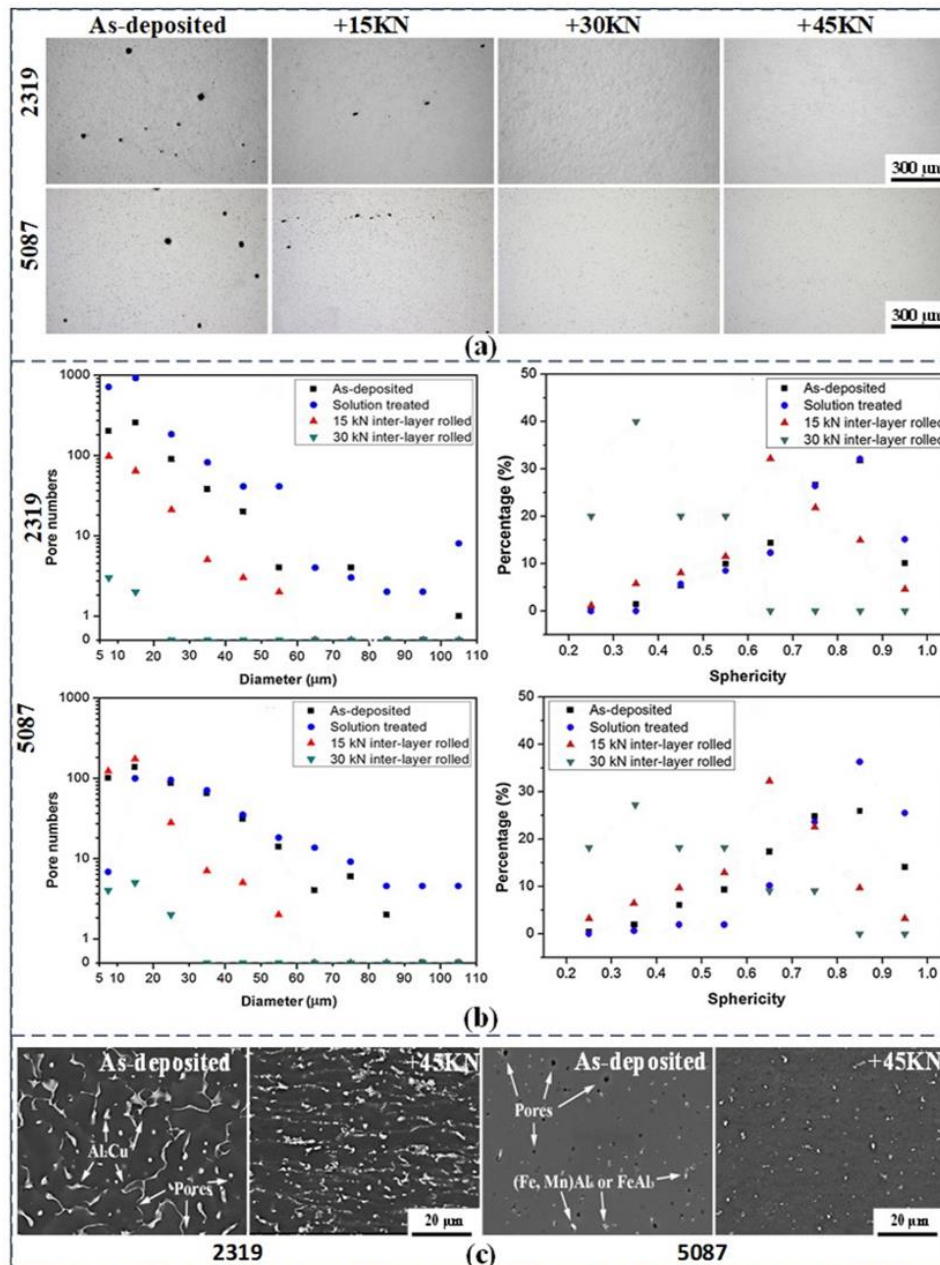


Fig. 32. (a) Optically observed porosity for the wire-arc DED Aluminum alloy with different state [55]. (b) Pore size distribution in numbers and pore sphericity distribution in percentage fraction for the as-deposited without rolling and heat treatment state, the post-deposition heat treated state, the 15 kN and 30 kN inter-layer rolled states [55]. (c) Electron microscopy scanned microstructures and pores for different state [55].

Fig. 33(a) displays optical images of fractured tensile specimens of 2319Al deposited specimens over 2219Al substrate under different processes. Fig. 33(b) exhibit the tensile fracture surfaces, revealing that the fracture surfaces of the rolled specimens are characterized by roughness and numerous defects. However, the porosity in the rolled specimens is considerably lower compared to the deposited samples [39]. Xie et al. [17] also successfully reduced pore defects in Al-Mg alloys using the hybrid in situ rolled wire-arc DED technique.

Emier et al. [75] conducted an investigation into the effect of inter-layer cold working on 2024 aluminum alloys, shown in Fig. 33(c). They found that inter-layer rolling significantly reduced the porosity level in specimens printed by the CMT-P and CMT-PA processes. In both processes with inter-layer rolling, pores were observed to be mainly appeared at the edge of the nearby wall. This is likely due to the uneven pressure distribution and strain field during rolling. Fig. 33(d) illustrates the number of pores per 100 mm³ as a function of pore volume. It shows that when the pore volume is large, the number of detected pores decrease sharply, and large porosities are detected only in the unrolled material. Thus, inter-layer rolling substantially reduces the number of porosities of all sizes.

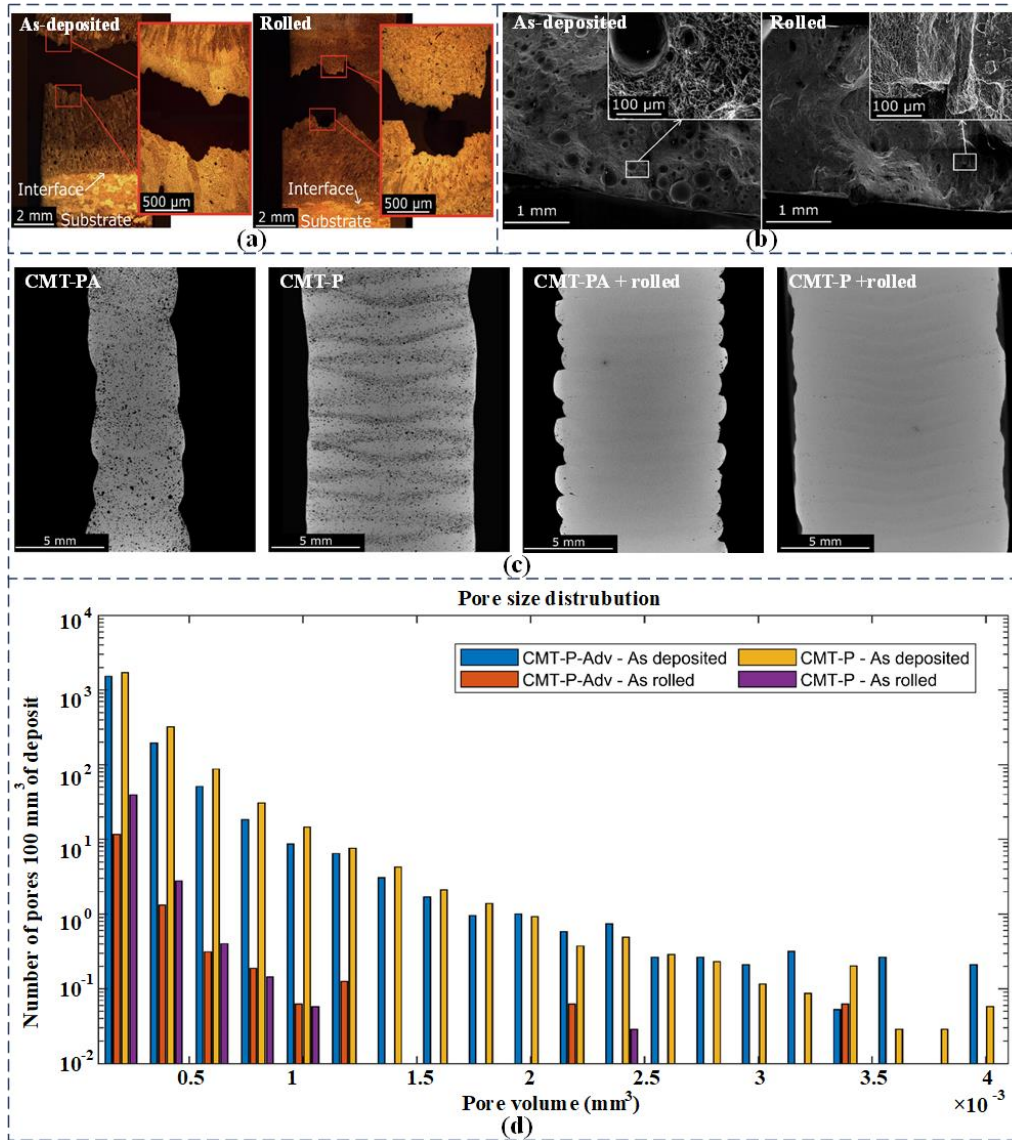


Fig. 33. (a) Optical images of broken tensile specimens representative [39]. (b) Fracture surface of specimens [39]. (c) Porosity detected by 3D tomography in a 5 mm thick cross section of material [75]. (d) Pore volume distribution [75].

Pore reduction after inter-layer rolling is mostly achieved through plastic deformation of the deposited material [74, 126]. According to the results shown in Fig. 34(b), as the applied load intensifies, the pore progressively transforms into an oblate or closed shape. The rate of pore closure is associated with the amount of alloy deformation and the size of the pore, with some dependence on the contact pressure or rolling pressure [53]. Higher rolling forces lead to greater alloy deformation and more complete pore closure. Most of the hydrogen originally present in the pore is absorbed in the dislocations, voids, and other defects created during inter-layer rolling, and it escapes through the dislocation ducts attached to the metal surface [70]. Fig. 32(a) demonstrates

that when a rolling force of 45kN is applied, with sufficient rolling loads, porosity cannot be observed by optical microscopy [55]. Furthermore, the relative depth of the pore from the stressed surface of the sample influences the effectiveness of pore closure [55, 127]. **After the interlayer rolling process, pores located close to the surface of the specimen and shallow internal pores undergo significant deformation, often adopting a flattened shape or even disappearing entirely. Conversely, pores situated near the substrate, which are located further away from the surface and have surpassed the plastic deformation region, exhibit minor changes in both pore morphology and pore number.**

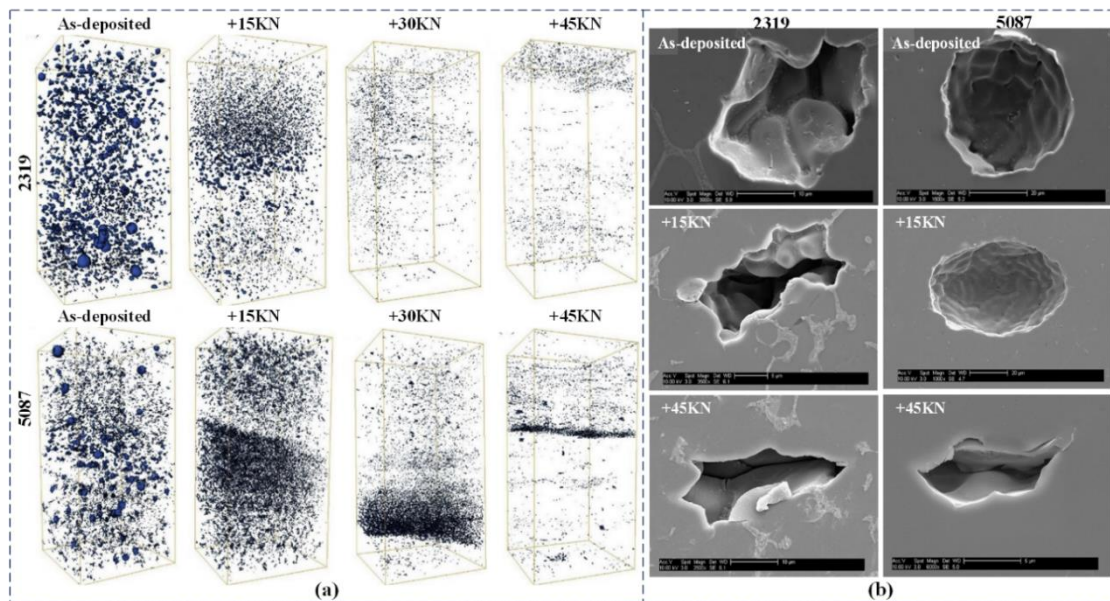


Fig. 34. (a) 3D view of micropores in wire-arc DED 2319 and 5087 alloy [53]. (b) Inner morphology of pores in the aluminum alloy [55].

To summarize, inter-layer rolling is an effective method for reducing porosity in wire-arc DED components and optimizing their structural properties. However, the extent of improvement can be influenced by factors such as the roller materials, roller shape, and rolling process parameters (load, temperature, and rate) [126]. Therefore, when implementing inter-layer rolling processes for complex wire-arc DED components, it's essential to optimize roller shape and process path to achieve specimens with lower porosity rates.

5.2.2. **Inter-layer** friction stir processing

Friction Stir Processing (FSP) is a new material processing technology based on Friction Stir Welding (FSW) [128-130]. The method employs a distinctive cutting tool to treat the surface of additively manufactured or other sample parts. A high-speed rotating stirring head is inserted into

the specimen, and the sample is heated to a thermoplastic state through the friction generated between the stirring needle (the shoulder of the stirring head) and the surface (the interior) of the workpiece [131]. By following specific commands and using reasonable parameters, the stirring head is operated to heat the metal at the front through friction, causing it to become thermoplastic and flow to the rear. The thermoplastic state of the metal is continually injected into the sample, resulting in the formation of a homogenous and compact structural component with relatively high performance. Compared to traditional processes, FSP offers advantages such as environmental friendliness and energy efficiency [40, 41, 132]. Currently, interlayer FSP is primarily used for grain refinement, preparation of wear-resistant surface materials, and elimination of defects within the material [131, 133-135]. Fig. 35(a) displays the experimental schematic.

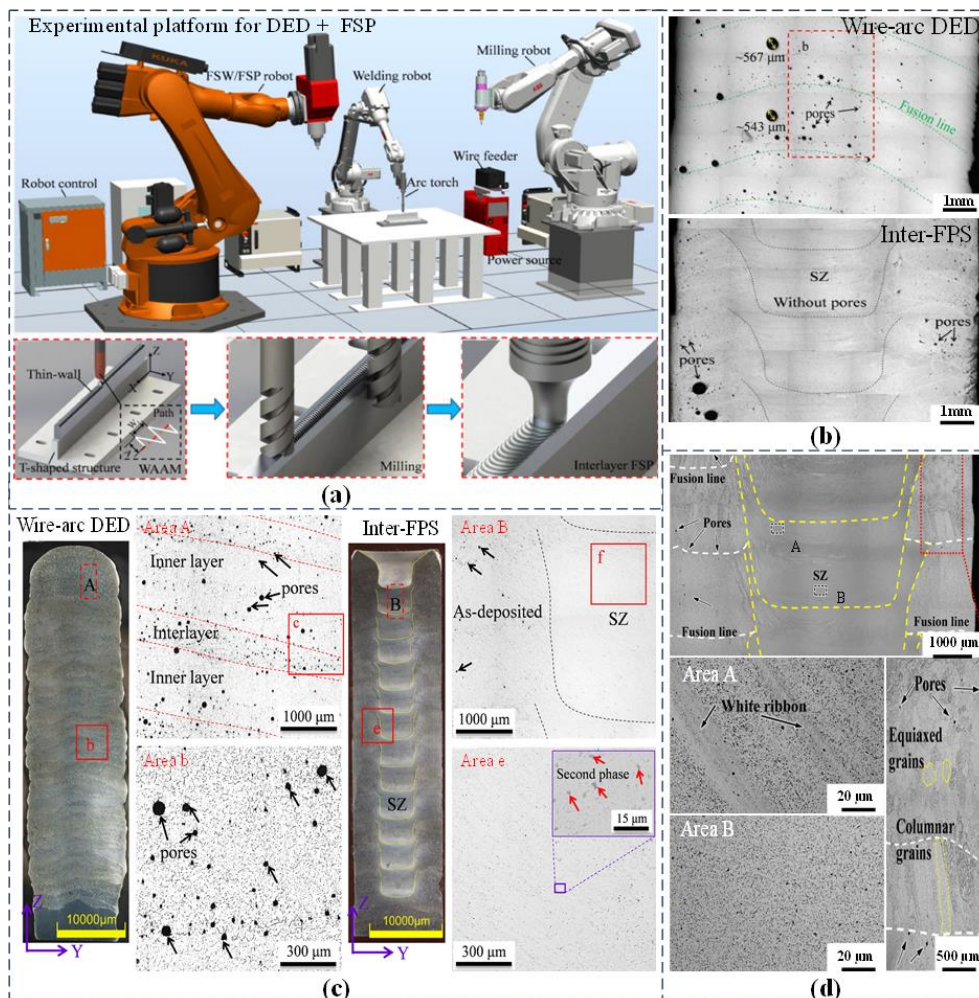


Fig. 35. (a) Schematic diagram of the wire-arc DED + interlayer FSP hybrid additive manufacturing [18]. (b) Pores distribution in the wire-arc DED and wire-arc DED + interlayer FSP Al-Si alloy [18]. (c) Macrostructure and porosity of the thin wall [40]. (d) Macro- and microstructure of XOZ section of the wire-arc DED + interlayer FSP

component [79].

The application of FSP has been demonstrated to refine, homogenize, densify, and alloy the surface structure of materials in numerous experiments [135, 136]. Yu et al. [91] observed that interlayer FSP significantly refined the grain size of wire-arc DED Aluminum alloy 2319 parts and eliminated internal defects. He et al. [18] used interlayer FSP to assist wire-arc DED 4043Al-Si alloy and found that the introduction of FSP between layers effectively eliminated pores, leading to significant improvements in ductility and fatigue properties. In their study, the pores in the wire-arc DED specimen were primarily concentrated near the fusion line, as shown in Fig. 35(b). The interlayer FSP deformation process subjected the deposited metal to high temperature and pressure, resulting in no visible porosity within the effective region of the produced specimen. These findings align with the measurements obtained through x-ray computed tomography by Zhao et al. [132].

Through the use of interlayer FSP, Wei et al. [40] successfully eradicated the presence of pore flaws in the deposited materials of 2219 aluminum alloy, resulting in enhanced mechanical properties of the components. As can be seen in Fig 35(c), prior to FSP, the thin walls prepared by wire-arc DED exhibited a periodic laminar structure divided into two regions, the inner layer and the middle layer, with a significant number of pores in the deposited material. The average porosity of the wire-arc DED aluminum alloy was calculated to be 1.1%, with a greater pore density in the interlayer region. However, after the introduction of interlayer FSP, the thin-wall macroscopic morphology exhibited a new distribution of lamellar structure, and the porosity in and around the stirring zone (SZ) was eliminated.

In Al-Zn alloys, Qie et al. [79] similarly found that interlayer FSP effectively eliminated metallurgical pore defects in the deposition zone and refined coarse columnar grains into fine equiaxial crystals, as in Fig. 35(d). This result was attributed to interlayer FSP, which removes the porosity concentrated at the top and top of the arc of the cladding metal. Additionally, it prevented surface oxides from being drawn into the melt pool, thus reducing the formation of hydrogen pores. Consequently, the number of pores in the AZ, especially interlayer pores, was significantly reduced when compared to the conventional microstructure obtained by wire-arc DED.

In summary, interlayer Friction Stir Processing (FSP) softens the material by generating frictional heat through the high-speed rotating stirring needle. The intense stirring action of the stirring head leads to plastic deformation, mixing, and crushing of the processed material. This

process effectively removes porosity concentrated at the top and eliminates surface oxides on the cladding metal, resulting in a reduction in porosity. Interlayer FSP thus plays a crucial role in improving the material's overall quality and reducing porosity defects.

Nevertheless, the utilization of inter-layer rolling and inter-layer friction stir processing techniques to produce intricate features and slender cantilever components with minimal radii of curvature is constrained by the significant plastic deformation involved. In response to the manufacturing challenges posed by progressively intricate components, scholars have investigated diverse interlayer reinforcement methodologies within wire-arc DED processes. Noteworthy approaches encompass Ultrasonic Peening Treatment (UPT), Laser Shock Peening (LSP), and Hot Isostatic Pressing (HIP).

5.2.3. Ultrasonic peening treatment

Ultrasonic Peening Treatment (UPT) is a technique used to enhance the strength of workpieces by subjecting their surfaces to high-frequency impacts. The technology operates using high-power ultrasonic waves, which transform electrical energy into high-frequency vibrations (20~55kHz) with a specific amplitude (20~50um) using a transducer. An amplifier further intensifies and focuses this energy before propelling an impact needle to strike the surface of the metal material. This process induces plastic deformation in the surface of the material and brings about beneficial effects such as the closure of pores, refinement of grain structure, and the enhancement of residual compressive stress [42, 137, 138]. The experimental setup is depicted in Fig. 36(a), while Fig. 36(b) illustrates the underlying experimental principles.

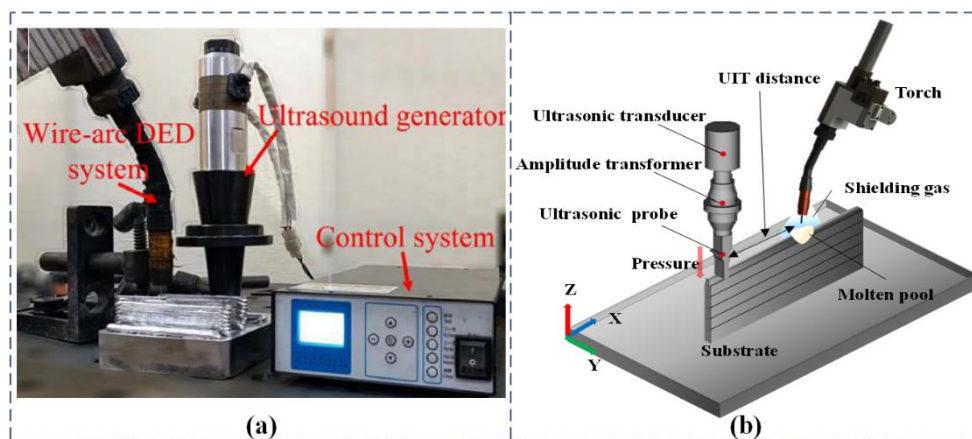


Fig. 36. (a) UTP experimental equipment drawing. (b) Schematic diagram of ultrasonic impact.

As depicted in Fig. 37(a) and detailed in Table 2, Wu et al. [139] conducted a study using

interlayer UPT on wire-arc DED 2219 Al alloy. Their research revealed that as the number of impacts increased, the number of pores, the average diameter of pores, and the roundness of the components decreased. Furthermore, some of the smaller diameter pores closed directly. This aligns with the findings reported by Guo et al. [138] in Ti6Al-4V alloy. The UPT induced plastic deformation in the deposited layer material and facilitated the partial transfer of ultrasonic energy in the form of vibrations into the liquid melt pool [140, 141]. This process resulted in improved surface characteristics and a reduction in porosity in the wire-arc DED components.

In the case of 4043 aluminum alloy, Tian et al. [43, 142] employed a layer-by-layer UPT technique after the solidification alloy to enhance the quality of aluminum alloy components. As depicted in Fig. 37(b), following the application of UPT, the spherical cavities experienced compressive deformation, resulting in a decrease in both the number of pores and the porosity of the specimen. Additionally, the grains on the metal surface exhibited significant refinement. Fig. 37(c) demonstrates the internal pore analysis of the deposited part using Matlab software, and Table 3 quantifies the pores while also calculating the percentage of pore area. The efficacy of the layer-by-layer UPT in pore elimination is also influenced by the location of the pores, as illustrated in Fig. 38. Following the UPT, the pores in Zone A (near the surface of the sedimentary layer) were severely compressed and in some cases even disappeared. In Zone B (located within the sedimentary layer), the pores underwent significant deformation and no longer retained their round or oval shape, appearing instead as flattened structures. In Zone C (close to the Partially Melted Zone), which is relatively distant from the UPT and beyond the range of plastic deformation, the morphology and the number of pores did not undergo significant changes [142].

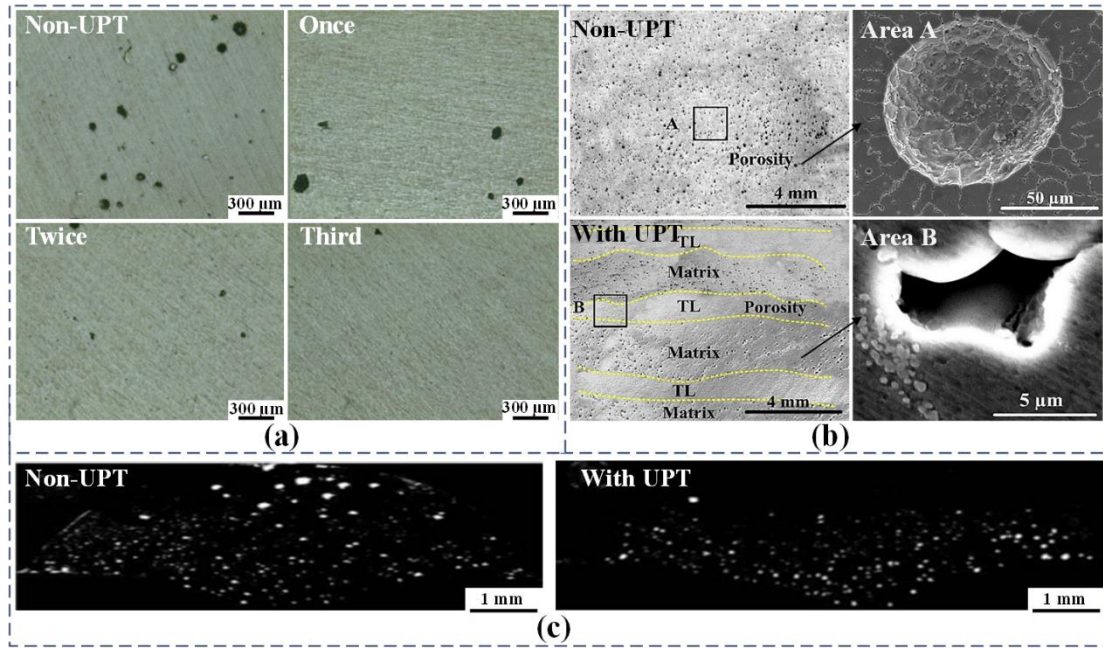


Fig. 37. (a) Pores in the samples with the different interlayered ultrasonic peening times [139]. (b) Porosity of components with different state [43]. (c) Morphology of pores extracted by Matlab software [142].

Table. 2. Pores of samples with the different interlayered ultrasonic peening times [139].

Index	NO-UTP	Once	Twice	Third
Number of pores (N)	986	856	785	679
Average diameter (μ m)	41	34	28	19
Porosity (%)	0.95	0.83	0.78	0.62
Degree of sphericity	0.86	0.75	0.71	0.66

Table. 3. Analysis results of porosity for welding seam of UPT and non-UPT [142].

Treatment	Porosity area percentage P (%)	Porosity number (N)
Non-UPT	4.3	770
UPT	2.31	420

Meanwhile, both the UPT amplitude and the location of UPT have an impact on the distribution of pores and the overall porosity of wire-arc DED aluminum alloy. Under the effect of repetitive local compressive deformation of UPT, the internal equilibrium structure of the pores is disrupted, and the internal hydrogen molecules re-enter the aluminum matrix. This process effectively closes the pores [143]. Consequently, the combination of specific UPT parameters can significantly reduce the porosity in wire-arc DED aluminum alloy components, contributing to enhanced component quality.

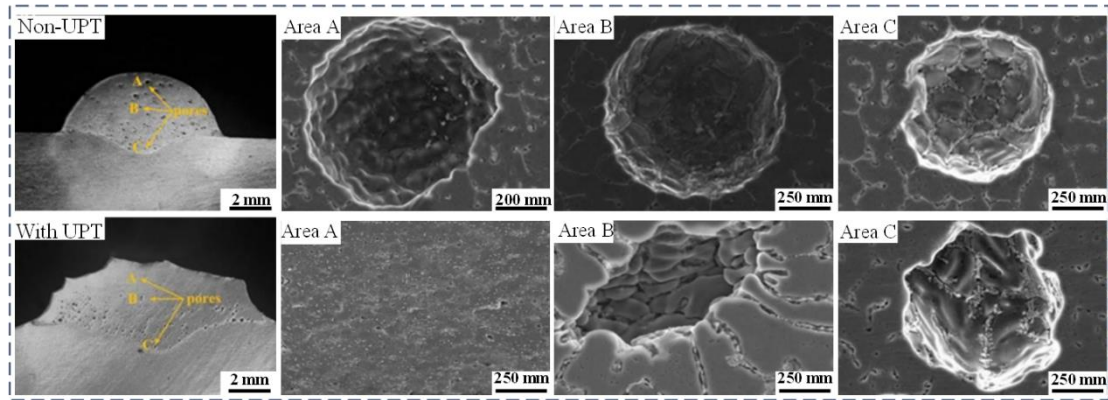


Fig. 38. Morphology of porosity with Non-UPT and with UPT [142].

In conclusion, interlayer UPT induces plastic deformation on the surface of the deposited layer, leading to an effective reduction in both the diameter and number of pores in wire-arc DED aluminum alloy components. It has also been suggested that the strengthening effect of UPT primarily stems from the combined influence of the impact process and ultrasonic oscillation [144]. This method represents an efficient approach to material strengthening by harnessing the synergistic effects of high-frequency impacts and UPT oscillations under high strains. It can yield favorable results even with relatively small applied loads(30-50N).

5.2.4. Laser shock peening

Laser Shock Peening (LSP) stands out as an advanced surface modification technology. The fundamental principle involves the application of a short pulse (on the order of nanoseconds), high peak power density ($>10\text{W}/\text{cm}^2$) laser beam onto the surface of metal parts. This results in the absorption of laser energy by the surface layer, leading to vaporization and explosion, thereby generating a high-temperature ($>10\text{K}$) and high-pressure ($>1\text{GPa}$) plasma. Constrained by the surface confinement layer, this plasma forms a high-pressure shock wave, inducing macroscopic plastic deformation in the surface material and microstructural alterations within the material [145, 146]. In comparison to alternative surface strengthening techniques, the stress induced by LSP can attain gigapascal levels within mere nanoseconds, providing LSP with a substantial depth of influence and virtually negligible deformation [45]. LSP exhibits exceptional flexibility in process design as it avoids direct contact with the workpiece, enabling precise control of the laser source [44]. Moreover, LSP demonstrates comprehensive performance benefits, including reduced deformation [147], optimized microstructure [148], pore elimination [149], and enhanced material resistance to fatigue [150], wear, and stress corrosion [151]. The experimental principle is illustrated

in Fig. 39.

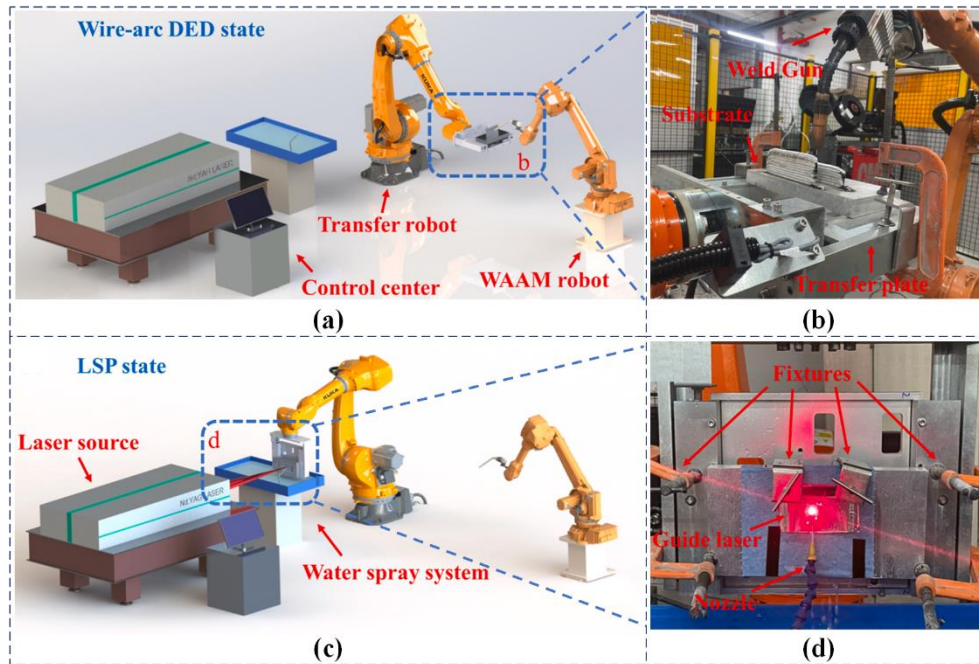


Fig. 39. Wire-arc DED +LSP equipment: (a) (b) wire-arc DED process; (c) (d) LSP process [44].

Employing LSP in combination with wire-arc DED, Sun et al. [32] observed that LSP had the capacity to diminish the grain size and optimize the residual stress distribution of 2319 aluminum alloys. Additionally, Jing et al. [44] introduced in-situ interlaminar LSP in the wire-arc DED 2319 aluminum alloy process. Illustrated in Fig. 40(a) and (b), the study revealed a remarkable reduction of 73.9% in the number of porosities and an 87.4% decrease in the total area of porosities in the LSP-treated interlayer samples compared to the deposited samples. Notably, LSP effectively reduced the number of porosities across various size categories. The LSP-treated samples, influenced by the combined factors of thermal input and dislocation density, formed a tightly knit metallurgical boundary around closed porosities, leading to enhanced strength and plasticity of the samples. Illustrated in Fig. 40(c) and (d), Huang et al. [45] conducted LSP on the surface of wire-arc DED 2319 aluminum alloy, creating an impact layer with a thickness of 1.3 mm. The concentrated compressive residual stress (CRS) surrounding porosity defects resulted in a notable reduction of 65.3% in porosity number density, accompanied by the collapse of large-sized pores. This treatment led to an increase in peak hardness and yield strength of the specimens, coupled with a doubling of the fatigue life. Two primary factors contribute to these outcomes. Firstly, the inherent strength of wire-arc DED 2319 aluminum alloy is comparatively lower when contrasted with steel and nickel-based high-temperature alloys. Consequently, the high-amplitude laser waves introduced

by the laser readily rupture these porosities. Secondly, during LSP, the interior of the porosity disrupts the propagation of the shock wave, generating substantial micro-strains (stress concentrations around the porosity), as depicted in Fig. 41.

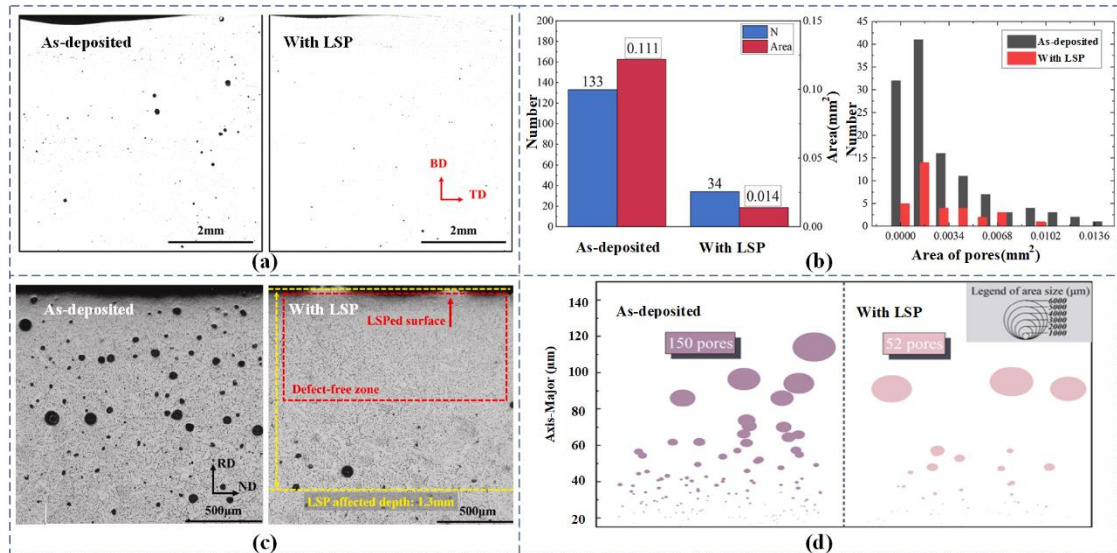


Fig. 40. (a) Cross-sectional view of pores in the different samples [44]. (b) Statistical comparison of the number and area of pores between different samples [44]. (c) Pore distribution without LSP and with LSP [44]. (d) Statistic of pore [45].

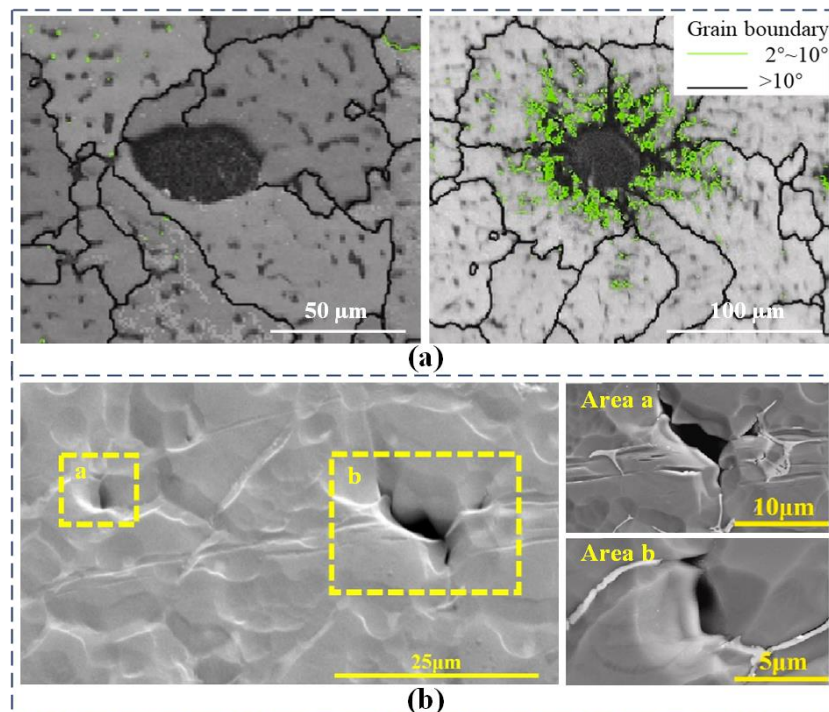


Fig. 41. (a) Using band contrast and grain boundary map to compare samples without LSP and with LSP pores [45]. (b) SEM image of collapsed pores in the near-surface zone of LSP sample [45].

In summary, LSP induces plastic deformation and residual stresses on the material surface, enhancing material properties such as microhardness, fatigue resistance, and corrosion resistance. Furthermore, the porosity defects within the material impede the propagation of the ultrasonic shock wave, leading to the generation of significant micro-strain around the porosity. Consequently, this phenomenon contributes to a reduction in specimen porosity.

5.2.5. Hot isostatic pressing

Hot Isostatic Pressing (HIP) is a prevalent heat treatment method employed for the reduction of porosity and enhancement of mechanical properties in cast metals [152]. This technique involves elevating the metal's temperature while applying isostatic pressure. Typically, a gas, such as Ar or N₂, is utilized as a medium due to its capacity for uniform pressure transfer. Hot Isostatic Pressing relies on a gaseous medium with constant pressure to uniformly exert pressure on the sintered specimen in all directions, thereby increasing specimen densities [153, 154]. In comparison with alternative sintering processes, HIP presents several advantages, including elevated specimen densities, uniformity, superior mechanical properties, abbreviated sintering cycles, concentrated processing, cost-effectiveness, and the ability to sinter complex-shaped specimens [155, 156]. The experimental principle is depicted in Fig. 42.

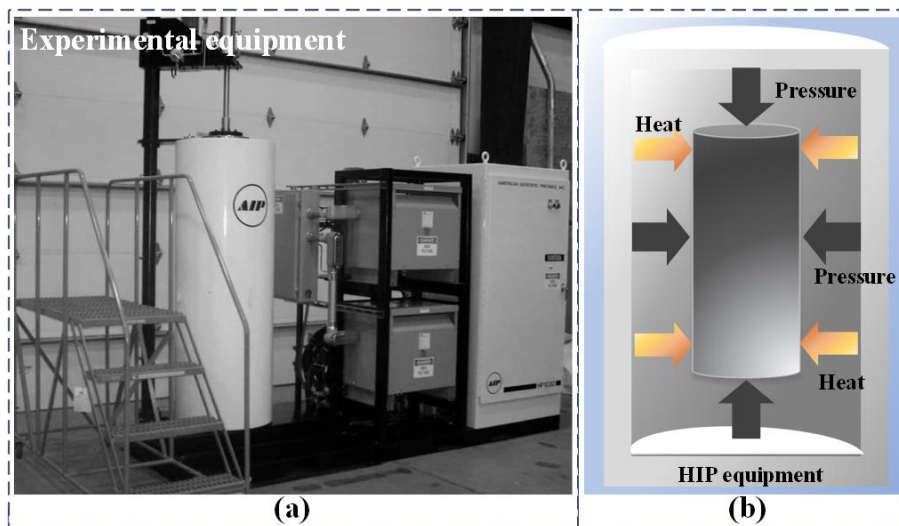


Fig. 42. Working principle diagram of HIP: (a) Equipment drawing. (b) Experimental schematic diagram.

Illustrated in Fig. 44(a), Mclean et al. [47] employed the Hot Isostatic Pressing (HIP) technique to mitigate the inherent challenges of porosity and lack of fusion in the wire-arc DED aluminum alloy process. Employing micro 3D computed tomography, they systematically investigated the process of porosity regeneration in specimens during HIP solution treatment and aging. Their study

revealed a substantial 95% reduction in overall porosity following the HIP process in comparison to the deposited samples. Gussev et al. [46] conducted an investigation into the impact of HIP on ultrasonically assisted forming specimens of 6061 aluminum alloy. Utilizing tensile testing and microstructure characterization, they observed successful closure of several porosities and an enhancement in tensile ductility following the HIP process, as depicted in Fig. 43(b). This improvement was attributed to the dual-phase action of plastic deformation and high-temperature creep on pore defects within the specimen during the HIP process, leading to a reduction in specimen porosity [156]. **Plastic deformation in this context refers to the destruction of internal pores and defects that result in the contact of internal surfaces as the specimen undergoes high temperatures and pressures within the HIP device, when the external pressure surpasses the material strength at elevated temperatures.** High-temperature creep occurs when the external pressure is lower than the high-temperature strength of the material, causing the plastic flow of the sample to cease. During this stage, mutual penetration, diffusion, and adhesion take place between the internal surfaces that came into contact during the plastic deformation stage, thereby eliminating defects and porosity [156].

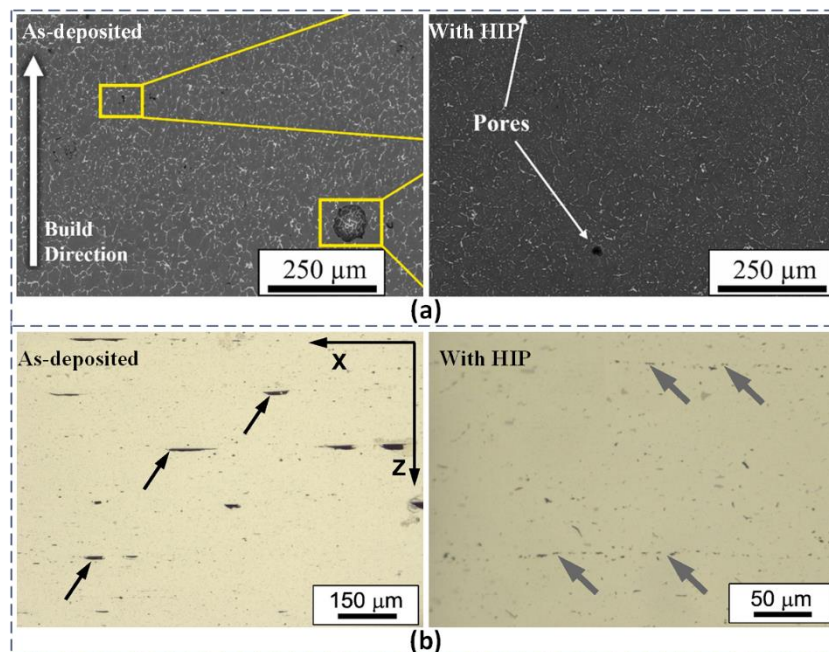


Fig. 43. (a) SEM images of Al 2319 produced by different state [47]. (b) Structure of the UAM-produced material [46].

In summary, the Hot Isostatic Pressing (HIP) process involves two essential phases—plastic deformation and high-temperature creep—acting on the porosity defects within the wire-arc DED

specimen. This dual-phase mechanism effectively facilitates the healing process of porosity, resulting in increased density of the specimen.

The rapid advancements in additive manufacturing and plastic deformation composite manufacturing have led to the development of various new processes aimed at reducing porosity defects in wire-arc DED aluminum alloys. These innovations have set the stage for further advancements in the preparation of high-strength aluminum alloys.

6. Conclusions and outlook

6.1. Conclusions

The porosity defects in wire-arc DED aluminum alloy are primarily linked to the disparity in hydrogen solubility in the liquid and solid phases of the alloy, as well as variations in the volume of liquid and solid phases during the solidification and shrinkage of the aluminum alloy. Different wire-arc DED processes, arc modes, process parameters, and shielding gas environments can impact the morphology and quantity of porosity in the final product. Adjusting the heat input and changing the shielding gas environment have proven effective in reducing tissue inhomogeneity and mechanical property anisotropy in wire-arc DED aluminum alloy, leading to significant improvements in pore defects. Composite manufacturing processes like **laser-arc hybrid additive manufacturing, ultrasonic vibration assistance, external magnetic field, inter-layer rolling, inter-layer friction stir processing, ultrasonic peening treatment, laser shock peening and hot isostatic pressing** have also demonstrated their ability to reduce porosity in additive components. The following are the conclusions:

(1) Porosity defects in wire-arc DED aluminum alloys can be clarified as three types: (I) gas pores (hydrogen porosity and shielding gas pores), (II) shrinkage cavities and (III) porosity formed by the evaporation of low-boiling elements (Mg, Li, Zn). Hydrogen, with its substantial solubility difference between the liquid and solid phases of aluminum alloys, is the primary reason for the formation of hydrogen pores, making up the majority of porosity defects in wire-arc DED aluminum alloys. These hydrogen pores often exhibit an interlayer distribution characteristic. Shielding gas pores are more likely to appear when the shielding gas is impure, or the wire dry extension length is too long. Shrinkage cavities primarily occur due to the volume difference between the solid and liquid phases during the alloy's solidification. The porosity resulting from the loss of elements is

also a significant concern due to its impact on mechanical properties.

(2) Porosity defects can be minimized or eliminated by both in-process optimization (e.g., heat input control, shielding gas) and post process treatments (e.g., HIP). In-process optimization can be achieved by effectively reducing heat input, i.e. decreasing the power supply current and wire feeding speed, while increasing the travel speed. Additionally, a properly handling of the interlayer temperature, the length of the dry depth of the wire material, and different arc modes can reduce porosity defects. Furthermore, the porosity in wire-arc DED aluminum alloy can also be minimized by changing shielding gas composition, shielding gas flow rate, and shielding gas purity. Similarly, post processing with heat treatment can also lead to the aggregation of micropores due to thermal stresses generated at high temperatures, resulting in an increase in both the total volume and size of micropores. The three primary mechanisms of this evolution include hydrogen micropore precipitation, phase particle dissolution, and micropore growth. Heat treatment plays a crucial role in altering the characteristics of micropores in the material.

(3) Porosity defects can be improved by hybrid wire-arc DED processes. Processes like laser-arc hybrid additive manufacturing, ultrasonic vibration assistance and external magnetic field enhance the flow of liquid metal in the melt pool, which helps facilitate the escape of internal bubbles. Additionally, the anode spot effect of the laser stabilizes the arc and effectively reduces porosity in aluminum alloy specimens. Techniques such as inter-layer rolling, inter-layer friction stir processing, ultrasonic peening treatment, laser shock peening and hot isostatic pressing aim to reduce porosity through plastic deformation of the deposited material. These methods contribute to improving the material's overall quality by reducing pore defects.

6.2. Outlook

As depicted in Fig. 44, addressing the porosity defects in wire-arc DED aluminum alloy components necessitates a multifaceted approach. This entails meticulous control and assurance of the quality of raw materials, specifically the aluminum alloy wire utilized. Furthermore, the determination and optimization of process parameters, the continual exploration of innovative multi-processes, and the deployment of intelligent, integrated, and high-efficiency customized equipment. These approaches are imperative to surmount the porosity challenges in extant processes.

Concomitantly, the establishment and development of a comprehensive theoretical knowledge system are imperative. This knowledge system aims to elucidate the scientific underpinnings

governing the formation of porosity in wire-arc DED aluminum alloys. By doing so, it not only seeks to unravel the intricacies of porosity formation but also endeavors to furnish a robust theoretical foundation for mitigating porosity in these alloys.

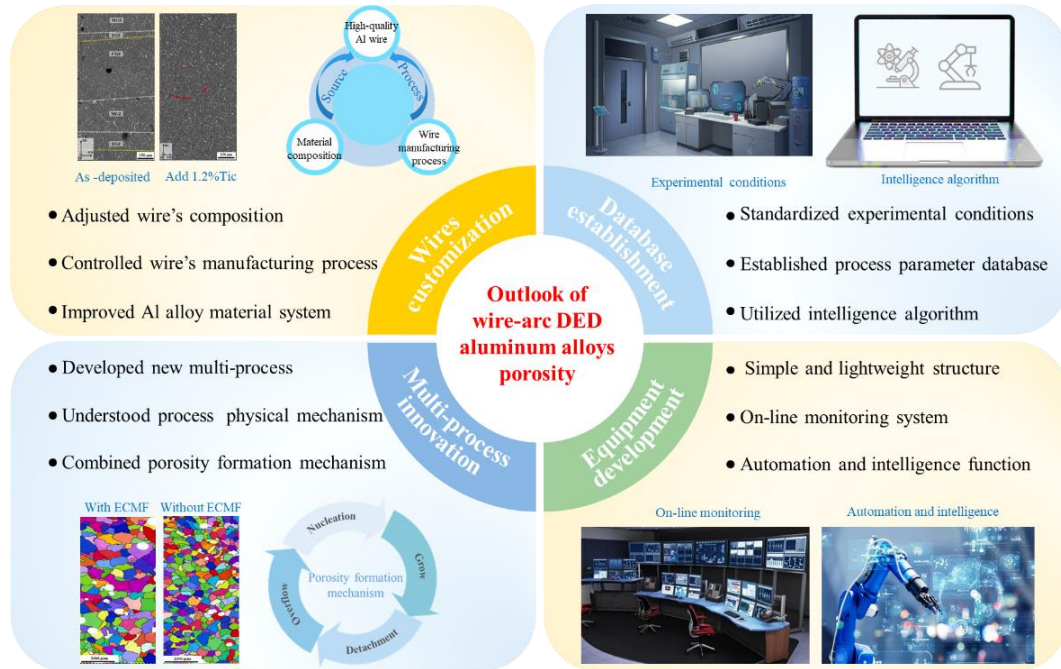


Fig. 44. Outlook of wire-arc DED aluminum alloys porosity reduction.

(1) Enhancing the quality of aluminum (Al) alloy wires is instrumental in mitigating hydrogen-related issues in aluminum alloys, thereby minimizing the occurrence of hydrogen porosity. The inherent properties of Al alloys, specifically the variation in hydrogen solubility between liquid and solid phases, along with the differences in volume during solidification and shrinkage, contribute significantly to the formation of hydrogen pore and shrinkage cavity throughout the forming process. A prospective avenue for addressing these challenges involves modifying the material composition of Al alloys. This may encompass judicious additions of trace elements, such as manganese and copper, to alter the hydrogen solubility characteristics. The establishment of a comprehensive wire-arc DED specialized aluminum alloy material system is paramount. Rigorous control over the Al wire manufacturing process is essential to realize the production of high-quality Al wires. These approaches facilitate a substantial amelioration of pore defects within the fabricated components.

(2) Owing to variations in experimental conditions and equipment across studies, replicating optimal process parameters, yielding low porosity and high performance achieved in prior research, is challenging. Consequently, it is crucial to develop standardized experimental conditions.

Meanwhile, establishing a systematic "process parameters-specimen porosity" relationship database holds great potential for predicting and optimizing pore defects in wire-arc DED aluminum alloy specimens. To enhance the efficacy of this database, an integration of extensive data is undertaken, leveraging intelligent algorithms such as machine learning and neural networks. These advanced techniques facilitate the prediction of optimal process parameters for achieving low porosity and superior mechanical properties under specific conditions. Furthermore, the database operates in real-time, ensuring dynamic updates as new data becomes available. This continuous refinement serves as a foundational resource for informed decision-making in the pursuit of fabricating large and intricate aluminum alloy components with minimal porosity.

(3) The incorporation of a multi-process into wire-arc DED emerges as an effective strategy for porosity reduction in aluminum alloy specimens. The ongoing exploration and advancement of novel multi-process methodologies, coupled with a profound comprehension of the underlying physical mechanisms intrinsic to these processes, establish a robust theoretical framework for porosity reduction and the enhancement of quality and performance in manufactured components. Illustratively, within the realm of multi-energy field coupling forming technology, a meticulous examination of the distribution of individual energy fields is imperative. Equally crucial is an understanding of the mechanisms arising from the coupling effect, superposition effect, and the interactions between diverse energy fields. By integrating these insights with a comprehensive grasp of the formation mechanisms of porosity in aluminum alloys, a nuanced exploration ensues, discerning their collective influence on the genesis of porosity in aluminum alloy components.

(4) Harnessing technological innovation, the imperative lies in designing highly efficient equipment that integrates sensing, monitoring, and feedback functionalities, thereby propelling the continuous industrialization of high-quality aluminum alloys. Confronting the challenge of accurately controlling pore formation and distribution during the aluminum alloy forming process, the development of systems and equipment featuring online monitoring capabilities is paramount. This entails the incorporation of sensor and detection systems to facilitate signal acquisition and real-time feedback. Such systems enable precise control over the forming process or post-processing stages. For instance, during the forming process, simultaneous implementation of extra conditions for melt pool bubble generation can be executed to mitigate pore formation. In post-processing, focused treatment strategies can be employed to address formed pores. The deployment of

automated, intelligent, and efficient custom equipment emerges as a pivotal assurance in reducing porosity in aluminum alloy specimens and ensuring superior forming quality. It is also a pivotal developmental trend in wire-arc DED aluminum alloys.

Acknowledgements

This work was supported by the National Natural Science Foundation of China (52375306), Joint Fund of Ministry of Education for Equipment Pre-research (8091B032107).

References

- [1] S. Fan, X. Guo, Z. Li, J. Ma, F. Li, Q. Jiang, A review of high-strength aluminum-copper alloys fabricated by wire arc additive manufacturing: microstructure, properties, defects, and post-processing, *J. Mater. Eng. Perform.* 32 (2023) 8517-8540.
- [2] S. Thapliyal, Challenges associated with the wire arc additive manufacturing (WAAM) of aluminum alloys, *Mater. Res. Express.* 6 (2019) 112006.
- [3] G.C. Liu, J. Xiong, L. Tang, Microstructure and mechanical properties of 2219 aluminum alloy fabricated by double-electrode gas metal arc additive manufacturing, *Addit. Manuf.* 35 (2020) 101375.
- [4] M.S. Kenevisi, Y.F. Yu, F. Lin, A review on additive manufacturing of Al-Cu (2xxx) aluminium alloys, processes and defects, *Mater. Sci. Technol.* 37 (2021) 805-829.
- [5] C.R. Cunningham, J.M. Flynn, A. Shokrani, V. Dhokia, S.T. Newman, Invited review article: Strategies and processes for high quality wire arc additive manufacturing, *Addit. Manuf.* 22 (2018) 672-686.
- [6] G. Langelandsvik, O.M. Akselsen, T. Furu, H.J. Roven, Review of aluminum alloy development for wire arc additive manufacturing, *Materials.* 14 (2021) 5370.
- [7] J. Xiong, C.F. Wen, Arc plasma, droplet, and forming behaviors in bypass wire arc-directed energy deposition, *Addit. Manuf.* 70 (2023) 103558.
- [8] B.O. Omiyale, T.O. Olugbade, T.E. Abioye, P.K. Farayibi, Wire arc additive manufacturing of aluminium alloys for aerospace and automotive applications: a review, *Mater. Sci. Technol.* 38 (2022) 391-408.
- [9] J. Gu, M. Gao, S. Yang, J. Bai, J. Ding, X. Fang, Pore formation and evolution in wire + arc additively manufactured 2319 Al alloy, *Addit. Manuf.* 30 (2019) 100900.

- [10] B. Wu, Z. Pan, D. Ding, D. Cuiuri, H. Li, J. Xu, J. Norrish, A review of the wire arc additive manufacturing of metals: properties, defects and quality improvement, *J. Manuf. Process.* 35 (2018) 127-139.
- [11] F. Wang, S. Williams, P. Colegrove, A.A. Antonysamy, Microstructure and mechanical properties of wire and arc additive manufactured Ti-6Al-4V, *Metall. Mater. Trans. A.* 44 (2012) 968-977.
- [12] P. Li, P.D. Lee, D.M. Maijer, T.C. Lindley, Quantification of the interaction within defect populations on fatigue behavior in an aluminum alloy, *Acta Mater.* 57 (2009) 3539-3548.
- [13] S. Sharma, Effect of friction stir processing on fatigue behavior of A356 alloy, *Scr. Mater.* 51 (2004) 237-241.
- [14] M. Muhammad, P.D. Nezhadfar, S. Thompson, A. Saharan, N. Phan, N. Shamsaei, A comparative investigation on the microstructure and mechanical properties of additively manufactured aluminum alloys, *Int. J. Fatigue.* 146 (2021) 106165.
- [15] H. Toda, T. Hidaka, M. Kobayashi, K. Uesugi, A. Takeuchi, K. Horikawa, Growth behavior of hydrogen micropores in aluminum alloys during high-temperature exposure, *Acta Mater.* 57 (2009) 2277-2290.
- [16] J. Gu, J. Ding, S.W. Williams, H. Gu, J. Bai, Y. Zhai, P. Ma, The strengthening effect of inter-layer cold working and post-deposition heat treatment on the additively manufactured Al-6.3Cu alloy, *Mater. Sci. Eng., A.* 651 (2016) 18-26.
- [17] C. Xie, S. Wu, Y. Yu, H. Zhang, Y. Hu, M. Zhang, G. Wang, Defect-correlated fatigue resistance of additively manufactured Al-Mg4.5Mn alloy with in situ micro-rolling, *J. Mater. Process. Tech.* 291 (2021) 117039.
- [18] C. He, J. Wei, Y. Li, Z. Zhang, N. Tian, G. Qin, L. Zuo, Improvement of microstructure and fatigue performance of wire-arc additive manufactured 4043 aluminum alloy assisted by interlayer friction stir processing, *J. Mater. Sci. Technol.* 133 (2023) 183-194.
- [19] H. Mayer, M. Papakyriacou, B. Zettl, S.E. Stanzl-Tschegg, Influence of porosity on the fatigue limit of die cast magnesium and aluminium alloys, *Int. J. Fatigue.* 25 (2003) 245-256.
- [20] L. Sheridan, O.E. Scott-Emuakpor, T. George, J.E. Gockel, Relating porosity to fatigue failure in additively manufactured alloy 718, *Mater. Sci. Eng., A.* 727 (2018) 170-176.
- [21] D. Liu, D. Wu, R. Wang, J. Shi, F. Niu, G. Ma, Formation mechanism of Al-Zn-Mg-Cu alloy

fabricated by laser-arc hybrid additive manufacturing: Microstructure evaluation and mechanical properties, *Addit. Manuf.* 50 (2022) 102554.

[22] Z. Zhang, Z. Ma, S. He, G. Song, L. Liu, Effect of laser power on the microstructure and mechanical properties of 2319-Al fabricated by wire-based additive manufacturing, *J. Mater. Eng. Perform.* 30 (2021) 6640-6649.

[23] X. Fang, G. Chen, J. Yang, Y. Xie, K. Huang, B. Lu, Wire and arc additive manufacturing of high-strength Al-Zn-Mg aluminum alloy, *Front. Mater.* 8 (2021) 656429.

[24] Z. Zhu, Z. Hu, H.L. Seet, T. Liu, W. Liao, U. Ramamurty, S.M. Ling Nai, Recent progress on the additive manufacturing of aluminum alloys and aluminum matrix composites: Microstructure, properties, and applications, *Int. J. Mach. Tool. Manu.* 190 (2023) 104047.

[25] Y. Liu, Z. Liu, G. Zhou, C. He, J. Zhang, Microstructures and properties of Al-Mg alloys manufactured by WAAM-CMT, *Materials.* 15 (2022) 5460.

[26] J. Xiong, Y. Li, R. Li, Z. Yin, Influences of process parameters on surface roughness of multi-layer single-pass thin-walled parts in GMAW-based additive manufacturing, *J. Mater. Process. Tech.* 252 (2018) 128-136.

[27] C. Zhu, X. Tang, Y. He, F. Lu, H. Cui, Characteristics and formation mechanism of sidewall pores in NG-GMAW of 5083 Al-alloy, *J. Mater. Process. Tech.* 238 (2016) 274-283.

[28] J. Ding, P. Colegrove, F. Martina, S. Williams, R. Wiktorowicz, M.R. Palt, Development of a laminar flow local shielding device for wire + arc additive manufacture, *J. Mater. Process. Tech.* 226 (2015) 99-105.

[29] I. Jurić, I. Garašić, M. Bušić, Z. Kožuh, Influence of shielding gas composition on structure and mechanical properties of wire and arc additive manufactured Inconel 625, *Jom.* 71 (2018) 703-708.

[30] S. Li, L.-J. Zhang, J. Ning, X. Wang, G.-F. Zhang, J.-X. Zhang, S.-J. Na, B. Fatemeh, Comparative study on the microstructures and properties of wire+arc additively manufactured 5356 aluminium alloy with argon and nitrogen as the shielding gas, *Addit. Manuf.* 34 (2020) 101206.

[31] D. Chen, Y. Cai, Y. Luo, J. Tu, F. Tang, Analysis on the microstructure regulation based on the pulsed laser oscillating molten pool in Laser-PTA additive manufacturing, *J. Manuf. Process.* 59 (2020) 587-594.

[32] R. Sun, L. Li, Y. Zhu, W. Guo, P. Peng, B. Cong, J. Sun, Z. Che, B. Li, C. Guo, L. Liu,

Microstructure, residual stress and tensile properties control of wire-arc additive manufactured 2319 aluminum alloy with laser shock peening, *J. Alloys Compd.* 747 (2018) 255-265.

[33] D. Wu, D. Liu, F. Niu, Q. Miao, K. Zhao, B. Tang, G. Bi, G. Ma, Al-Cu alloy fabricated by novel laser-tungsten inert gas hybrid additive manufacturing, *Addit. Manuf.* 32 (2020) 100954.

[34] F. Ji, X. Qin, Z. Hu, X. Xiong, M. Ni, M. Wu, Influence of ultrasonic vibration on molten pool behavior and deposition layer forming morphology for wire and arc additive manufacturing, *Int. Commun. Heat. Mass.* 130 (2022) 105789.

[35] Y. Wu, R. Kovacevic, Mechanically assisted droplet transfer process in gas metal arc welding, *Proc. Inst. Mech. Eng., Part B.* (2002) 555-564.

[36] H. Yi, Q. Wang, W. Zhang, H. Cao, Wire-arc directed energy deposited Mg-Al alloy assisted by ultrasonic vibration: Improving properties via controlling grain structures, *J. Mater. Process. Tech.* 321 (2023) 118134.

[37] Y. Wang, J. Chen, X. Wu, M. Chen, H. Su, L. Wang, C. Wu, Investigation on high-deposition-rate directed energy deposition of Al-5%Mg alloy via external compound magnetic fields, *Addit. Manuf.* 61 (2023) 103299.

[38] W. Zhao, Y. Wei, X. Zhang, J. Chen, W. Ou, Comparative investigation of wire arc additive manufacturing of Al-5%Mg alloy with and without external alternating magnetic field, *Int. J. Adv. Manuf. Tech.* 119 (2022) 2571-2587.

[39] E. Eimer, S. Williams, J. Ding, S. Ganguly, B. Chehab, Mechanical performances of the interface between the substrate and deposited material in aluminium wire Direct Energy Deposition, *Mater. Design.* 225 (2023) 111594.

[40] J. Wei, C. He, Y. Zhao, M. Qie, G. Qin, L. Zuo, Evolution of microstructure and properties in 2219 aluminum alloy produced by wire arc additive manufacturing assisted by interlayer friction stir processing, *Mater. Sci. Eng., A.* 868 (2023) 144794.

[41] L. Zhao, J.G. Santos Macías, A. Dolimont, A. Simar, E. Rivière-Lorphèvre, Comparison of residual stresses obtained by the crack compliance method for parts produced by different metal additive manufacturing techniques and after friction stir processing, *Addit. Manuf.* 36 (2020) 101499.

[42] E.S. Statnikov, V.O. Muktepavel, Technology of ultrasound impact treatment as a means of improving the reliability and endurance of welded metal structures, *Soldag. Insp.* 17 (2003) 741-

744.

[43] Y. Tian, J. Shen, S. Hu, J. Han, Q. Wang, Y. Cai, Effects of ultrasonic peening treatment layer by layer on microstructure of components fabricated by wire and arc additive manufacturing, *Mater. Lett.* 284 (2021) 128917.

[44] Y. Jing, X. Fang, Y. Geng, Y. Duan, K. Huang, Simultaneous strength and ductility enhancement of wire-arc directed energy deposited Al–Cu alloy by interlayer laser shock peening, *Mater. Sci. Eng., A.* 887 (2023) 145699.

[45] Y. Jing, X. Fang, N. Xi, T. Chang, Y. Duan, K. Huang, Improved tensile strength and fatigue properties of wire-arc additively manufactured 2319 aluminum alloy by surface laser shock peening, *Mater. Sci. Eng., A.* 864 (2023) 144599.

[46] M.N. Gushev, N. Sridharan, Z. Thompson, K.A. Terrani, S.S. Babu, Influence of hot isostatic pressing on the performance of aluminum alloy fabricated by ultrasonic additive manufacturing, *Scr. Mater.* 145 (2018) 33-36.

[47] N. McLean, M.J. Bermingham, P. Colegrove, A. Sales, N. Soro, C.H. Ng, M.S. Dargusch, Effect of Hot Isostatic Pressing and heat treatments on porosity of Wire Arc Additive Manufactured Al 2319, *J. Mater. Process. Tech.* 310 (2022) 117769.

[48] B. Cong, J. Ding, S. Williams, Effect of arc mode in cold metal transfer process on porosity of additively manufactured Al-6.3%Cu alloy, *Int. J. Adv. Manuf. Tech.* 76 (2014) 1593-1606.

[49] B.Q. Cong, H.Y. Sun, P. Peng, B.J. Qi, G. Zhao, J.L. Ding, Porosity control of wire plus arc additively manufactured Al-6.3Cu alloy deposition using AC-GTAW process, *Rare. Metal. Mat. Eng.* 46 (2017) 1359-1364.

[50] B. Cong, X. Cai, Z. Qi, B. Qi, Y. Zhang, R. Zhang, W. Guo, Z. Zhou, Y. Yin, X. Bu, The effects of ultrasonic frequency pulsed arc on wire + arc additively manufactured high strength aluminum alloys, *Addit. Manuf.* 51 (2022) 102617.

[51] Z. Zhang, C. Sun, X. Xu, L. Liu, Surface quality and forming characteristics of thin-wall aluminium alloy parts manufactured by laser assisted MIG arc additive manufacturing, *Int. J. Lightw. MaterManuf.* 1 (2018) 89-95.

[52] C. Zhang, M. Gao, X. Zeng, Workpiece vibration augmented wire arc additive manufacturing of high strength aluminum alloy, *J. Mater. Process. Tech.* 271 (2019) 85-92.

[53] J. Gu, S. Yang, M. Gao, J. Bai, Y. Zhai, J. Ding, Micropore evolution in additively manufactured

- aluminum alloys under heat treatment and inter-layer rolling, *Mater. Design.* 186 (2020) 108288.
- [54] H. Yi, L. Jia, J.L. Ding, H.J. Li, Achieving material diversity in wire arc additive manufacturing: Leaping from alloys to composites via wire innovation, *Int. J. Mach. Tools Manuf.* 194 (2024) 104130.
- [55] J. Gu, J. Ding, S.W. Williams, H. Gu, P. Ma, Y. Zhai, The effect of inter-layer cold working and post-deposition heat treatment on porosity in additively manufactured aluminum alloys, *J. Mater. Process. Tech.* 230 (2016) 26-34.
- [56] Z. Snow, A.R. Nassar, E.W. Reutzel, Invited Review Article: Review of the formation and impact of flaws in powder bed fusion additive manufacturing, *Addit. Manuf.* 36 (2020) 101457.
- [57] S. Li, L.-J. Zhang, J. Ning, X. Wang, G.-F. Zhang, J.-X. Zhang, S.-J. Na, Microstructures and mechanical properties of Al–Zn–Mg aluminium alloy samples produced by wire + arc additive manufacturing, *J. Mater. Res. Technol.* 9 (2020) 13770-13780.
- [58] T. Hauser, R.T. Reisch, P.P. Breese, B.S. Lutz, M. Pantano, Y. Nalam, K. Bela, T. Kamps, J. Volpp, A.F.H. Kaplan, Porosity in wire arc additive manufacturing of aluminium alloys, *Addit. Manuf.* 41 (2021) 101993.
- [59] Q. Li, Z. Luo, C. Feng, R. Zhang, H. Li, C. Sun, F. Wang, X. Zeng, Influence of arc mode and wire properties on porosity of additively manufactured Al-6.3Cu alloy, *Guti. Huojian. Jishu.* 42 (2019) 801-807.
- [60] E.M. Ryan, T.J. Sabin, J.F. Watts, M.J. Whiting, The influence of build parameters and wire batch on porosity of wire and arc additive manufactured aluminium alloy 2319, *J. Mater. Process. Tech.* 262 (2018) 577-584.
- [61] B.Q. Cong, J.L. Ding, Influence of CMT Process on Porosity of Wire Arc Additive Manufactured Al-Cu Alloy, *Rare. Metal. Mat. Eng.* 43 (2014) 3149-3153.
- [62] M. Yang, Z. Yang, B. Cong, B. Qi, How ultra high frequency of pulsed gas tungsten arc welding affects weld porosity of Ti-6Al-4V alloy, *The International Journal of Advanced Manufacturing Technology.* 76 (2015) 955-960.
- [63] H. Zheng, M. Yang, Z. Yang, B. Qi, Analysis of pore in Ti-6Al-4V UHF pulsed GTAW welds, *Hanjie. Xuebao.* 38 (2017) 37-40+130.
- [64] J. Gu, S. Yang, M. Gao, J. Bai, K. Liu, Influence of deposition strategy of structural interface on microstructures and mechanical properties of additively manufactured Al alloy, *Addit. Manuf.*

34 (2020) 101370.

[65] J. Gu, J. Bai, J. Ding, S. Williams, L. Wang, K. Liu, Design and cracking susceptibility of additively manufactured Al-Cu-Mg alloys with tandem wires and pulsed arc, *J. Mater. Process. Tech.* 262 (2018) 210-220.

[66] B.J. Qi, M.X. Yang, B.Q. Cong, F.J. Liu, The effect of arc behavior on weld geometry by high-frequency pulse GTAW process with 0Cr18Ni9Ti stainless steel, *Int. J. Adv. Manuf. Tech.* 66 (2013) 1545-1553.

[67] Y. Feng, L. He, K. Wang, X. E, The effects of low frequency on the microstructure and mechanical properties of high-strength al-mg aluminum alloys by wire and double-pulsed arc additive manufacturing, *J. Mater. Eng. Perform.* 27 (2018) 5591-5604.

[68] C. Xue, Y. Zhang, P. Mao, C. Liu, Y. Guo, F. Qian, C. Zhang, K. Liu, M. Zhang, S. Tang, J. Wang, Improving mechanical properties of wire arc additively manufactured AA2196 Al-Li alloy by controlling solidification defects, *Addit. Manuf.* 43 (2021) 102019.

[69] J.Y. Bai, C.L. Yang, S.B. Lin, B.L. Dong, C.L. Fan, Mechanical properties of 2219-Al components produced by additive manufacturing with TIG, *Int. J. Adv. Manuf. Tech.* 86 (2015) 479-485.

[70] H. Toda, P.C. Qu, S. Ito, K. Shimizu, K. Uesugi, A. Takeuchi, Y. Suzuki, M. Kobayashi, Formation behaviour of blister in cast aluminium alloy, *Int. J. Cast. Metal. Res.* 27 (2014) 369-377.

[71] Z. Qi, B. Cong, B. Qi, H. Sun, G. Zhao, J. Ding, Microstructure and mechanical properties of double-wire+ arc additively manufactured Al-Cu-Mg alloys, *J. Mater. Process. Tech.* 255 (2018) 347-353.

[72] J.L. Gu, S.L. Yang, M.J. Gao, J. Bai, K. Liu, Influence of deposition strategy of structural interface on microstructures and mechanical properties of additively manufactured Al alloy, *Addit. Manuf.* 34 (2020) 101370.

[73] X.W. Bai, H.O. Zhang, G.L. Wang, Electromagnetically confined weld-based additive manufacturing, *Procedia CIRP.* 6 (2013) 515-520.

[74] J. Gu, M. Gao, S. Yang, J. Bai, Y. Zhai, J. Ding, Microstructure, defects, and mechanical properties of wire + arc additively manufactured Al Cu4.3-Mg1.5 alloy, *Mater. Design.* 186 (2020) 108357.

[75] E. Eimer, S. Ganguly, S. Czink, S. Dietrich, B. Chehab, J. Ding, S. Williams, Effect of inter

layer cold work on 2024 aluminium alloy produced by wire directed energy deposition, *Mater. Sci. Eng., A.* 880 (2023) 145272.

[76] S.K. Manjhi, B.S.S. Kumar, J.P. Rodrigues, P. Sekar, S. Bontha, A. Balan, An Experimental Investigation on Microstructure, Mechanical Properties and Corrosion Performance of CMT-Wire Arc Additively Manufactured Al-4043 Alloy, *Trans. Indian Inst. Met.* (2023) 1-12.

[77] Y. Li, C. Su, J. Zhu, Comprehensive review of wire arc additive manufacturing: Hardware system, physical process, monitoring, property characterization, application and future prospects, *Results in Engineering.* 13 (2022) 100330.

[78] M. Köhler, S. Fiebig, J. Hensel, K. Dilger, Wire and arc additive manufacturing of aluminum components, *Metals-Basel.* 9 (2019) 608.

[79] M. Qie, J. Wei, C. He, Microstructure evolution and mechanical properties of wire-arc additive manufactured Al-Zn-Mg-Cu alloy assisted by interlayer friction stir processing, *J. Mater. Res. Technol.* 24 (2023) 2891-2906.

[80] Z. Geng, G. Zhang, Y. Deng, L. Li, S. Yin, Processing property of variable polarity power in TIG arc welding of aluminium alloys, *Han jie. Xue bao.* (1997) 42-47.

[81] L. Xu, Z. Tian, X. Zhang, Y. Peng, Effect of shielding gas on weld microstructure and porosity sensitivity of high strength aluminum alloy, *Han jie. Xue bao.* (2006) 69-73+116.

[82] P.N. Anyalebechi, Hydrogen-induced gas porosity formation in Al-4.5 wt% Cu-1.4 wt% Mg alloy, *J. Mater. Sci.* 48 (2013) 5342-5353.

[83] B. Dong, X. Cai, S. Lin, X. Li, C. Fan, C. Yang, H. Sun, Wire arc additive manufacturing of Al-Zn-Mg-Cu alloy: Microstructures and mechanical properties, *Addit. Manuf.* 36 (2020) 101447.

[84] R. Fu, W. Lu, Y. Guo, H. Lei, Y. Cui, J. Wang, G. Di, J. Wang, C. Liu, Achieving high strength-ductility of Al-Zn-Mg-Cu alloys via hot-wire arc additive manufacturing enabled by strengthening precipitates, *Addit. Manuf.* 58 (2022) 103042.

[85] M. Wiczorowski, A. Pereira, D. Carou, B. Gapinski, I. Ramírez, Characterization of 5356 Aluminum Walls Produced by Wire Arc Additive Manufacturing (WAAM), *Materials.* 16 (2023) 2570.

[86] N. McLean, M.J. Bermingham, P. Colegrove, A. Sales, M.S. Dargusch, Understanding the grain refinement mechanisms in aluminium 2319 alloy produced by wire arc additive manufacturing, *Sci. Technol. Weld. Join.* 27 (2022) 479-489.

- [87] Z.Y. Li, M.F. Zhu, T. Dai, Modeling of microporosity formation in an Al-7%Si alloy, *Acta. Metall. Sin.* 49 (2013) 1032-1040.
- [88] C. Zhang, M. Gao, D. Wang, J. Yin, X. Zeng, Relationship between pool characteristic and weld porosity in laser arc hybrid welding of AA6082 aluminum alloy, *J. Mater. Process. Tech.* 240 (2017) 217-222.
- [89] P. Jiangang, Y. Bo, G. Jinguo, R. Yu, C. Hongjun, Z. Liang, L. Hao, Influence of arc mode on the microstructure and mechanical properties of 5356 aluminum alloy fabricated by wire arc additive manufacturing, *J. Mater. Res. Technol.-JMRT.* 20 (2022) 1893-1907.
- [90] E. Aldalur, A. Suárez, F. Veiga, Metal transfer modes for Wire Arc Additive Manufacturing Al-Mg alloys: Influence of heat input in microstructure and porosity, *J. Mater. Process. Tech.* 297 (2021) 117271.
- [91] L. Yu, Investigation on the process of wire arc additive manufacturing of high strength aluminum alloy. Beijing Institute of Technology, 2017.
- [92] X. Fang, L. Zhang, H. Li, C. Li, K. Huang, B. Lu, Microstructure evolution and mechanical behavior of 2219 aluminum alloys additively fabricated by the cold metal transfer process, *Materials.* 11 (2018) 812.
- [93] Z. Qi, B. Cong, B. Qi, H. Sun, G. Zhao, J. Ding, Microstructure and mechanical properties of double-wire + arc additively manufactured Al-Cu-Mg alloys, *J. Mater. Process. Tech.* 255 (2018) 347-353.
- [94] Z. Qi, B. Qi, B. Cong, H. Sun, G. Zhao, J. Ding, Microstructure and mechanical properties of wire + arc additively manufactured 2024 aluminum alloy components: As-deposited and post heat-treated, *J. Manuf. Process.* 40 (2019) 27-36.
- [95] Q. Shen, X. Kong, X. Chen, Fabrication of bulk Al-Co-Cr-Fe-Ni high-entropy alloy using combined cable wire arc additive manufacturing (CCW-AAM): Microstructure and mechanical properties, *J. Mater. Sci. Technol.* 74 (2021) 136-142.
- [96] B.Y. Kang, Y.K.D.V. Prasad, M.J. Kang, H.J. Kim, I.S. Kim, Characteristics of alternate supply of shielding gases in aluminum GMA welding, *J. Mater. Process. Tech.* 209 (2009) 4716-4721.
- [97] E.E.N. Nuñez, J. Unfried Silgado, J.E. Torres Salcedo, A.J. Ramírez, Influence of gas mixtures Ar-He and Ar-He-O₂ on weldability of aluminum alloy AA5083-O using automated GMAW-P, *Soldag. Insp.* 30 (2016) 423-431.

- [98] B.Q. Cong, Y. Su, B.J. Qi, G. Zhao, Q. Wang, Z.W. Qi, Wire + arc additive manufacturing for aluminum alloy deposits, *Aerospace Manufacturing Technology*. (2016) 29-32+37.
- [99] K.E.K. Vimal, M. Naveen Srinivas, S. Rajak, Wire arc additive manufacturing of aluminium alloys: A review, *Mater. Today: Proc.* 41 (2021) 1139-1145.
- [100] J.W. McPherson, C.F. Dunn, A model for stress-induced metal notching and voiding in very large-scale-integrated Al-Si (1%) metallization, *J. Vac. Sci. Technol. B.* 5 (1987) 1321-1325.
- [101] D. Liu, D. Wu, G. Ma, C. Zhong, F. Niu, A. Gasser, J.H. Schleifenbaum, G. Bi, Effect of post-deposition heat treatment on laser-TIG hybrid additive manufactured Al-Cu alloy, *Virtual. Phys. Prototy.* 15 (2020) 445-459.
- [102] P. Gao, Study on the microstructure and properties of 2196 Al-Li alloy fabricated by wire and arc additive manufacturing. Shandong University, 2022.
- [103] A.K. Sinha, S. Pramanik, K.P. Yagati, Effect of interlayer time interval on GTAW based wire arc additive manufacturing of 2319 aluminium alloy, *Sādhanā*. 48 (2023) 122.
- [104] W.M. Steen, Arc augmented laser processing of materials, *J. Appl. Phys.* 51 (1980) 5636-5641.
- [105] Q. Miao, D. Wu, D. Chai, Y. Zhan, G. Bi, F. Niu, G. Ma, Comparative study of microstructure evaluation and mechanical properties of 4043 aluminum alloy fabricated by wire-based additive manufacturing, *Mater. Design*. 186 (2020) 108205.
- [106] D. Ding, Z. Pan, D. Cuiuri, H. Li, Wire-feed additive manufacturing of metal components: technologies, developments and future interests, *The International Journal of Advanced Manufacturing Technology*. 81 (2015) 465-481.
- [107] L. Zhao, T. Sugino, G. Arakane, S. Tsukamoto, Influence of welding parameters on distribution of wire feeding elements in CO₂ laser GMA hybrid welding, *Sci. Technol. Weld. Join.* 14 (2009) 457-467.
- [108] W. Chen, Y. Chen, T. Zhang, T. Wen, Z. Yin, X. Feng, Effect of ultrasonic vibration and interpass temperature on microstructure and mechanical properties of Cu-8Al-2Ni-2Fe-2Mn alloy fabricated by wire arc additive manufacturing, *Metals (Basel)*. 10 (2020) 215.
- [109] J. Zhang, Y. Xing, J. Cao, Effect of ultrasonic vibration on micro-structure and properties of aluminum alloy produced by CMT wire arc additive manufacturing, *Heat Treat. Met.* 47 (2022) 159-164.
- [110] X. Jian, H. Xu, T.T. Meek, Q. Han, Effect of power ultrasound on solidification of aluminum

A356 alloy, *Mater. Lett.* 59 (2005) 190-193.

[111] J. Zhang, Y.F. Xing, J.J. Zhang, J.Y. Cao, F.Y. Yang, X.B. Zhang, Effects of In-Process Ultrasonic Vibration on Weld Formation and Grain Size of Wire and Arc Additive Manufactured Parts, *Materials*. 15 (2022) 5168.

[112] Y. Tian, J. Shen, S. Hu, Z. Wang, J. Gou, Effects of ultrasonic vibration in the CMT process on welded joints of Al alloy, *J. Mater. Process. Tech.* 259 (2018) 282-291.

[113] N.S. Biradar, R. Raman, Grain refinement in Al-Mg-Si Alloy TIG welds using transverse mechanical arc oscillation, *J. Mater. Eng. Perform.* 21 (2012) 2495-2502.

[114] T. Watanabe, M. Shiroki, A. Yanagisawa, T. Sasaki, Improvement of mechanical properties of ferritic stainless steel weld metal by ultrasonic vibration, *J. Mater. Process. Tech.* 210 (2010) 1646-1651.

[115] H. Wu, Y. Chang, L. Lu, J. Bai, Review on magnetically controlled arc welding process, *Int. J. Adv. Manuf. Tech.* 91 (2017) 4263-4273.

[116] L. Wang, C. Wu, J. Chen, J. Gao, Experimental measurement of fluid flow in high-speed GMAW assisted by transverse magnetic field, *J. Manuf. Process.* 56 (2020) 1193-1200.

[117] Y. Wang, X. Chen, Q. Shen, C. Su, Y. Zhang, S. Jayalakshmi, R.A. Singh, Effect of magnetic Field on the microstructure and mechanical properties of inconel 625 superalloy fabricated by wire arc additive manufacturing, *J. Manuf. Process.* 64 (2021) 10-19.

[118] Q. Sun, J. Li, Y. Liu, Y. Jiang, K. Kang, J. Feng, Arc characteristics and droplet transfer process in CMT welding with a magnetic field, *J. Manuf. Process.* 32 (2018) 48-56.

[119] Y. Cui, Y. Kang, Y. Shi, J. Chen, Z. Wang, J. Wang, Investigation into the arc profiles and penetration ability of axial magnetic field-enhanced K-TIG welding by means of a specially designed sandwich, *J. Manuf. Process.* 68 (2021) 32-41.

[120] D.R. Corradi, A.Q. Bracarense, B. Wu, D. Cuiuri, Z. Pan, H. Li, Effect of Magnetic Arc Oscillation on the geometry of single-pass multi-layer walls and the process stability in wire and arc additive manufacturing, *J. Mater. Process. Tech.* 283 (2020) 116723.

[121] B. Yang, F. Liu, C. Tan, L. Wu, B. Chen, X. Song, H. Zhao, Influence of alternating magnetic field on microstructure and mechanical properties of laser-MIG hybrid welded HG785D steel joint, *J. Mater. Res. Technol.* 9 (2020) 13692-13705.

[122] Y. Zhong, Z. Zheng, J. Li, C. Wang, Effect of in-situ transverse magnetic field on

microstructure, mechanical properties and corrosion resistance of the directed energy deposited 316L stainless steel, *Addit. Manuf.* 68 (2023) 103508.

[123] B. Wu, Z. Qiu, B. Dong, D. Wexler, Z. Pan, K. Carpenter, D.R. Corradi, H. Li, Effects of synchronized magnetic arc oscillation on microstructure, texture, grain boundary and mechanical properties of wire arc additively manufactured Ti6Al4V alloy, *Addit. Manuf.* 54 (2022) 102723.

[124] J.R. Hönnige, P.A. Colegrove, S. Ganguly, E. Eimer, S. Kabra, S. Williams, Control of residual stress and distortion in aluminium wire + arc additive manufacture with rolling, *Addit. Manuf.* 22 (2018) 775-783.

[125] F. Martina, M.J. Roy, B.A. Szost, S. Terzi, P.A. Colegrove, S.W. Williams, P.J. Withers, J. Meyer, M. Hofmann, Residual stress of as-deposited and rolled wire+arc additive manufacturing Ti-6Al-4V components, *Mater. Sci. Technol.* 32 (2016) 1439-1448.

[126] P.A. Colegrove, H.E. Coules, J. Fairman, F. Martina, T. Kashoob, H. Mamash, L.D. Cozzolino, Microstructure and residual stress improvement in wire and arc additively manufactured parts through high-pressure rolling, *J. Mater. Process. Tech.* 213 (2013) 1782-1791.

[127] J. Gu, X. Wang, J. Bai, J. Ding, S. Williams, Y. Zhai, K. Liu, Deformation microstructures and strengthening mechanisms for the wire+arc additively manufactured Al-Mg4.5Mn alloy with inter-layer rolling, *Mater. Sci. Eng., A.* 712 (2018) 292-301.

[128] R.S. Mishra, Z.Y. Ma, I. Charit, Friction stir processing: a novel technique for fabrication of surface composite, *Mater. Sci. Eng., A.* 341 (2003) 307-310.

[129] S. Jana, R.S. Mishra, J.B. Baumann, G. Grant, Effect of stress ratio on the fatigue behavior of a friction stir processed cast Al-Si-Mg alloy, *Scr. Mater.* 61 (2009) 992-995.

[130] H.J. Jiang, C.Y. Liu, Z.X. Yang, Y.P. Li, H.F. Huang, F.C. Qin, Effect of Friction Stir Processing on the microstructure, damping capacity, and mechanical properties of Al-Si alloy, *J. Mater. Eng. Perform.* 28 (2019) 1173-1179.

[131] I. Charit, R.S. Mishra, Effect of friction stir processed microstructure on tensile properties of an Al-Zn-Mg-Sc alloy upon subsequent aging heat treatment, *J. Mater. Sci. Technol.* 34 (2018) 214-218.

[132] Z. Zhao, X. Yang, S. Li, D. Li, Interfacial bonding features of friction stir additive manufactured build for 2195-T8 aluminum-lithium alloy, *J. Manuf. Process.* 38 (2019) 396-410.

[133] S. Palanivel, P. Nelaturu, B. Glass, R.S. Mishra, Friction stir additive manufacturing for high

structural performance through microstructural control in an Mg based WE43 alloy, *Mater. Design*. 65 (2015) 934-952.

[134] A.K. Srivastava, N. Kumar, A.R. Dixit, Friction stir additive manufacturing - An innovative tool to enhance mechanical and microstructural properties, *Mater. Sci. Eng., B*. 263 (2021) 25.

[135] Z.Y. Ma, R.S. Mishra, M.W. Mahoney, R. Grimes, High strain rate superplasticity in friction stir processed Al-Mg-Zr alloy, *Mater. Sci. Eng., A*. 351 (2003) 148-153.

[136] R.S. Mishra, Z.Y. Ma, Friction stir welding and processing, *Mat. Sci. Eng. R*. 50 (2005) 1-78.

[137] L. Sun, L. Huang, R. Huang, K. Xu, P. Wu, W. Long, F. Jiang, N. Fang, Progress in the effect of Ultrasonic Impact Treatment on microstructure improvement and strengthening mechanism in additive manufacturing, *Acta. Metall. Sin.* (2023) 1-22.

[138] C. Guo, Z. Wang, D. Wang, S. Hu, Numerical analysis of the residual stress in ultrasonic impact treatment process with single-impact and two-impact models, *Appl. Surf. Sci.* 347 (2015) 596-601.

[139] Y. Wu, W. Deng, K. Liu, Z. Zhang, D. Wu, M. Chen, J. Bai, Effect of inter-layer ultrasonic peening on the micro-structure and mechanical properties of 2219 aluminum alloy by TIG wire arc additive manufacturing, *Aeronautical Science & Technology*. 32 (2021) 80-86.

[140] B.N. Mordyuk, G.I. Prokopenko, Ultrasonic impact peening for the surface properties' management, *J. Sound. Vib.* 308 (2007) 855-866.

[141] T. Roland, D. Reirant, K. Lu, J. Lu, Fatigue life improvement through surface nanostructuring of stainless steel by means of surface mechanical attrition treatment, *Scr. Mater.* 54 (2006) 1949-1954.

[142] Y. Tian, J. Shen, S. Hu, Y. Liang, P. Bai, Effects of ultrasonic peening treatment on surface quality of CMT-welds of Al alloys, *J. Mater. Process. Tech.* 254 (2018) 193-200.

[143] H. Toda, T. Yamaguchi, M. Nakazawa, Y. Aoki, K. Uesugi, Y. Suzuki, M. Kobayashi, Four-Dimensional Annihilation Behaviors of Micro Pores during Surface Cold Working, *Mater. Trans.* 51 (2010) 1288-1295.

[144] H.Y. V., Treatment of metal welded joints by ultrasound aimed on residual stress decreasing, *Svar.Proizvod.* (1973) 12-200.

[145] J. Chi, Z. Cai, Z. Wan, H. Zhang, Z. Chen, L. Li, Y. Li, P. Peng, W. Guo, Effects of heat treatment combined with laser shock peening on wire and arc additive manufactured Ti17 titanium

- alloy: Microstructures, residual stress and mechanical properties, *Surf. Coat. Technol.* 396 (2020) 125908.
- [146] A. Ermakova, J. Braithwaite, N. Razavi, S. Ganguly, F. Berto, A. Mehmanparast, The influence of laser shock peening on corrosion-fatigue behaviour of wire arc additively manufactured components, *Surf. Coat. Technol.* 456 (2023) 129262.
- [147] Y. Deng, Y. Zhang, C.P. Tsui, Z. Guo, R. Zhao, S. Wang, The Jet formation in Ring-shape Laser Induced forward transfer, *Procedia CIRP.* 95 (2020) 138-142.
- [148] Z. Tong, H. Liu, J. Jiao, W. Zhou, Y. Yang, X. Ren, Microstructure, microhardness and residual stress of laser additive manufactured CoCrFeMnNi high-entropy alloy subjected to laser shock peening, *J. Mater. Process. Tech.* 285 (2020) 116806.
- [149] A. du Plessis, D. Glaser, H. Moller, N. Mathe, L. Tshabalala, B. Mfusi, R. Mostert, Pore Closure Effect of Laser Shock Peening of Additively Manufactured AlSi10Mg, *3D Print. Addit. Manuf.* 6 (2019) 245-252.
- [150] L. Hackel, J.R. Rankin, A. Rubenchik, W.E. King, M. Matthews, Laser peening: A tool for additive manufacturing post-processing, *Addit. Manuf.* 24 (2018) 67-75.
- [151] T. Chang, H. Zhang, X. Fang, Y. Jing, N. Xi, K. Huang, Tailoring precipitation of directed energy deposited Al-Cu alloy via laser shock peening, *Addit. Manuf.* 73 (2023) 103652.
- [152] M. Brummer, H. Hoffmann, E. Werner, J. Yokohama, S. Kumai. Heat treatment of aluminum castings combined with hot isostatic pressing; proceedings of the Proceedings of the 12th International Conference on Aluminium Alloys, Yokohama, Japan, F, 2010 [C].
- [153] J.C. Hastie, M.E. Kartal, L.N. Carter, M.M. Attallah, D.M. Mulvihill, Classifying shape of internal pores within AlSi10Mg alloy manufactured by laser powder bed fusion using 3D X-ray micro computed tomography: Influence of processing parameters and heat treatment, *Mater. Charact.* 163 (2020) 110225.
- [154] W.H. Kan, Y. Nadot, M. Foley, L. Ridosz, G. Proust, J.M. Cairney, Factors that affect the properties of additively-manufactured AlSi10Mg: Porosity versus microstructure, *Addit. Manuf.* 29 (2019) 100805.
- [155] M.J. Birmingham, L. Nicastro, D. Kent, Y. Chen, M.S. Dargusch, Optimising the mechanical properties of Ti-6Al-4V components produced by wire + arc additive manufacturing with post-process heat treatments, *J. Alloys Compd.* 753 (2018) 247-255.

[156] C.C. Chama, Elimination of porosity from aluminum-silicon castings by hot isostatic pressing, J. Mater. Eng. Perform. 1 (1992) 773-779.